ESCUELA INTERNACIONAL DE DOCTORADO
Programa de Doctorado en Tecnologías de la Computación
e Ingeniería Ambiental

Impact of climate variability and human activities on water resources

Autor:

Sitian Liu

Directores:

Dr. D. Javier Senent Aparicio
Dr. D. Francisco Javier Alcalá García

Murcia, septiembre de 2022

ESCUELA INTERNACIONAL DE DOCTORADO
Programa de Doctorado en Tecnologías de la Computación
e Ingeniería Ambiental

Impact of climate variability and human activities on water resources

Autor:

Sitian Liu

Directores:

Dr. D. Javier Senent Aparicio
Dr. D. Francisco Javier Alcalá García

Murcia, septiembre de 2022

AUTORIZACIÓN DEL DIRECTOR DE LA TESIS
PARA SU PRESENTACIÓN

El Dr. D. Javier Senent Aparicio y el Dr. D. Francisco Javier Alcalá García como Directores[1] de la Tesis Doctoral titulada "Impact of climate variability and human activities on water resources" realizada por Dña. Sitian Liu en el Programa de Doctorado en Tecnologías de la Computación e Ingeniería Ambiental, **autoriza su presentación a trámite** dado que reúne las condiciones necesarias para su defensa.

Lo que firmo, para dar cumplimiento al Real Decreto 99/2011 de 28 de enero, en Murcia a 01 de septiembre de 2022.

Fdo.: Javier Senent Aparicio   Fdo.: Francisco Javier Alcalá García

[1] Si la Tesis está dirigida por más de un Director tienen que constar y firmar ambos

COMPENDIO DE PUBLICACIONES

Esta Tesis Doctoral se presenta bajo la modalidad de compendio de publicaciones. Los artículos publicados en revistas indexadas que integran la tesis son los siguientes:

- **Publicación 1:** Senent-Aparicio, J.; Liu, S.; Pérez-Sánchez, J.; López-Ballesteros, A., Jimeno-Sáez, P. Assessing Impacts of Climate Variability and Reforestation Activities on Water Resources in the Headwaters of the Segura River Basin (SE Spain). Sustainability 2018, 10, 3277. https://www.mdpi.com/2071-1050/10/9/3277

  Impact Factor 2018 (JCR): 3.251; Category (JCR): ENVIRONMENTAL STUDIES; Ranking: 120/265 (Q2); Date of Publication: 2018.

- **Publicación 2:** Senent- Aparicio, J.; Alcalá, F.J.; Liu, S.; Jimeno-Sáez, P. Coupling SWAT Model and CMB Method for Modelling of High–Permeability Bedrock Basins Receiving Interbasin Groundwater Flow. Water, 2020, 12, 657. https://doi.org/10.3390/w12030657

  Impact Factor 2020 (JCR): 3.103; Category (JCR): WATER RESOURCES; Ranking: 31/94 (Q2); Date of Publication: 2020.

- **Publicación 3:** Liu, S.; Pérez-Sánchez, J.; Jimeno-Sáez, P.; Alcalá, F.J.; Senent-Aparicio, J. A novel approach to assessing the impacts of dam construction on ecohydrological conditions in the Castril River basin. Ecohydrology & Hydrobiology, 22(2022), 598-608. https://doi.org/10.1016/j.ecohyd.2022.08.004

  Impact Factor 2021 (JCR): 2.957; Category (JCR): ECOLOGY; Ranking: 84/173 (Q2); Date of Publication: 2022.

ACKNOWLEDGEMENTS

I would like to extend my deep gratitude to all those who have offered me a lot of help and support during my doctoral study.

First and foremost, my sincere thanks go to Prof. Dr. Javier Senent Aparicio, my director and supervisor, who has offered me numerous valuable comments and suggestions with incomparable patience and encouraged me profoundly throughout my doctoral study. I also want to express my thanks to Prof. Dr. Francisco Javier Alcalá García, without his painstaking teaching and insightful advice, the completion of this thesis would have been impossible.

Secondly, I would like to express my heartfelt thanks to all those who helped and cooperated with me in the process of my thesis writing. Also, I owe many thanks to my dear friends, Cynthia, Fannie, Queenie, Mareike.

Last but not least, I would like to express my thanks to my beloved parents for their unfailing love and support. For so many years, they have always been supporting me and respecting me. Their love and care are the greatest fortune of my life. Mom and dad, I love you!

"There is No Planet B".

INDEX

14

ACRONYMS AND ABBREVIATIONS

AEMET	Spanish National Meteorological Agency
ALPHA_BF	Baseflow alpha factor (days)
BFLOW	Baseflow Automated Digital Filter Program
BIOMIX	Biological mixing efficiency
CANMX	Maximum amount of water that can be trapped in the canopy when it is fully developed (mm)
CEDEX	Centre for Public Works Studies and Experimentation
CH_K1	Effective hydraulic conductivity in tributary channel alluvium
CH_K2	Effective hydraulic conductivity in main channel alluvium
CH_N1	Manning's "n" value for the tributary channels
CH_N2	Manning's "n" value for the main channel
CH_S1	Average slope of tributary channels (m/m)
CH_S2	Average slope of main channel along the channel length (m/m)
CMB	Atmospheric Chloride Mass Balance
CN2	Soil Conservation Service curve number
CRB	Castril River basin
DEM	Digital Elevation Model
EPCO	Plant uptake compensation factor
EQR	Ecological Quality Ratio
ESCO	Soil evaporation compensation factor
ET	Evapotranspiration
FDC	Flow duration curve
GIS	Geographic Information System
GRW	Guadalquivir River watershed
GW_DELAY	Groundwater delay (days)
GW_REVAP	Groundwater revap coefficient
GWQMN	Threshold water level in shallow aquifer for base flow (mm)
HRU	Hydrologic response units

HRU_SLP	Average slope steepness (m/m)
HWSRB	Headwaters of the Segura River basin
HWSM	Harmonized World Soil Map
IAG	Index of Global Alteration
IAHRIS	Indicators of Hydrologic Alteration in RIverS
IGF	Interbasin Groundwater Flow
IGME	Geological Survey of Spain
IGN	Spanish National Geographic Institute
IHA	Indicators of Hydrologic Alteration
InNSE	Inverse Nash-Sutcliffe Efficiency
IPF	Instantaneous Peak Flow
LAT_TTIME	Lateral flow travel time
LULC	Land-use and land-cover changes
MAKESENS	Microsoft Excel template application
MAPAMA	Ministry of Agriculture, Fisheries and Food of Spain
MK	Mann–Kendall
MMDF	Maximum mean daily flow
MSE	Mean square error
NAO	North Atlantic oscillation
NSE	Nash–Sutcliffe Efficiency
OV_N	Manning's "n" value for overland flow
PBIAS	Percent bias
QSWAT	QGIS interface for SWAT
R²	Coeficient of determination
RCHRG_DP	Deep aquifer percolation fraction
RCP	Representative Concentration Pathways
REDIAM	Andalusian Environmental Information Network
REVAPMN	Threshold depth of water in shallow aquifer for revap or percolation to deep aquifer to occur (mm)
RMSE	Root mean square error
RSR	Observations standard deviation ratio
SCS	Soil Conservation Service
SLSOIL	Slope length for lateral subsurface flow (m)

SLSUBBSN	Average slope length (m)
SOL_AWC	Available water capacity of the soil layer
SOL_BD	Moist bulk density
SOL_K	Saturated hydraulic conductivity
SPI	Standardized Precipitation Index
SRI	Standardized Runoff Index
SRW	Segura River watershed
SUFI-2	Sequential Uncertainty Fitting version 2
SURLAG	Surface runoff lag coefficient
SVR	Support Vector Regression machines
SWAT	Soil and Water Assessment Tool
SWAT-CUP	SWAT–Calibration Uncertainly Procedures
USDA-ARS	Agricultural Research Service of the United States Department of Agriculture
USGS	United States Geological Survey
WFD	Water Framework Directive

INDEX OF FIGURES

20

INDEX OF TABLES

ABSTRACT

This PhD Thesis assess the extent to which the global driving forces (climate change, groundwater dynamics, etc.) and human activities (land-use/land-cover changes, dam construction, etc.) interact and affect the hydrological regime in some selected basins in the semi-arid region of southeastern Spain. To conduct a comprehensive causal analysis, this PhD Thesis used the Soil and Water Assessment Tool (SWAT) hydrological model as the main tool and combined it with the Interbasin Groundwater Infiltration (IHA) method and the Chloride Mass Balance (CMB) method to make calculations of specifics water balance components.

Climate change and land-use and land-cover changes (LULC) caused by human activities are significant contributors to ecosystem degradation and the availability of a basin's water resources. Climate change forecasts for the Mediterranean region this century reveal that rising temperatures, combined with less precipitation, have resulted in a 20% drop in water resources. Human activities, such as agricultural irrigation expansion and urbanization alter runoff regimes and have an impact on the availability of water resources. Significant LULC has occurred in southeastern Spain since the 1970s, as a result of the increasing abandonment of dryland farming and the implementation of reforestation programs to prevent ecoservices degradation in watersheds. It is critical to understand how these activities impact the quantity of water resources in the headwater of large basins in southeastern Spain like the Segura River basin. The SWAT model was used to investigate the aforementioned impacts.

SWAT is the most widely used model for simulating the quality and quantity of surface water and groundwater balance components at different basin spatial scales, predicting the effects of climate change on the water balance components, and extrapolating the influence of anthropogenic activities on water resources. However, when it comes to modelling groundwater flow and storage, SWAT has substantial conceptual constraints, and other specifics techniques are needed.

Because the earth's surface water resources can no longer supply the needs of living things, which is especially evident in drylands, groundwater resources have become the focal point of water resource development. As the most important form of freshwater on land, groundwater and surface water are transformed into each other on a spatiotemporal distribution as an indivisible whole. The laws and simulations of surface water and groundwater have not been carried out jointly due to the complexity

of the hydrological cycle and the varied modes of occurrence and movement. The interaction between regional surface water and groundwater has become more and more common as a result of global changes and human activities, particularly large-scale groundwater extraction and inter-basin water transfer projects, especially in arid and semi-arid watersheds where water resources are scarce, surface water-groundwater exchange is more intense, and surface water and groundwater conversion is a factor that must be taken into account in the analysis of surface water and groundwater conversion. This study attempted to consider groundwater and surface water as a whole to provide a more trustworthy and accurate basis for water resource planning and management in order to better reflect the hydrological cycle process.

Although the SWAT model considers shallow and deep groundwater in the structure, it is solely used to calculate watershed water balance; there is no dynamic mechanism to simulate and output the net groundwater resource. The Chloride Mass Balance (CMB) is a robust method to estimate net groundwater. SWAT model and CMB method were coupled in order to accurately replicate the specific groundwater situation of the Castril River basin (CRB) in the Guadalquivir River basin. This basin was chosen to assess the reliability of combining the SWAT model and the CMB method to improve streamflow modeling in high–permeability bedrock basins receiving Interbasin Groundwater Flow (IGF), in this case from the Segura River basin.

Dam construction is also seen as having a significant impact on hydrological regime and ecosystems in the CRB. The impact of human activities has continued to change the hydrological regime of rivers and dependent ecosystems. The hydrological situation is the basic attribute and important driving force of the river ecosystem, and changes in the morphology of rivers and riparian zones, flow patterns, water quality, flora and fauna, and riparian vegetation, which affect the normal structure and function of the river ecosystem, and even an irreversible ecological crisis, will result from intra- and inter-annual variation. We provide a framework for assessing the effects of the El Portillo dam construction on streamflow regime and river ecosystem downstream. The streamflow regime data was compared with and without dam impact. IAHRIS (Indicators of Hydrologic Alteration in RIverS) which is a free Spanish software based on IHA method to assess the hydrologic alteration in rivers was used in this calculation.

The introduced methodology and the conducted analysis of results make this PhD Thesis valuable to design water resources management strategies aimed to combat the negative effects of climate change and human activities in the headwaters of large river basins in semi-arid southeastern Spain, including the relevance of interbasin groundwater flow in streamflow and the effect of dam construction on river ecosystem downstream.

RESUMEN

Esta tesis doctoral evalúa la medida en que las principales fuerzas impulsoras a escala global (cambio climático, dinámica de las aguas subterráneas, etc.) y las actividades humanas (cambios en el uso del suelo/cobertura del suelo, construcción de presas, etc.) interactúan y afectan el régimen hidrológico en algunas cuencas ubicadas en regiones semiáridas del sureste español. Para realizar un análisis causal completo, esta tesis doctoral utilizó el modelo hidrológico de la herramienta de evaluación de suelos y aguas (SWAT) como herramienta principal y lo combinó con el cálculo de indicadores de alteración hidrológica (IHA) y el método de balance de masa de cloruro (CMB) para realizar los cálculos de componentes específicos del balance hídrico.

El cambio climático y los cambios en el uso y la cobertura de la tierra (LULC, por sus siglas en inglés) causados por las actividades humanas contribuyen significativamente a la degradación de los ecosistemas y la disponibilidad de los recursos hídricos de una cuenca. Las previsiones de cambio climático para la región mediterránea de este siglo revelan que el aumento de las temperaturas, combinado con menos precipitaciones, ha provocado una caída del 20 % en los recursos hídricos. Las actividades humanas, como la expansión del riego agrícola y la urbanización, alteran los regímenes de escorrentía y tienen un impacto en la disponibilidad de los recursos hídricos. Se han producido LULC significativos en el sureste de España desde la década de 1970, como resultado del creciente abandono de la agricultura de secano y la implementación de programas de reforestación para evitar la degradación de los servicios ecosistémicos en las cuencas hidrográficas. Es fundamental entender cómo estas actividades impactan en la cantidad de recursos hídricos en la cabecera de grandes cuencas en el sureste de España como la cuenca del río Segura. El modelo SWAT se utilizó para investigar los impactos antes mencionados.

SWAT es el modelo más utilizado para simular la calidad y cantidad de los componentes del balance de aguas superficiales y subterráneas en diferentes escalas espaciales de cuencas, predecir los efectos del cambio climático en los componentes del balance hídrico y extrapolar la influencia de las actividades antropogénicas en los recursos hídricos. Sin embargo, cuando se trata de modelar el flujo y el almacenamiento de aguas subterráneas, SWAT tiene restricciones conceptuales sustanciales y se necesitan otras técnicas específicas.

Debido a que los recursos hídricos superficiales de la tierra ya no pueden satisfacer las necesidades de los seres vivos, lo cual es especialmente evidente en las tierras secas, los recursos hídricos subterráneos se han convertido en el punto central del desarrollo de los recursos hídricos. Como la forma más importante de agua dulce en la tierra, las aguas subterráneas y superficiales se transforman entre sí en una distribución espaciotemporal como un todo indivisible. Las leyes y simulaciones de aguas superficiales y subterráneas no se han realizado de manera conjunta debido a la complejidad del ciclo hidrológico y los variados modos de ocurrencia y movimiento. La interacción entre las aguas superficiales y subterráneas regionales se ha vuelto cada vez más común como resultado de los cambios globales y las actividades humanas, particularmente la extracción de aguas subterráneas a gran escala y los proyectos de transferencia de agua entre cuencas, especialmente en cuencas áridas y semiáridas donde los recursos hídricos son escasos, el intercambio de aguas superficiales y subterráneas es más intenso, y la conversión de aguas superficiales y subterráneas es un factor que debe tenerse en cuenta en el análisis de conversión de aguas superficiales y subterráneas. Este estudio intentó considerar las aguas subterráneas y superficiales como un todo para proporcionar una base más confiable y precisa para la planificación y gestión de los recursos hídricos a fin de reflejar mejor el proceso.

Aunque el modelo SWAT considera aguas subterráneas superficiales y profundas en la estructura, se utiliza únicamente para calcular el balance hídrico de la cuenca; no existe un mecanismo dinámico para simular y producir el recurso neto de agua subterránea. El balance de masa de cloruro (CMB) es un método robusto para estimar el agua subterránea neta. El modelo SWAT y el método CMB se acoplaron para replicar con precisión la situación específica de las aguas subterráneas de la cuenca del río Castril (CRB) en la cuenca del río Guadalquivir. Esta cuenca fue elegida para evaluar la confiabilidad de combinar el modelo SWAT y el método CMB para mejorar el modelado de caudales en cuencas de lecho rocoso de alta permeabilidad que reciben flujo de agua subterránea entre cuencas (IGF), en este caso de la cuenca del río Segura.

También se considera que la construcción de presas tiene un impacto significativo en el régimen hidrológico y los ecosistemas en la cuenca del río Castril. El impacto de las actividades humanas ha ido modificando el régimen hidrológico de los ríos y los ecosistemas dependientes. La situación hidrológica es el atributo básico y motor importante del ecosistema fluvial, y los cambios en la morfología de los ríos y zonas ribereñas, patrones de caudal, calidad del agua, flora y fauna, y vegetación ribereña, que afectan la estructura y función normal del ecosistema fluvial, e incluso una crisis ecológica irreversible, resultará de la variación intra e interanual. Proporcionamos un marco para evaluar los efectos de la construcción del embalse del Portillo en el régimen de flujo y el ecosistema del río aguas abajo. Los datos del régimen de caudales se

compararon con y sin impacto de presa. En este cálculo se utilizó IAHRIS (Indicators of Hydrologic Alteration in RIverS), que es un software español gratuito basado en el método IHA para evaluar la alteración hidrológica en los ríos.

La metodología presentada y el análisis de resultados realizado hacen que esta Tesis Doctoral sea valiosa para diseñar estrategias de gestión de los recursos hídricos dirigidas a combatir los efectos negativos del cambio climático y las actividades humanas en las cabeceras de las grandes cuencas hidrográficas del sureste semiárido de España, incluyendo la relevancia del flujo de agua subterránea entre cuencas en el flujo de corriente y el efecto de la construcción de presas en el ecosistema del río aguas abajo.

Palabras clave: Modelo SWAT, método CMB, método IHA, software IAHRIS, hidrología de cabecera, flujo de agua subterránea entre cuencas, construcción de presas, ecosistema fluvial, Hidrología, Ingeniería Civil, Geografía Física, Geología Ambiental.

I - INTRODUCTION

I- **INTRODUCTION**

I.1   INTRODUCTION

Water is the fundamental element for the survival of all living things on the Earth. The hydrological cycle is the link between geosphere-biosphere-atmosphere of the Earth ecosystems. As a result of global driving forces and human activities, the hydrological cycle mechanism in the formation and transformation of water resources at different scales in basins, regions and territories has become more and more complicated. The dichotomy between water and climate, water and ecology, water and society, water and economy has become increasingly prominent (Vörösmarty C. et al., 2004; Xia Jun, 2002).

In recent decades, water resources have decreased significantly due to human activities and the effects of climate change (Li Y. Y. et al., 2016). This is particularly true in semi-arid regions, where water resources have become a key element of socio-economic development (Li Z. et al., 2016).

Hydrological models have become indispensable tools to cope with water management problems, due to the capability to simulate the hydrological cycle through holistic and multidisciplinary approaches under different climate, land use and water management scenarios (Trolle D. et al., 2012). The reliability of such models depends on the spatial and temporal scales covered, as well as the ability to conceptualize the functioning of the system (Hojberg A.L. et al., 2005; Beven K., 2007; Alcalá F.J. et al., 2015). These basin-scale hydrological models are powerful decision support tools as they can provide insight into water management dilemmas, including the development of watershed management plans (Francesconi W. et al., 2016). Among them, the Soil and Water Assessment Tool (SWAT) is a physics-based semi-distributed eco–hydrological public domain model (Arnold J. G. et al., 1998), which has been used worldwide to simulate the hydrological cycle at different spatial scales in general, and the impacts of climate changes and human activities on watershed hydrology in particular (Zhang L. et al., 2017).

I.2   JUSTIFICATION OF THE INVESTIGATION

Climate change projections during this century in the Mediterranean region show that rising temperatures, accompanied by reduced precipitation, have led to a reduction in water resources of more than 20 percent (Giorgi F. and Lionello P., 2008). Human activities such as agricultural irrigation expansion and urbanization affect the availability of water resources by affecting runoff, especially true in Mediterranean Europewhere human activities have changed the landscape (Serra P. et al., 2008; Morán-Tejeda E. et al., 2012; García C. et al., 2017). A number of recent studies have examined the drivers of the hydrological cycle, concluding that climate change and land use/land cover change (LULC) are two key factors influencing hydrological processes in watersheds (Yang L., et al., 2017). Since the 1970s, significant LULC has occurred in southeastern Spain as a result of the gradual abandonment of dryland farming activities and the implementation of reforestation programmes to prevent ecoservices degradation in watersheds (Boix-Fayos C. et al., 2008). Due to severe water stress, it is important to assess the impact of forest restoration on water yields. Therefore, for Mediterranean basins with scarce data, SWAT models were used to analyze the effects of climate variability and reforestation activities on runoff and evapotranspiration (ET).

SWAT can be used to simulate the quality and quantity of surface and groundwater balance components at different basin scales, and predict the effects of climate change on the water balance (Molina-Navarro E. et al., 2018; Blanco-Gómez P. et al., 2019), and extrapolate the impact of anthropogenic activities on water resources (Senent-Aparicio J. et al., 2018). So far SWAT is the most commonly used model (Fu B., et al., 2019). However, one disadvantage of SWAT is that it has significant conceptual limitations in simulating groundwater flow and storage (Luo Y. et al., 2012).

At present, the surface water resources on the Earth can no longer meet the survival and development of living things, so that groundwater resources become the focus of water resources development. The conversion of surface water and groundwater is an important process of water circulation, and almost surface water bodies in nature interact with groundwater (Hu LiTang et al., 2007).

Groundwater and surface water, as the most important form of freshwater on land, are transformed into each other on spatio-temporal distribution as an

indivisible whole. However, due to the complexity of the hydrological cycle itself, and the different modes of occurrence and movement, the laws and simulations of surface water and groundwater have been carried out in respective relatively independent fields for a long time (Maxwell R.M. and Miller N.L., 2005). Such simplification will inevitably lose some important dynamic factors in the hydrological cycle, making the established model greatly reduced in reflecting the physical process of the water cycle in the basin.

With the impact of global changes and human activities, especially large-scale groundwater extraction and inter-basin water transfer project, the interaction between regional surface water and groundwater has become more and more frequent, especially in arid and semi-arid watersheds where water resources are scarce, surface water-groundwater exchange is more evident, and surface water and groundwater conversion is the factor must be taken into account in the analysis of water circulation and water resources management in the basin. In order to reflect the hydrological cycle process more reasonably, groundwater and surface water should be simulated as a whole to provide a more reliable and accurate basis for water resources planning and management (Sophocleous M., 2002).

In this complicated situation we cannot only use SWAT to model a watershed. Although SWAT model considers shallow groundwater and deep groundwater in the structure, it is only for the calculation of the watershed water balance, and there is no dynamic process to simulate and output the groundwater resource. SWAT model cannot perfectly simulate the regime flow in a watershed with interbasin groundwater flow. In order to accurately simulate the specific situation of a particular watershed, other specific methods should be coupled the SWAT model such as the Chloride Mass Balance (CMB) method (Alcalá and Custodio, 2008a; 2008b; 2014; 2015). To evaluate the reliability of coupling SWAT model and CMB method to improve the streamflow modelling in high–permeability bedrock basins receiving Interbasin Groundwater Flow (IGF), the Castril River basin (CRB) in the headwater of the Guadalquivir River watershed (GRW) was taken as the research area.

In CRB, the effect of dam construction is also considered as a key impact on hydrological alternation and river ecosystems. With the development and progress of economy and society, the impact of human activities on the ecosystem of rivers

and lakes continues to expand, and the hydrological situation of rivers is constantly changing, and even long-term degrading (Dong Z. et al., 2017). The hydrological situation is the basic attribute and important driving force of the river ecosystem (Jiang L. et al., 2014), and its intra- and inter-annual variation will cause changes in the morphology of rivers and riparian zones, flow patterns, water quality, flora and fauna, and riparian vegetation, which in turn affect the normal structure and function of the river ecosystem, and even an irreversible ecological crisis (Zuo Q. et al., 2015). In recent decades, due to the intensification of human activities, such as the construction and operation of a large number of water conservancy projects, the acceleration of urbanization, the destruction of vegetation and environmental pollution, as well as the impact of climate change, have had a profound impact on the river and destroyed the original river ecosystem. Therefore, carrying out hydrological change assessment, analyzing the characteristics of changes in hydrological conditions before and after human interference, and assessing the impact of hydrological changes on river ecosystems have become important research objects for river health assessment, river ecological management and ecological restoration in the world.

I.3   OBJECTIVES

In order to assess the extent to which the global driving forces (climate change, groundwater dynamics, etc.) and human activities (LULC, dam construction, etc.) affect the hydrological conditions, this study used the SWAT model as the main tool and combined with IHA method and CMB method to conduct a comprehensive analysis in the semi-arid region of southeastern Spain. Through the calculation and analysis of the results, suggestions for water resources management were given.

To cope with this main objective, other partial objectives of this PhD Thesis were scheduled as follows:

- To analyze the impact of climate variability and reforestation activities on runoff and evapotranspiration (ET).
- To simulate high permeability bedrock basins receiving IGF by coupling SWAT model and CMB method

- To present a framework to assess the impacts of dam construction on streamflow regime and river ecosystem.

- To explore the long-term trend of hydrologic metrics.

- To analyze the possible causes behind flow changes and the possible ecological impacts in downstream reaches.

- To provide several recommendations can be considered as management strategies to improve the hydrological conditions of the river, which in turn can greatly affect the ecological sustainability.

I.4   STRUCTURE OF THE THESIS

The overall structure of this PhD Thesis was divided into six chapters and an appendix. Following the brief introduction, **Chapter I** introduced the significance of the research and main objectives of the study. **Chapter II** overviewed research background and latest studies in hydrological models and associated research, such as coupling models. **Chapter III** described the study area and research methodologies. **Chapter IV** reproduced the three publications that make up this PhD Thesis and synthesized the results and discussions obtained. **Chapter V** presented conclusions and determined future research directions. **Chapter VI** contained a bibliography of references cited in this thesis. Finally, in the **Appendix A**, all information about the quality of the three published publications that make up this PhD Thesis is provided.

II – BACKGROUND AND LITERATURE REVIEW

II- BACKGROUND AND LITERATURE REVIEW

This chapter presented the literature review that frames the theoretical context on which this research is based. On the one hand, the most recent hydrological modeling research was included. In addition, the state of the art of research methods on hydrologic and ecological alteration due to natural variability and human intervention was inquired.

Hydrological modeling is used to assess the influence that changes in climate, land use, topography, geology, vegetation cover, and soils have on hydrological processes (Kiros G. et al., 2015; Krysanova V. and Srinivasan R., 2014; Singh and Woolhiser, 2002). All of these variables have non-uniform distributions, timings, and responses, which affects the complexity of physical models that attempt to explain a basin's hydrology (Srivastava et al., 2006; Singh and Woolhiser, 2002).

Hydrological modeling has a long history. It all started with the development of civil engineering in the nineteenth century, which was used to create highways, canals, rrigation systems, dams, bridges, and sewage and water delivery systems. Until the mid-1960s, hydrologic modeling was largely concerned with the creation of concepts, theories, and models to describe the many mechanisms involved in the hydrologic cycle, such as infiltration, evaporation, overland flow, and baseflow (Singh and Woolhiser, 2002).

From then to now, model development has coincided with increases in computer processing power, resulting in numerous models being developed, their typologies multiplying, their practical applications expanding, and the modeling theory itself advancing significantly (Cabezas F., 2015; Jodar-Abellán A. et al., 2019). The integration of models of diverse components of the hydrological cycle, and thus the simulation of almost the entire basin, was made possible by this significant advancement in computer technology. The Stanford Watershed Model-SWM (now termed HSPF) was the first comprehensive example of conceptual modeling of the hydrological cycle (Crawford and Linsley, 1966). Beginning in the 1970s, computer processing power expanded at an exponential rate, resulting in unprecedented breakthroughs in basin hydrology. Numerous models were developed, including the SSARR model (Rockwood D.M., Davis E.D., and

Anderson J.A., 1972), the HYOM model (Williams J.R. and Hann R.W., 1973), the Sacramento model (Burnash R. J., Ferral R. L., and McGuire R. A., 1973), the tank model (Sugawara M., Ozaki E., Wantanabe I., and Katsuyama Y., 1976), TOPMODEL (Beven K. J. and Kirkby M. J, 1979), CREAMS (Knisel W. G., 1980), HEC-1 (Hydrologic Engineering Center [HEC], 1981), SHE (Systeme Hydrologique europeen) (Abbott M. B., Bathurst J. C., Cunge J. A., O'Connell P. E., and Rasmussen J., 1986), and the ARNO model (Todini E., 1996). Some of the earlier models had flaws, such as missing critical processes like evapotranspiration or subsurface flow, which rendered them useless. Furthermore, even models that could include more processes did not do so with enough spatial resolution to be truly successful in replicating basin processes (Arnold J.G. et al., 1998). Early hydrological models handled input parameters as aggregates for the entire basin, ignoring the spatial diversity of hydrological processes, due to still limited computational capacity and geographic databases (Zhang et al., 2016).

It was not until the twenty-first century, with significant advances in computing and software development – particularly with the introduction of Geographic Information Systems (GIS) and the development of databases – that it was realized. Consider the territory's existing spatial dispersion, which is causing a proliferation of physically based distributed models.

Water management in arid and semi-arid regions, large-scale floods, the influence of climate change, and the impacts of land management have all prompted the development of models that simulate large areas. The US Agricultural Research Service (ARS) developed SWAT, which has the added benefit of being free software. It is a conceptual, semi-distributed, physically based model that is one of the most widely used hydrological models at the basin scale (Grusson Y. et al., 2017). According to Jodar-Abellán A., Pla-Bru C., and Valdés-Abellán J. (2019), the reference paper received 2,391 citations in 2017, far more than other hydrological models' corresponding articles.

SWAT has been effectively employed for a variety of applications around the world, including evaluating water supplies, water quality, land use changes, and the impact of climate change (Krysanova V. and White M., 2015). Many earlier research has demonstrated SWAT's capacity to model runoff under various environmental and physical conditions, and it has been frequently utilized for

modeling the rainfall-runoff process (Srivastava P. et al., 2006; Gassman P.W. et al., 2007; Cibin R. et al., 2010; Rahman K. et al., 2013; Wang G. et al., 2014).

SWAT is a basin-wide and well-established hydrologic model that is frequently used to simulate streamflow. Climate change, land cover change, and human activities are all assumed to be influencing runoff in the basin. In recent decades, human activities and climate change have contributed to a growing scarcity of water resources in most river basins (Vorosmarty C.J. et al., 2000). As a result, determining and measuring the factors that influence runoff variation has become a popular research issue. Because hydrological responses to climate change and human activities differ depending on location, they are usually investigated at the basin scale. Many studies on the variation analysis of hydro-climatic parameters have been conducted around the world (Hamlet A.F. et al., 2007; Yang Y.H. and Tian F., 2009; Kliment Z., 2009).

Climate change and land-use/land-cover changes (LULC) are two well-known elements that influence watershed hydrological processes (Wei X. et al., 2013). Recently, researchers have focused their efforts on better understanding the relative affects and contributions of the two variables on hydrological cycles and water resources (Karlsson I.B. et al., 2016). Increased air temperature raises atmospheric water vapor levels and modifies regional weather circulation patterns, resulting in changes in precipitation occurrence, frequency, and severity, as well as intensification of the hydrological cycle. Soil erosion is mostly caused by intense but brief precipitation episodes; thus, variations in precipitation frequency and intensity affect soil erosion and vegetation cover (Lal R. and Pimentel D., 2008; Routschek A. et al., 2014).

On the other hand, LULC is known to disrupt the hydrological cycle, including transpiration, interception, and conservation (Tomer M.D. and Schilling K.E., 2009). Increased flooding and drought occurrences, land degradation related to soil erosion, reduced agricultural productivity, and deterioration of fragile natural eco systems have all resulted from land-use change such as afforestation/deforestation, desertification, urbanization, and wetlands reclamation (Lorup J.K. et al., 1998). Deforestation, for example, might improve streamflow, resulting in short-term positive feedbacks. Furthermore, forest removal increases the likelihood of damaging floods and increases soil erosion.

Deforestation can also result in lower precipitation due to decreased evapotranspiration (ET) (Panday P.K. et al., 2015). Several research has looked into the potential decline in water production owing to forestation practices. The influence of vegetation changes on water output was investigated in 94 distinct basins (Bosch J.M. and Hewlett J.D., 1982). The result showed that eucalypt and pine forest types reduce water yield by 40 mm per 10% change in cover, but shrubland reduces yield by four times (10 mm). Another research used a fuzzy linear regression approach to analyze 145 basins and came to similar findings (Sahin V. and Hall M.J., 1986). Brown A.E. et al. (2005) analyzed 166 basins, focusing not only on water yield but also on low flows. Sun G. et al. (2006) investigated the possible magnitude of yearly water production reduction due to forestation across China, finding that it can range from 30% in tropical areas to 50% in semiarid regions. The regeneration with pine trees reduced runoff by up to 18% in a Mediterranean mountain basin was presented (Llorens P. et al., 2003). Vegetation types and distributions can impact air humidity, temperature, precipitation, and as a result, the hydrological cycle. Several pioneering research have investigated the relationships of forest change, climate, and hydrological activity, despite the fact that the corpus of scientific literature on this topic appears to be sparse (Tague G. et al., 2008).

The identification of climate change and LULC consequences on streamflow variability in arid to semi-arid regions (Gao L. et al., 2016) is always fascinating. The majority of research explored the influence of climate change on hydrological components (Lee M.H. and Bae D.H., 2015), and just a few looked at the combined effects of climate change and LULC change on a river basin's water resources (Zhang A.J. et al., 2012; Zhang Y. et al., 2014). Most studies used hydrological modeling to examine differences in hydrological processes at the river-basin size (Fossey M. et al., 2016; Marhaento H. et al., 2017). To evaluate the attribution of these fluctuations in streamflow in a river basin, some research employed hydrological models and classical statistical approaches (Wagner P.D. et al., 2016; Woldesenbet T.A. et al., 2017; Yan, R. et al., 2017).

When establishing a hydrological model, it is generally assumed that the aquifer boundary is consistent with the basin boundary and is determined by the topography. However, in many cases aquifers usually extend to more than one basin and in many cases this assumption cannot be met (Mul M. L. et al., 2007).

Water abstraction by pumping (Ladouche B. et al., 2014; Charlier J.B. et al., 2015), overbank flow phenomena (Bates P.D. and De Roo A.P.J., 2000; Moussa R. and Bocquillon C., 2009], and IGF (Eakin T.E., 1966, Pedro-Monzonis M. et al., 2014) are examples of hardly or not measurable flows that can have a noticeable impact on water balance.

Natural IGF, i.e. groundwater flow under surface topographic divides can have a big impact on water and chemical fluxes to surface water and important consequences for watershed science and management. IGF, which is typically present at sites catalogued as groundwater bodies over the world (Genereux D.P. et al., 2002), is an expected feature of some groundwater flow systems. Given the correct topography and length/depth ratio of the groundwater system, IGF can be achieved even in homogenous isotropic geological materials (To'th J.A., 1963).

IGF may obey structural and lithostratigraphic controls in more realistic heterogeneous and anisotropic geological settings (e.g. Eakin T.E., 1966; Parker J.M. et al., 1988; Hudson M.R. and Mott D.N., 1997; Thyne G.D. et al., 1999). Physical techniques such as soil–water budget and water–table fluctuation (when sufficient data are available) (Rahayuningtyas C. et al., 2014; Han M. et al., 2015), tracer techniques measuring mostly environmental chemicals and stable isotope contents of stream water (Obuobie E., 2008; Alcalá, F.J. et al., 2018), and groundwater modeling tools for indirect evaluations (Kim N.W. et al., 2008; Bouaziz L. et al., 2018) have traditionally been used to identify and quantify IGF. Palanisamy and Workman (2014) created the KarstSWAT Model to model IGF in watersheds characterized by typical karst features, determining input (preferential recharge in sinkholes) and output (punctual discharge in springs) water component dynamics. The KSWAT model was developed by Malagó et al. (2016), and it was based on a combination of two previous SWAT applications: (1) a SWAT model adaptation to consider fast preferential infiltration through caves and sinkholes up to deep aquifers developed by Baffaut and Benson (2009), and (2) a karst–flow model in Excel to simulate punctual spring flow discharge developed by Nikolaidis et al. (2013). In a karst–dominated location in Germany, Nguyen et al. (2020) suggested a two–linear–reservoir model to capture the duality of aquifer recharge and discharge processes. Although there is still interest in the SWAT model, to our knowledge, it has yet to be integrated with the CMB method to improve the

hydrological cycle simulation in basins where groundwater flow divides and surface topographic divides disagree.

The hydrological situation is the basic attribute and important driving force of the river ecosystem (Jiang L. et al., 2014), and its intra- and inter-annual variation will cause changes in the morphology of rivers and riparian zones, flow patterns, water quality, flora and fauna, and riparian vegetation, which in turn affect the normal structure and function of the river ecosystem, and even an irreversible ecological crisis (Zuo Q. and Liang S., 2018). In recent decades, due to the intensification of human activities, such as the construction and operation of a large number of water conservancy projects, the acceleration of urbanization, the destruction of vegetation and environmental pollution, as well as the impact of climate change, have had a profound impact on the river and degradated the original river ecosystem.

Large dams became significant and visible technologies for water resource management in the twentieth century. The construction of dams for development and economic progress increased dramatically from the 1930s to the 1970s, and the trend culminated in the 1970s (WCD, 2000). Dams, on the other hand, play both positive and negative roles in the context of environmental flow, depending on the space and time (Dwivedi V.K. et al., 2010). According to the World Resources Institute (WRI), at least one large dam alters 46 percent of the world's 106 primary watersheds. Furthermore, dam development has regulated more than 60% of the world's rivers (Revenga C., Brunner J., Henninger N., Kassem K. and Payne R., 2000). Dams are the most significant physical danger to watershed ecosystems, fragmenting and changing aquatic and terrestrial ecosystems with a variety of consequences that vary in duration, magnitude, and degree of reversibility.

River damming has long been employed in Mediterranean areas to deal with precipitation's natural cycle (Hooke J.M., 2006). Precipitation and runoff are out of phase with water demand in these areas, and rivers are more severely dammed than in humid areas, resulting in artificially lowered flood peaks and higher summer base flows (Kondolf G.M. and Batalla R.J., 2005; Grantham T.E. et al., 2013). Flow management in Spain became more intense in the second part of the twentieth century, when more than 1300 big dams were built (MMA, 2006), causing significant changes in the volume of flows and reversals of natural seasonal cycles

in the rivers (Batalla R.J. et al., 2004; Grindlay A.L. et al., 2011; Lorenzo-Lacruz J. et al., 2012).

Dams and reservoirs have changed natural hydrological regimes, reducing ecological services and endangering freshwater biodiversity (Magilligan F.J. and Nislow K., 2005). Hydrological alteration caused by river damming have a global environmental impact, affecting the volume and timing of natural flow regimes and endangering the biodiversity of fluvial ecosystems (Poff N.L. et al., 2007; Döll P. et al., 2009). The dam's water holding structure obstructs the natural river flow regime, causing environmental, ecological, and aquatic life problems, as well as morphological changes in the river (Mitra S. and Singh A., 2018). Non-native species may thrive in the riparian environment downstream of a dam (Zeiringer B. et al. 2018). Because the evolution, adaptation, development, and preservation of river habitats rely on water availability, the natural river flow is critical for fluvial communities and their ecological integrity (McManamay R.A. and Bevelhimer M.S., 2013).

Dam construction has resulted in significant reductions in native fish variety in many Spanish rivers (Aparicio E. et al., 2000). Reduced hydrological variability and sediment supply downstream of dams has altered river geomorphic patterns and increased vegetation encroachment, which prevents natural riparian zone dynamic succession (González del Tánago M. et al., 2015; Lobera G. et al., 2015). As a result, a better knowledge of reservoirs' cumulative ecohydrological impacts on flow regime through time is required.

In order to assess the river's ecological health and the degree of hydrological alteration caused by reservoirs and dams, and to redesign environmental flows for river management departments, indicators are needed to assess the river's ecological health and the degree of hydrological alteration caused by reservoirs and dams. The "natural flow regime" concept was established in the 1990s for the ecological restoration of rivers that had been disrupted by anthropogenic activities (Matteau M. et al. 2009). The reconstruction of natural flow regimes has been studied numerous times since the notion was introduced (Karr J.R. 1991; Ritcher B.D. et al. 1996; Poff N.L. et al. 1997).

Over 170 hydrological metrics have been published to characterize various characteristics of the flow regime (Olden J.D. and Poff N.L., 2003), but there has

been little study of the association between indicators or the statistical redundancy involved (Gao Y., Vogel R.M., Kroll C.N., Poff N.L., and Olden J.D., 2009). Richter, Baumgartner, Powell, and Braun (1996) established the Indicators of Hydrologic Alteration (IHA), which have been the most commonly used metrics for evaluating the influence of regulation on flow regimes. Many regulated rivers across the world have effectively employed the IHA method to assess hydrological disturbance (Hu W. et al., 2008; Shiau J.T. and Wu F.C., 2004; Chen Y.D. et al., 2010; Yang Z. et al., 2012; Jiang L. et al., 2014; Wang Y. et al., 2015). The IHA evaluates hydrological alterations using 33 parameters that describe the magnitude, timing, frequency, duration, and rate of change in streamflow. Changes in these streamflow features must be assessed in order to understand and forecast the impact of changing flow regimes on riverine biota, including fish (Fantin-Cruz I. et al., 2015; Sakaris P.C., 2013).

The concepts of "ecodeficit" and "eco-surplus," which are based on flow duration curves (FDCs), were first suggested by Homa et al. (2005) and Vogel et al. (2007) in an effort to construct an overall measure of habitat alteration based on streamflow data. These metrics can be calculated for any time period (season or year) and show the shortage or excess of streamflow caused by flow regulation during that time period. These two ecoflow metrics illustrate the tradeoff between human and ecological demands for available water in a numerical and graphical format. The eco-deficit and eco-surplus statistics might be useful in determining how much a river has altered hydrologically. Among all the indices in the simulated data set, the yearly eco-deficit appears to be the best generalized index (Gao B. et al., 2012; Gao Y. et al., 2009; Zhang Q. et al., 2015).

For optimizing the natural biogeochemical process and for varied hydrophytic communities, environmental flow design necessitates freshwater quantity, quality, and timing of water flow. One strategy to reduce the escalating impacts of hydrological alteration in the world's rivers is to use environmental low management in the river system (Tonkin J.D., Jähnig S.C., and Haase P., 2014).

As a result, there is a need to manage the environmental flow in order to recover and preserve the socially, environmentally, and economically feasible choice while reducing the negative impacts of dams and supporting freshwater and estuarine ecosystems (The Brisbane Declaration, 2007).

III – RESEARCH METODOLOGY

III- **RESEARCH METODOLOGY**

Chapter III was divided into four parts. Section **III.1** described the main characteristics of the study areas. **Section III.2** presented the SWAT hydrological model, as well as the sensitivity analysis, calibration and validation of the model. **Section III.3** described the CMB method. Finally, **Section III.4** presented the IAH method and the IAHRIS software.

III.1 CHARACTERISTICS OF THE STUDY AREAS

The two study areas are located in the semi-arid region of southeastern Spain. The first is the headwater of the Segura River Basin (HWSRB) at Segura River Watershed (SRW) and the second is the Castril River Basin (CRB) headwater at Guadalquivir River Watershed (GRW). The GRW is adjacent to the SRW (Figure 1). The HWSRB flows to the Anchuricas Reservoir, which has a capacity of 6 Mm³ for power generation (Figure 1a). The CRB headwater extends from the GRW–SRW divide to the El Portillo Reservoir, which has a capacity of 33 Mm³ (Figure 1b).

III.1.1 Headwater of the Segura River Basin (HWSRB)

The Segura River Basin is one of the most arid regions in the Mediterranean area, and its flow pattern shows great heterogeneity (Belmar O., et al., 2011). The HWSRB is in the province of Andalusia, and was selected mainly to study how climate change and land-use/land-cover changes (LULC) determine the flow pattern in this semiarid region. As mentioned earlier, the LULC of HWSRB has changed dramatically since the 1970s due to the reduction of rainfed agriculture and the increase of forest cover. The HWSRB reforestation strategy was to introduce pine species, using pinus nigra in the upper part of the basin, and using pinus pinaster and pinus halepensis in the middle and lower parts (Araque Jiménez E. F, 2017). Former research shown how the increase in vegetation cover leads to a decrease in both sediment yield and runoff generation (Quiñonero-Rubio J.M., et al., 2016). Even worse, other research predicted that water volumes of the HWSRB would

decline by more than 50% by the end of the century (Senent-Aparicio J. et al., 2017). The Anchuricas Reservoir was built in 1957.
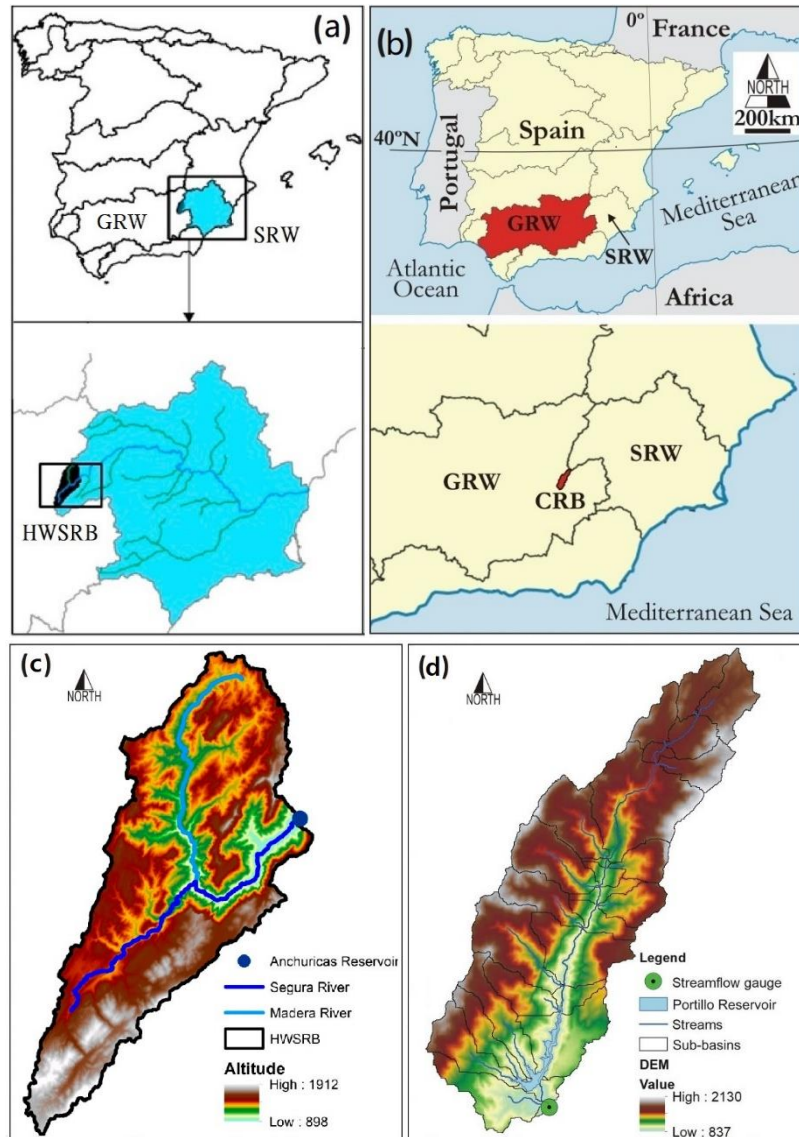
Figure 1. (a) Location of the headwater of the Segura River Basin (HWSRB) at Segura River Watershed (SRW); (b) Location of the Castril River Basin (CRB) headwater at Guadalquivir River Watershed (GRW); (c) Digital Elevation Model (DEM) of HWSRB; (d) DEM of CRB.

As a typical Mediterranean climate, precipitation is mainly concentrated in spring and autumn. Based on data from 1951 to 2015, the average annual precipitation was above 800 mm, ranging from 381 mm to 1447 mm. The HWSRB has an area of 235 km^2 with elevation ranging from 898 to 1912 m. The average annual temperature is 11.8 °C.

The average monthly flow varies from 0.74 m^3/s in August to 4.82 m^3/s in February. The land cover in the basin is predominantly (approximately 81%) dominated by forests characterized by Mediterranean shrub vegetation; the rest being bareland areas at summits. The predominant soil type is Rendzic Leptosol, stony, high carbon content and well drained (Senent-Aparicio J. et al., 2017).

Table 1 compares the land use situation in HWSRB in 1956 and 2007. As can be seen, from 1956 to 2007, the area devoted to shrubland and rainfed agriculture decreased and forests increased. Compared to 1956, the urban areas, water bodies, and barren lands have not changed much, but the grassland and forest area increased by 5.56 and 34.26 km^2, respectively. During the same period, the area devoted to rainfed agriculture, shrubland and woodland/shrub transition decreased by 11.56, 14.79 and 15.60 km^2, respectively.

Table 1. Land-use change in the HWSRB from 1956 to 2007

Land Cover Type	Area Coverage (km2)		Area Coverage (%)		Change 1956–2007	
	1956	2007	1956	2007	By km²	By %
Urban Areas	0.16	0.21	0.07	0.09	0.05	+0.02
Water Bodies	0.00	0.44	0.00	0.19	0.44	+0.19
Barren Land	0.49	2.13	0.21	0.90	1.64	+0.69
Grassland	30.96	36.52	13.13	15.49	+5.56	+2.36
Forests	54.91	89.17	23.29	37.82	+34.26	+14.53
Rainfed Agriculture	17.04	5.48	7.23	2.32	−11.56	−4.91
Shrubland	82.16	67.37	34.85	28.57	−14.79	−6.28
Transitional Woodland/Shrub	50.06	34.46	21.23	14.62	−15.6	−6.61

III.1.2 Castril River Basin (CRB) headwater

The Castril River is a mountain stream supplied by aquifers at the headwater of GRW in the province of Granada in Andalusia, adjacent to SRW (Figure 1b). The headwater sector of the CRB covers 120 km². The Castril River flows 40km from the carbonate southern slopes of the Segura Mountains and southward among the Sierra de Castril (West) and Sierra Seca (East) Mountains (Paz C. et al., 2017) to the El Portillo Reservoir (Figure 2) with elevation ranging from 2,130 to 837. The El Portillo Reservoir was built in 1999.

Figure 2. Location of El Portillo Reservoir

The climate is typical continental Mediterranean with dry summers and cold winters (Capel-Molina J.J., 1981). The annual average temperature is about 8°C, with winter temperature lower than 0°C and summer temperature over 40°C. Average annual precipitation is about 770 mm and average annual potential evapotranspiration is about 800 mm (Vanderlinden K. et al., 2004). Most rainfall occurs from autumn to spring. Winter is dominated by cold north wind and humid west wind, while in summer and autumn it is dominated by southeast wind. The summer high temperature and less rainfall coincide with each other (Trigo R. et al., 2004).

The CRB headwater is located in the Sierra de Castril Natural Park, so the land use is dominated by forests, grasslands, woodlands and shrublands, sparse vegetation areas, barren lands, and marginal irrigated crops (Figure 3). The absence of permanent human settlements avoids the impact of human production and domestic water use on the research.
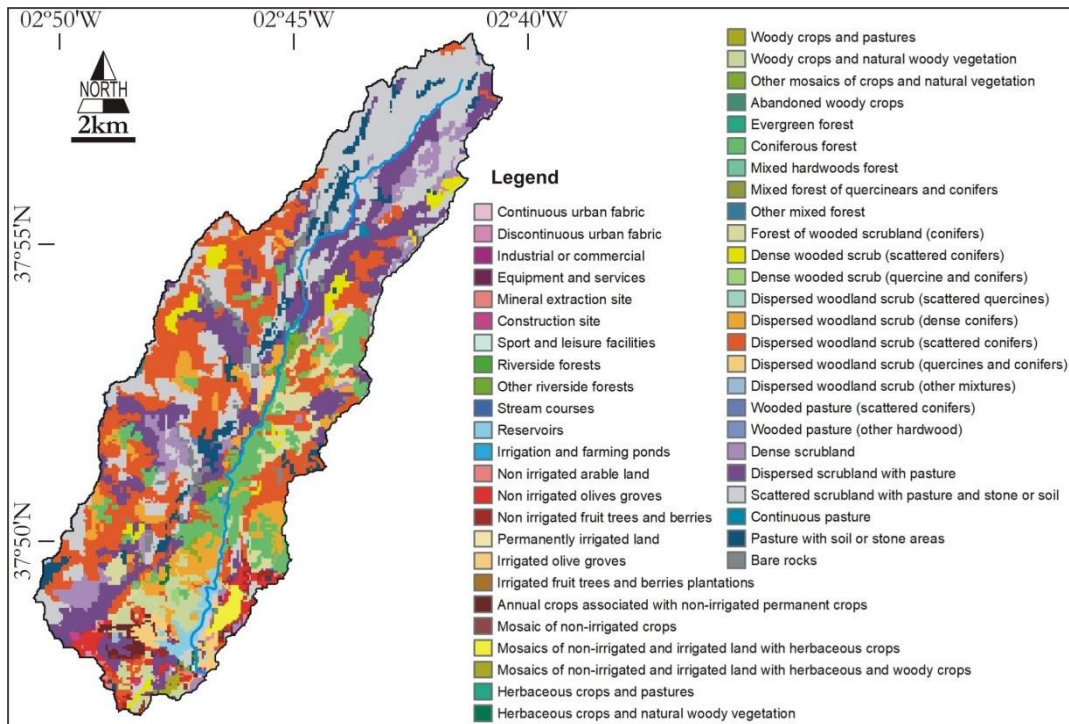
Figure 3. Land-use map (scale 1:25,000) of the CRB headwater from the Andalusian Environmental Information Network (REDIAM).

Two studies were conducted in this high-permeability bedrock basin, namely, modeling of received Interbasin Groundwater Flow (IGF) and assessing of the impacts of the El Portillo Reservoir construction on hydrologic alternation and river ecosystem.

The CRB water balance is influenced by IGF, which is a naturally occurring groundwater flow below the topographic divide between SRW and GRW. The magnitude of the IGF may be particularly relevant in high-permeability bedrock areas, which can maintain permanent streamflow during the dry seasons, thereby

modifying the water balance of the area that most rainfall-runoff modeling tools can evaluate (Nguyen V.T., et al., 2004).

Geologically, this study area belongs to the Prebetic domain of the External Zone of the Alpine Betic Chain. According to the types of permeability and storage capacity reported by the Geological Survey of Spain (IGME) (1988, 1995) and ITGE–CGH–DGCA (2001), and the bottom-top lithostratigraphic distribution in the region, the geological structure can be divided into four main formations with different hydraulic bahaviour: (1) Triassic gypsum–rich marls and clays with occasional limestones are low permeable formation that form the impervious boundary of local aquifers; (2) Jurassic and Cretaceous carbonate formations form highly permeable aquifers with a thickness of up to 300 m; (3) Jurassic and Cretaceous marls and calcareous marls are low permeable formation; (4) Late Quaternary alluvial deposits appear intermittently in the valley, forming temporary unconfined aquifers (Figure 4).

Figure 4. Hydrogeological map of the CRB (scale 1:200,000)
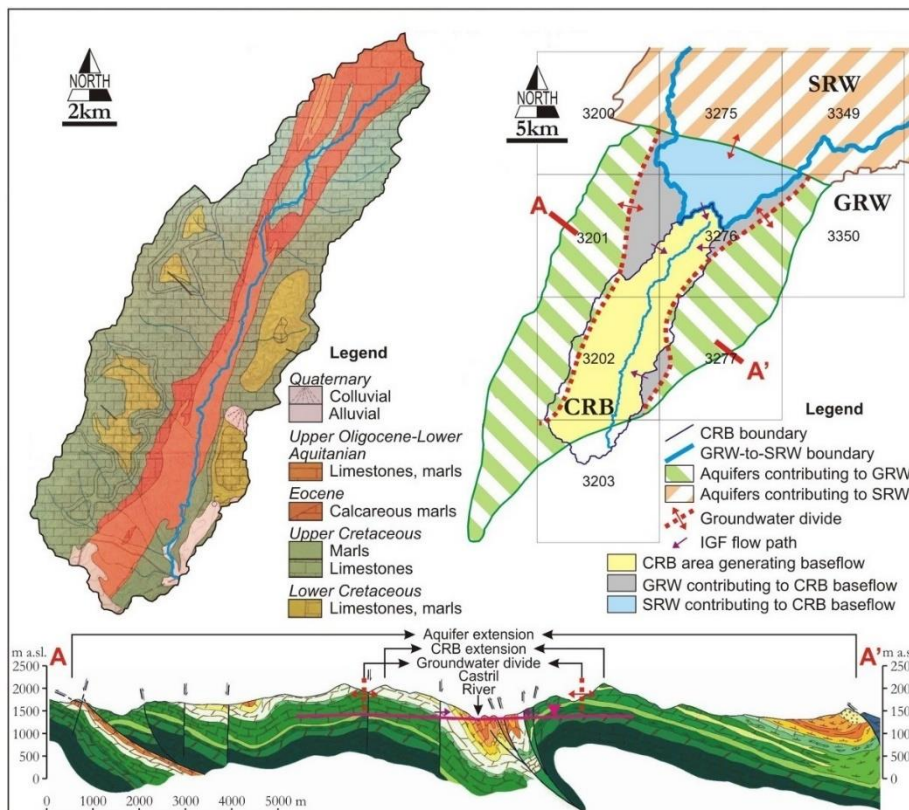
III.2   SWAT MODEL

Since the mid-1980s, with the continuous development of computer technology and Geographic Information Systems (GIS) and Remote Sensing (RS) technology, distributed hydrological model which can easily and objectively reflect the impact of climate and uncertainty in spatial distribution of surface attributes on runoff generation, has gradually become one of the important tools and methods for modern water resources and water environment research. Among them, the SWAT (Soil and Water Assessment Tool) model plays an important role in the distributed hydrological model with powerful function, advanced model structure and efficient calculation, and can be modeled in the area where the data is lacking. SWAT is a physically based, semi-distributed, continuous simulation model that operates on a daily scale. SWAT was jointly developed in 1994 by the Agricultural Research Service of the United States Department of Agriculture (USDA-ARS) and Texas A&M AgriLife Research, part of The Texas A&M University System. SWAT was primarily created to predict the impact of human activities on water resources and sediments in large and complex watersheds, with a variety of soil types, different land uses and exploitation conditions over time. Combined with the GIS platform, the model uses spatial data information provided by GIS and RS to simulate a variety of different hydrophysical processes in complex watersheds, including the transport and transformation of water, sediments, chemicals and pesticides, and has been widely used in many countries around the world (Arnold J.G. et al., 1998).

The simulation of SWAT model includes atmospheric precipitation, surface runoff, subsurface flow, evapotranspiration, groundwater flow, river network flow concentration and other processes. SWAT requires a digital elevation model (DEM), a soil map, and a land use map for the hydrological division of the basin, the climate data is also integral. The integration of this spatial information is done with the help of GIS systems, with specific plugins in ArcGIS and QGIS. These data are used as inputs for the hydrological simulation analysis of surface runoff and groundwater recharge. The SWAT model first divides the study area into several hydrological response units (HRUs) based on DEM map, land use, soil type and meteorological data, and then establishes a hydrophysical conceptual model on

each HRU, with runoff calculation on each unit the model finally connects all the HRUs by the river network in the whole study area.

The hydrological simulation in SWAT is separated into two phases: land phase and routing phase (Neitsch et al., 2011). The land phase of the hydrologic cycle (Figure 5) determines the amount of water, sediments, nutrients and pesticides incorporated into the main channel of each sub-basin. The movement of water, sediments and other components determined in the first phase to the watershed outlet is controlled through the routing phase.
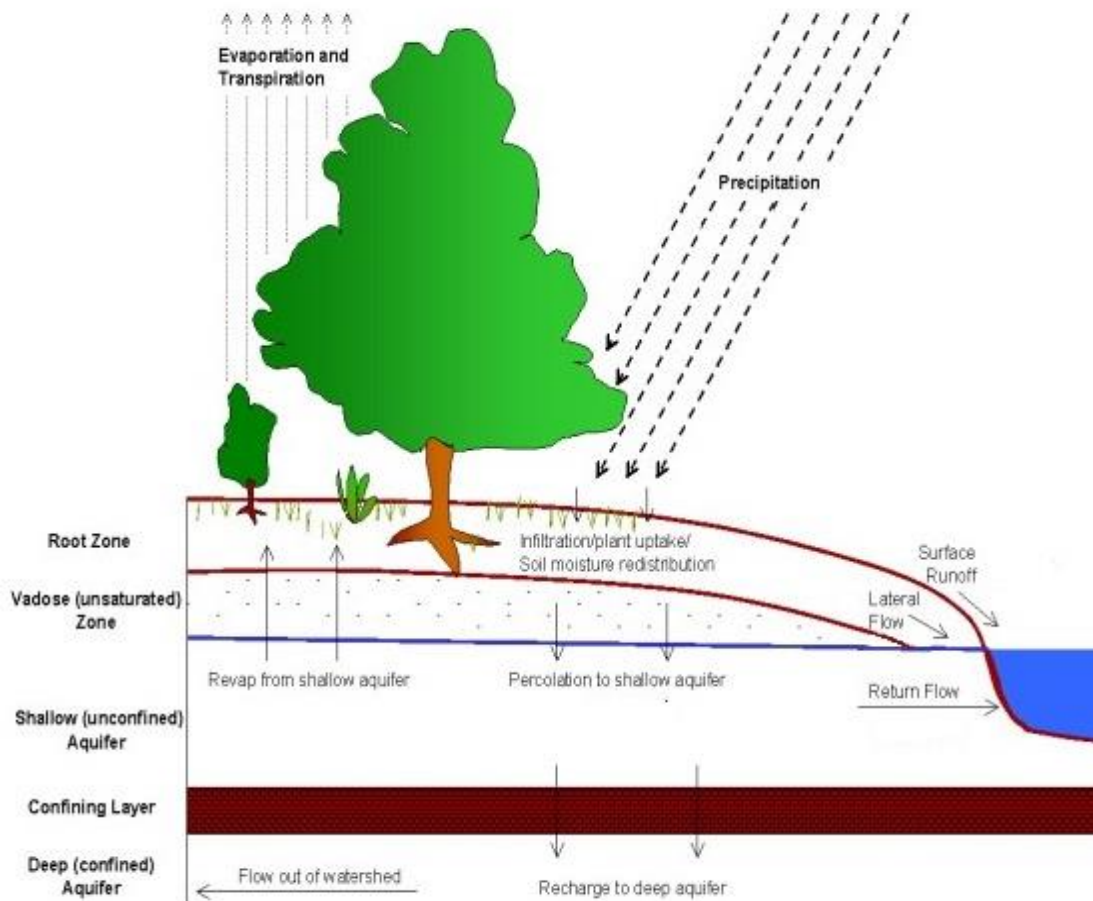
Figure 5. The land phase of the hydrological cycle in SWAT (Neitsch et al., 2011)

SWAT simulates the water balance components taking precipitation, runoff, evapotranspiration, permeation and return flow variables into accout (Abbaspour et al., 2015). The water balance equation that governs the hydrological components modeling of the SWAT model is as follows:

$$SW_t = SW_0 + \sum_{i=1}^{t} \left(R_{day} - Q_{surf} - ET_i - W_{seep} - Q_{gw} \right) \tag{1}$$

where SW_t is the final soil water content (mm H_2O), SW_0 is the initial soil water content (mm H_2O), t is the time (days), R_{day} is the amount of precipitation on day i (mm H_2O), Q_{surf} is the surface runoff amount on day i (mm H_2O), ET_i is the amount of evapotranspiration on day i (mm H_2O), W_{seep} is the amount of water that enters the vadose zone from the soil profile on day i (mm H_2O), and Q_{gw} is the return flow amount on day i (mm H_2O).

The recharge of underground water is calculated by:

$$W_{rchrg,i} = (1 - \exp[-1/\delta_{gw}]) \cdot W_{seep} + \exp[-1/\delta_{gw}] \cdot W_{rchrg,i-1} \tag{2}$$

where $W_{rchrg,i}$ is the amount of recharge entering the aquifers on day i (mm H_2O), δ_{gw} is the delay time or drainage time of the overlying geologic formations (days), W_{seep} is the total amount of water exiting the bottom of the soil profile on day i (mm H_2O), and $W_{rchrg,i-1}$ is the amount of recharge entering the aquifers on day i-1 (mm H_2O).

The climate of a basin determines the moisture and energy inputs that control the water balance. The climatic variables required by SWAT are daily precipitation, maximum and minimum air temperature, solar radiation, wind speed and relative humidity. These variables can be entered as observed data or generated during the simulation.

The SWAT model assumes for the modeling of the water in the channel circulates through trapezoidal channels and in a free sheet regime. SWAT uses Manning's equation to define the rate and velocity of flow. The water circulates through the channel network using the variable storage routing method or the Muskingum method. With this procedure, the flows generated in each HRU are aggregated along the drainage network until reach the model outlet.

III.2.1 Hydrological components of the SWAT model

When water precipitates from the atmosphere to the land surface, a part can be intercepted by the vegetation cover and the rest infiltrates through the soil reaching the underlying aquifer or forms surface and subsurface flows, which by runoff reach the main water channels, thus contributing to increase the flow of rivers in the short term. A variable fraction evapotranspirates and returns to the atmosphere.

All the processes involved in the land phase of the hydrological cycle are described in the next sub-sections.

III.2.1.1 Surface runoff

Surface runoff occurs when precipitation reaching the land surface exceeds its infiltration capacity. This infiltration decreases as soil moisture increases. In SWAT, surface runoff can be calculated using two different methods: (i) the United States Soil Conservation Service (SCS) curve number (CN) method (USDA-SCS, 1972) and (ii) the Green & Ampt infiltration method (1911). This research has used the curve number method to estimate surface runoff in the hydrological models of the study areas.

The curve number varies nonlinearly with soil moisture content and decreases as the soil approaches wilting point from values close to 0 for very high permeability conditions (e.g. sinkholes in kastic areas) to 100 for very low permeability conditions (e.g. pavemented urban areas) or when soil is fully saturated or frozen.

III.2.1.2 Interception by vegetation

A fraction of the precipitation never reaches the land surface. This fraction is intercepted by the vegetation cover and is available for direct evaporation. When the curve number method is used to calculate surface runoff, the water intercepted by the vegetation cover is considered in the runoff balance. The maximum value of intercepted water by each type of vegetation in the basin is defined in SWAT, this being the first water that disappears when evaporation is considered.

III.2.1.3 Infiltration

Infiltration is the amount of water that enters the soiland flows downward below the soil root zone through the unsaturated zone. In this process, the soil becomes increasingly moist, causing saturation. The excess of water flowing downward below the root zone (the zone of influence of evapotranspiration) is named infiltration and decreases over time. Infiltration is determined as the difference between the amount of precipitation and surface runoff.

III.2.1.4 Subsurface flow

The subsurface flow originates in the unsaturated zone, including the soil root zone. This fraction of in-transit infiltrating water does not reach the saturated zone and leaves the unsaturated zone to contribute to the channels water flow. In SWAT it is calculated by a kinematic storage model developed by Sloan, Morre, Coltharp, & Eigel (1983). This model takes the variation in conductivity, slope and soil water contentinto account for its calculation.

III.2.1.5 Evapotranspiration

Evapotranspiration is the sum of two water balance components: evaporation and transpiration. Evaporation encompasses all the processes by which liquid or solid water present on or near the land surface and in the soil turns into vapor, including evaporation from rivers and lakes, water on the land surface, the soil and the vegetation cover, and sublimation from ice and snow. Transpiration includes the water fraction that plants exchange to the atmosphere to complete its functional cycles, including direct flows from the stems and leaves and indirect ones from the roots in the soil.   Evapotranspiration may be defined as a potential, possible value without water limitations or an actual value attending to the net available amount of water to be evapotranspired.

The SWAT model offers three methods to calculate potential evapotranspiration: Penman-Monteith (Monteith, 1965), Hargreaves (Hargreaves, Hargreaves, & Riley, 1985), and Priestley-Taylor (Priestley & Taylor, 1972).

Penman-Monteith, uses data on solar radiation, temperature, relative humidity and wind speed are required, Priestley-Taylor uses data on solar radiation, temperature and relative humidity, and Hargreaves uses maximum and

minimum temperature data only. Due to the easy access to the data, Hargreaves and Penman-Monteith are more widely used methods to calculate evapotranspiration. In this research, Hargreaves is the method chosen to calculate evapotranspiration.

III.2.1.6 Percolation

Percolation is the infiltration water fraction minus the percolation flow that moves downward through unsaturated zone. It is calculated for each soil layer in the unsaturated zone. When the soil water content exceeds the soil field capacity of one layer, then the water percolates to the next layer. When the soil layer is frozen, SWAT does not calculate the water flow of the layer. Temperature is a determining factor in this process, which means when the temperatures below 0°C, the water in the ground is frozen and the flow does not occur.

III.2.1.7 Channels

Two different types of channels are considered in SWAT (i) the main channel network and (ii) tributary or secondary channels. The tributary channels are responsible for collecting surface runoff from the sub-basins and directing it to the network of main channels. The subsurface flow in SWAT connects directly with the main network. Secondary channel attributes are used to calculate the time of concentration for each of the sub-basins.

III.2.1.8 Return flow and aquifer recharge

Return flow, or baseflow, is the groundwater fraction that contributes to the channels water flow from the aquifers. Aquifer recharge is the fraction of percolation flow that reaches the saturated zone and contributes to the aquifer storage. The SWAT model divides the groundwater dynamics into two layers (i) a shallow, unconfined aquifer, which provides baseflow to surface streams in the basin; and (ii) a deep, confined aquifer that supplies baseflow to surface streams outside the basin (Arnold, Allen, & Bernhardt, 1993). In addition to return flow, the groundwater stored in the shallow aquifer can replenish moisture in the soil in very dry conditions or be directly removed by phreatophytic vegetation when the water table is shallow.

III.2.2 Sensitivity analysis, calibration and validation of the SWAT model

The adjustment of the defining parameters of SWAT is carried out through a calibration procedure consisting of three different stages: sensitivity analysis, calibration and validation.

Sensitivity analysis determines how much changes in model parameters affect the model outputs. It is a necessary process to identify the key parameters needed for calibration (Ma L. et al., 2000), and to select those parameters that have a significant impact on the model results. Model calibration is the process of estimating the value of parameters by comparing model simulation outputs with observed data for the same conditions. The validation process consists of running the model using the parameters determined in the calibration to demonstrate that the model is sufficiently accurate for the case study.

The calibration can be done manually or automatically. Manual calibration is based on a trial-and-error process, which means when the number of parameters is large manual calibration becomes a slow and complex task. Automatic calibration optimizes parameter values using numerical methods. As SWAT is a model with a multitude of parameters and complex operation, automatic calibration is recommended. For this purpose, the SUFI-2 (Sequential Uncertainty Fitting version 2) (Abbaspour K. C. et al., 2004) algorithm implemented in the SWAT-CUP (SWAT – Calibration Uncertainly Procedures) software package has been used in the different models developed in this PhD Thesis. As a calibration algorithm, the SUFI-2 algorithm requires fewer simulations to achieve the same level of performance compared to the other calibration options. Furthermore, SUFI-2 was found to be quite efficient for time-consuming large-scale models (Yang J. H. et al., 2008).

The calibration process for adjusting the values of the selected parameters using SUFI-2 algorithm includes the following steps:

1. Definition of the objective function dependent on the project objectives.

2. Definition of the absolute maximum and minimum values of the parameters based on their physical characteristics.

3. Sensitivity analysis of the parameters selected in the model.

4. Definition of the initial values of the calibration parameters.

5. Running N simulations (n > 500) and saving the output variables
   obtained, including the following steps:

   a. Calculation of the objective function of each simulation.

   b. Calculation of the sensitivity of each parameter.

   c. Calculation of 95% of the prediction sensitivity (95PPU).

6. Definition of the updated intervals for each parameter and repetition
   of the simulations until the desired adjustment is achieved.

Sensitivity analysis is estimated according to the variations in the objective function that evaluates the model calibration's effectiveness. It is computed by altering each parameter one by one, while all other parameters remain the same. The SUFI-2 algorithm calculates the statistical values of the t-stat and p-value by a multiple regression analysis in the sensitivity analysis of each of the parameters.

The higher the value of t-stat and lower the p-value statistic (values less than 0.05), the more sensitive the parameter considered (Abbaspour K. C. et al., 2007).

The parameter calibration and validation process begins when the most sensitive parameters have been detected, in many cases depending on the results of their initial values. The warm-up period (first 2 - 5 years) is used to stabilize the model and improve the quality of the simulation, and the parameter values at the end of the warm-up period are taken as the initial values.

Validation consists executing the model with the values of the parameters that were determined during the calibration process, and comparing the predictions to observed data not used in the calibration. In this way, the validity of the model is guaranteed in conditions other than the calibration phase.

III.2.3 Performance Evaluation Criteria of the SWAT model

Quantitative information is used to cross-validate the SWAT model results. For model efficiency criteria, the most common statistics are Nash-Sutcliffe efficiency (NSE), inverse Nash-Sutcliffe Efficiency (lnNSE), coeficient of determination (R2), percent bias (PBIAS), root mean square error (RMSE), and observations standard deviation ratio (RSR) (Table 2).

Table 2. Equations, ranges, and optimal values for SWAT model performance statistics, after Moriasi D. N. et al. (2012).

Statistic and Equation	Description
NSE: Nash–Sutcliffe Efficiency Coefficient. $$= 1 - \frac{\sum_{i=1}^{n}(Q_{obs\ i} - Q_{sim\ i})^2}{\sum_{i=1}^{n}(Q_{obs\ i} - \overline{Q})^2}$$	NSE indicates a perfect match between observed and simulated data and the range is between $-\infty$ and 1. Higher than 0.5 is considered satisfactory.
lnNSE $$= 1 - \frac{\sum_{i=1}^{n}(\ln(Q_{obs\ i}) - ln(Q_{sim\ i}))^2}{\sum_{i=1}^{n}(\ln(Q_{obs\ i}) - \overline{\ln(Q)})^2}$$	lnNSE is the logarithmic form of the model efficiency coefficient. NSE emphasizes the high flows, and lnNSE emphasizes the low flows.
R^2: *Coefficient of Determination* $$= \left(\frac{\sum_{i=1}^{n}(Q_{obs\ i} - \overline{Q})\,(Q_{sim\ i} - \overline{Q_{sim\ \iota}})}{\sqrt{\sum_{i=1}^{n}(Q_{obs\ i} - \overline{Q})^2}\,\sqrt{\sum_{i=1}^{n}(Q_{sim\ i} - \overline{Q_{sim\ \iota}})^2}} \right)^2$$	R^2 indicates the degree of linear relationship between simulated and observed data and the range is from 0 to 1. Higher than 0.5 is considered satisfactory.
PBIAS: Percent Bias $$= \frac{\sum_{i=1}^{n}(Q_{obs\ i} - Q_{sim\ i}) \cdot 100}{\sum_{i=1}^{n}(Q_{obs\ i})}$$	PBIAS calculates the average trend of the simulated data to be larger or smaller than their observed counterparts. The optimal value is 0, and between ±25 is acceptable.
RMSE: Root Mean Square Error $$= \sqrt{\sum_{i=1}^{n}(Q_{obs\ i} - Q_{sim\ i})^2}$$	RMSE indicates a perfect match between observed and predicted data when it equals to zero. Increasing RMSE values indicate that matching is getting worse.

RSR: Ratio of RMSE to Standard deviation of observations data.

$$= \frac{RMSE}{STDEV_{obs}} = \frac{\sqrt{\sum_{i=1}^{n}(Q_{\text{obs } i} - Q_{\text{sim } i})^2}}{\sqrt{\sum_{i=1}^{n}(Q_{obs \ i} - \overline{Q_{sim \ i}})^2}}$$

RSR is the ratio of the RMSE to standard deviation of observed data, and its range is between 0 and ∞. The lower RSR, the lower RMSE and better the model performance. Lower than 0.7 is acceptable.

where n is the total number of observations, $Q_{\text{obs } i}$ and $Q_{\text{sim } i}$ are the observed and simulated discharges at i th observation, $\bar{Q}$ is the mean of the observed data over the simulation period, and $\overline{Q_{sim \ i}}$ is the mean of the simulated data over the simulation period.

III.3 CMB METHOD

SWAT has significant conceptual limitations in simulating groundwater flow and storage (Luo Y. et al., 2012), which can lead to poor model performance in groundwater-dominated watersheds (Ficklin D.L. et al., 2012). One of these limitations is SWAT's inability to consider the Interbasin Groundwater Flow (IGF). IGF is defined as the naturally occurring groundwater flow beneath the surface topographic divide that defines the basin boundary introduced by SWAT model or other hydrological models, and contributes to the baseflow of another basin different to what it was generated (Genereux D.P. et al., 2005). The magnitude of IGF may be particularly associated with high-permeability bedrock areas, such as steep karst massifs. IGF maintains streamflow in dry seasons, thereby significantly altering the water balance of a region (Nguyen V.T. et al., 2020). IGF is often difficult to measure, although it is a common hydrological process in high-permeability bedrock areas.

Long-term net aquifer recharge (R) and discharge in steep basins with increased flow in natural (undisturbed) states can be equated when groundwater extraction, direct evapotranspiration from shallow aquifers, and underflow into deep aquifers are almost zero (Alcalá F.J. et al., 2011; Andreu, J.M. et al., 2011). In this undisturbed hydrological regime, net aquifer recharge is equal to the baseflow component of streamflow (Rutledge A.T. et al., 1996; Lim K.J. et al., 2005; Plesca I. et al., 2012; Lee J. et al., 2018), narrowing down to the implementation of

appropriate and feasible techniques to determine R. Average R can be determined using different methods (Scanlon B.R. et al., 2002; McMahon P.B. et al., 2011), one of which is independent and well-known method is atmospheric chloride mass balance (CMB) (Claasen H.C. et al., 1986; Dettinger, M.D., 1989; Wood, W.W.; et al., 1995; Sami K. et al., 1996; Scanlon B.R. et al., 2006).The CMB method has been widely used for different topographical, climatic, and geological changes to measure long-term R when the chloride content of the water table is a function of the atmospheric chloride content and can be used as a proxy for the recharge chloride content. By validating the long-term stability of the CMB variables (Alcalá F.J. et al., 2014; Alcalá F.J. et al., 2015), the CMB method has recently been used to assess the spatial distribution of average R from precipitation and its uncertainty in continental Spain. This data availability is why the CMB method was chosen to assess IGF in areas where there are no human activities neither geological features contributing non-atmospheric hloride sources.

III.3.1 CMB Method application for aquifer recharge

As described above, the CMB is one of the most widely used methods to estimate R. The CMB is a global method based on the principle of mass conservation of a conservative tracer, in this case the chloride ion, atmospherically contributing to the land surface.

By validating the long-term stability for the CMB variables: atmospheric chloride bulk deposition, chloride output fluxe from surface runoff, and chloride content in recharge water, the CMB method has recently been used to determine the spatial average R and its natural uncertainty (standard deviation) on continental Spain (Alcalá F.J. et al., 2014; Alcalá F.J. et al., 2015; Alcalá F.J. et al., 2008a). This assessment analyzed the effects of hydraulic properties (permeability and storability) of different aquifer lithologies on the R estimates and the potential contribution of non-atmospheric chloride sources (Alcalá F.J. et al., 2008b).

The hydrological significance and reliability of distributed R was determined by comparing with local potentially trustworthy R values, including some aquifers near the study areas with similar typology. The CMB variable is regionalized by using ordinary kriging on the same 4976 nodes of a 10 km x 10 km regular grid to estimate average R and its uncertainty in each grid node. The assessment covered

10 years, which is a critical balance period for achieving a relatively stable CMB mean and standard deviation. This period coincides with the ten-year global climate cycles acting on the Iberian Peninsula, with roughly five years of positive and negative phases not perfect along with the North Atlantic Oscillation trend (Hurrell J.W., 1995; Trigo R. et al., 2004).

III.3.2 IGF series generation

As mentioned earlier, under natural (undisturbed) regime when groundwater extraction, direct evaporation of shallow aquifers, and underflow into deep aquifers are almost zero, long-term steady R and IGF in steep high-permeability bedrock basins with gaining streams can be equated (Rutledge A.T. et al., 1996; Lim K.J. et al., 2005; Plesca I. et al., 2012; Lee J. et al., 2018). When the human water use is virtually null and the hydrogeological functioning is well defined, the fraction of R produced in upstream contributing areas can be used as a reliable proxy for the baseflow component.

A procedure was introduced to obtain the yearly R series, by adopting the temporal structure of the yearly P series of the control period (Pulido-Velazquez D. et al., 2018). The model uses a correction function that forces the control R series to have the same relative deviation as the control P series, while maintaining the magnitude of its initial mean and standard deviation. The calibration function is used to obtain the yearly R series, assuming that the correction function is unchanged. The process consists of the following steps:

Average change of mean and standard deviation of P and R for the same control period:

$$\Delta\mu = \frac{\mu(R) - \mu(P)}{\mu(P)} \tag{3a}$$

$$\Delta\sigma = \frac{\sigma(R) - \sigma(P)}{\sigma(P)} \tag{3b}$$

where $\Delta\mu$ is the change in mean and $\Delta\sigma$ is the change in standard deviation.

Standardization of the yearly P series:

$$Pn_i = \frac{P_i - \bar{P}}{\sigma_R} \tag{4}$$

where P_i is i–year P and Pn_i is its standardised value, $\bar{P}$ is mean P, and σ_R is standard deviation of mean R.

Generation of yearly R series from yearly P series:

$$R_i = \mu_C + \sigma_C \cdot Pn_i \tag{5}$$

where R_i is i–year R, and μ_C and σ_C are expressed as:

$$\mu_C = \mu(P) \cdot (1 + \Delta\mu) \tag{6a}$$

$$\sigma_C = \sigma(P) \cdot (1 + \Delta\sigma) \tag{6b}$$

III.3.3 BFLOW programme

The Baseflow Automatic Digital Filter (BFLOW) was employed to divide daily streamflow records into baseflow and surface runoff components. This recursive digital filter technique was first used for baseflow analysis (Nathan and McMahon, 1990). Filtering baseflow (low-frequency signal) from streamflow (high-frequency signal) is equivalent to filtering low-frequency signals in signal processing, according to the BFLOW hypothesis (Arnold J.G. et al., 1995). Despite the lack of a true physical basis for this technique, it is objective and repeatable, and it produces results that are comparable to those achieved using other most sophisticated automated models or tedious manual techniques. Many research including the SWAT Model (Plesca I. et al., 1995; Meaurio, M. et al., 2015) have employed BFLOW. BFLOW's baseflow was enhanced by adding IGF.

III.4 IHA METHOD AND IAHRIS

In order to quantitatively assess the extent to which human activities affect the hydrological regime, many researchers have implemented different methods since the 1970s, the most widely used was the IHA (Indicators of Hydrologic Alteration) method. This PhD Thesis used the IAHRIS (Indicators of Hydrologic Alteration in RIverS) version 2.2 software package to calculate the IHA of CRB.

IAHRIS is a free software developed by the Centre for Public Works Studies and Experimentation (CEDEX).

III.4.1 Indicators of hydrologic alteration (IHA)

The IHA method established 33 quantifiable hydrological parameters related to the ecological environment from the five aspects of flow regime, timing, frequency, duration and rate of change (Richter B.D. et al., 1996). IHA was originally designed to analyze hydrologic effects of dams by comparing streamflow in "with dam" and "without dam" periods. The method assumes that natural flow modification alters the ecosystem. The numerical changes of hydrological parameters reflect the degree of hydrological changes, while the differences in hydrological parameters can also reflect the differences in ecological hydrology, and certain hydrological parameters depict a certain aquatic environment.

The IHA parameters contains five categories (Table 3): (1) magnitude of monthly streamflow, (2) magnitude of annual extreme flow, (3) frequency and duration of high and low pulses, (4) rate and frequency of flow changes, and (5) timing of annual extreme flow. The IHA covers most flow components and can be used to analyze high information and non-redundant indices.

Table 3. Indicators of hydrological alteration (IHA).

Group	Parameter
Magnitude of monthly streamflow	Mean flow in January, mean flow in February, mean flow in March, mean flow in April, mean flow in May, mean flow in June, mean flow in July, mean flow in August, mean flow in September, mean flow in October, mean flow in November, mean flow in December.
Magnitude of annual extreme flow	One-day maximum flow, three-day maximum flow, seven-day maximum flow, 30-day maximum flow, 90-day maximum, one-day minimum flow, three-day minimum flow, seven-day minimum flow, 30-day minimum flow, 90-day minimum flow.

Frequency and duration of high and low pulses	Low pulse count, low pulse duration, high pulse count, high pulse duration.
Rate of flow change	Rise rate, Fall rate, Number of reversals.
Timing of flow	Date of annual maximum flow, date of annual minimum flow, number of zero flow days.

III.4.2 IAHRIS

IAHRIS (Martínez C. and Fernández J.A., 2010a & 2010b) is a free software developed by CEDEX to evaluate the degree of hydrological changes through a series of indicators. IHARIS is suitable for Spain because the hydrological alteration is assessed according to the criteria established by the Spanish Hydrological Planning Instruction. In IAHRIS, the IHA value is obtained by comparing 19 parameters (Table 4) of the natural flow and the altered flow. Three of them are derived from annual flow, six are derived from monthly flow, and the rest are from daily flow. These indicators are divided into usual values, maximum extreme values (floods) and minimum extreme values (droughts). The impact on the ecosystem is considered from five aspects: magnitude, variability, seasonality, duration and frequency at each level.

Table 4. Parameters of IAHRIS

Group		Aspect	Description	Parameter
Usual values	Annual and Monthly volumes	Magnitude	Mean of annual volumes.	P1
		Variability	Difference between maximum and minimum volume in the year.	P2
		Seasonality	Months of maximum and minimum volume in the year.	P3
	Daily flows	Variability	Differences between average flows of 10% and 90% percentiles.	P4

Extreme values	Maximum daily flow (floods)	Magnitude and frequency	Average of Yearly maximum daily flow.	Q_c (P5)
			Effective discharge.	Q_{GL} (P6)
			Connectivity flow.	Q_{CONEC} (P7)
			Usual flow in flooding (5% exceedance percentile).	$Q_{5\%}$ (P8)
		Variability	Coefficient of variation of yearly maximum daily flow.	$Cv\ (Q_c)$ (P9)
			Coefficient of variation of usual flow in flooding.	$Cv\ (Q_{5\%})$ (P10)
		Duration	Consecutive days in a year with exceedance percentile below 5%.	Duration of flooding (P11)
		Seasonality	Average number of days per month with exceedance percentile above 5%.	One value per month (P12)
	Minimum daily flow (droughts)	Magnitude and frequency	Average of yearly minimum.	Q_s (P13)
			Usual flow in droughts (95% exceedance percentile).	$Q_{95\%}$ (P14)
		Variability	Coefficient of variation of yearly minimum daily flow.	$Cv\ (Q_s)$ (P15)
			Coefficient of variation of usual flow in droughts.	$Cv\ (Q_{95\%})$ (P16)
		Duration	Consecutive days in a year with exceedance percentile below 95%.	Duration of droughts (P17)
			Average number of days per month with null flow.	One value per month (P18)

Seasonality		Average number of days per month with exceedance percentile below 95%.	One value per month (P19)

By comparing and calculating these parameters, 21 IHA values can be obtained (Table 5). Each IHA value can correspond to the original and altered hydrological conditions. The natural parameter value vs. the altered parameter value ratio ranges from 0 to 1, where 1 means no alteration and 0 means total alteration. When IAH is higher than 1, the obtained value is substituted by its inverse in order to maintain proportionality in the variation of both regimes (natural vs. altered), avoiding the compensations that would arise in global alteration index calculus for indices lower and higher than 1. Fernández et al. (2012) and Pérez-Sánchez et al. (2020) provide a detailed description of the IAHRIS method.

Table 5. List of parameters used by IAHRIS to obtain the IHA

Group	Aspect	IHA Indicator	Description	Parameter
Usual Values	Magnitude	IAH1	Magnitude of annual volume.	P1
		IAH2	Magnitude of monthly volume.	P1
	Variability	IAH3	Habitual variability.	P4
		IAH4	Extreme variability.	P2
	Seasonality	IAH5	Seasonality of maximums.	P3
		IAH6	Seasonality of minimums.	P3
Floods	Magnitude and frequency	IAH7	Magnitude of maximum floods.	P5
		IAH8	Magnitude of effective discharge.	P6
		IAH9	Frequency of connectivity flow.	P7
		IAH10	Magnitude of usual floods.	P8

Variability	IAH11	Variability of maximum floods.	P9
	IAH12	Variability of usual floods.	P10
Duration	IAH13	Floods duration.	P11
Seasonality	IAH14	Seasonality of floods (1 for each month).	P12
Magnitude and frequency	IAH15	Magnitude of extreme droughts.	P13
	IAH16	Magnitude of usual droughts.	P14
Variability	IAH17	Variability of extreme droughts.	P15
	IAH18	Variability of usual droughts.	P16
Duration	IAH19	Duration of droughts.	P17
	IAH20	Number of days of null flow (1 for each month).	P18
Seasonality	IAH21	Seasonality of droughts (1 for each month).	P19

(Row group label at left: **Droughts** spans from IAH15 to IAH21.)

Significant inter-annual and seasonal variability, as well as frequent floods, characterize Mediterranean rivers (Fernández J.A. et al., 2012). As a result, typical inter-annual values must first be studied and discretized. The goal of discretisation is to define streamflow thresholds such that years can be classed as wet, normal, or dry. In a natural regime, a year is deemed wet if its annual volume is higher than the 25th percentile. The year is termed dry if the annual volume is less than the 75th percentile, and the years between the 25th and 75th percentiles are classified as normal. As a result, for each type, an indicator is obtained. The following equation can be used to produce a weighted year indicator.

$$\text{Indicator weighted year} = 0.25\ \text{Indicator wet year} + 0.5\ \text{Indicator normal year} + 0.25\ \text{Indicator dry year} \tag{7}$$

IAHRIS uses the colors recommended by the Ecological Quality Ratios (EQR) (WFD, 2000) to classify the IHA into five hydrological states (Table 6). The higher the value of the index is, the lower the hydrologic alteration is, which indicates excellent ecological status with blue color. And respectively green, yellow, orange and red means good, moderate, deficient and very deficient status.

Table 6. Ranking of hydrological states in IAHRIS.

Category	Level I Excellent	Level II Good	Level III Moderate	Level IV Deficient	Level V Very deficient
Range	0.8 < IHA ≤ 1	0.6 < IHA ≤ 0.8	0.4 < IHA ≤ 0.6	0.2 < IHA ≤ 0.4	0 < IHA ≤ 0.2

Two types of results for each of the three groups (usual, droughts and floods) are also provided by IAHRIS. On one side, there is a spider chart that shows the value of each IHA (Figure 6). On the other side, an index of global alteration (IAG) is calculated for usual values, droughts and floods. The IAG is quantified by the ratio between the areas of the natural and altered polygons of the spider chart. A color code has been established to display the hydrological states (Table 7).
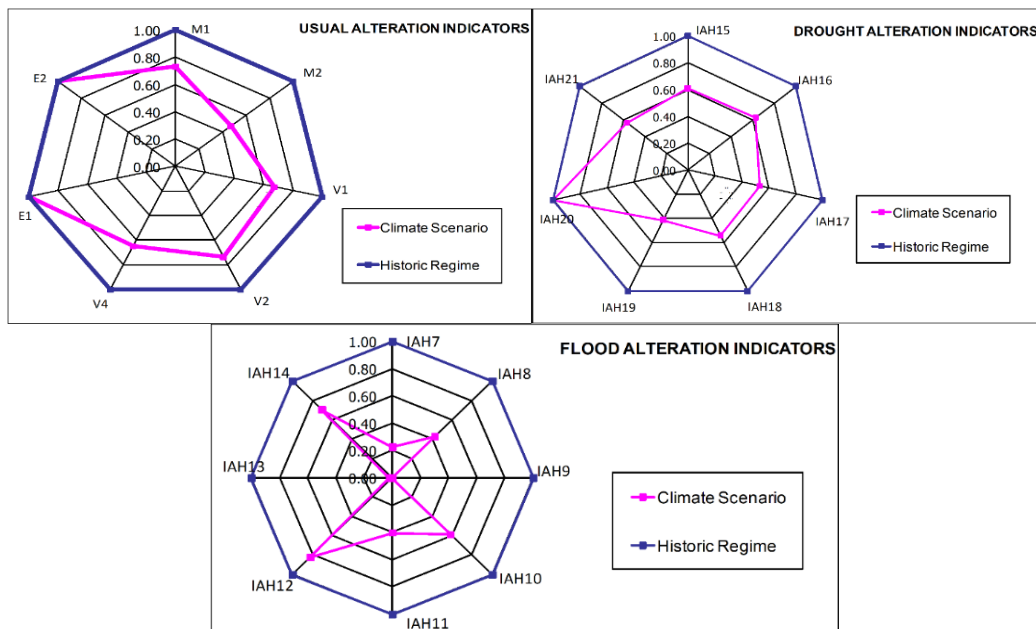
Figure 6. Spider charts of IAHRIS for usual, droughts and floods hydrological states.

Table 7. Hydrological state of IAG in IAHRIS.

Category	Level I Excellent	Level II Good	Level III Moderate	Level IV Deficient	Level V Very deficient
Range	0.64 < IAG ≤ 1	0.36 < IAG ≤ 0.64	0.16 < IAG ≤ 0.36	0.04 < IAG ≤ 0.16	0 < IAG ≤ 0.04

III.4.3 FDC

A modest collection of representative indicators has been designed for efficiently determining the shift of flow regimes in order to solve the problem of a large number of parameters and redundant information. The flow duration curve (FDC) is constructed from the runoff data in specific time intervals and to provide a measurement of the time percentage during which a specific flow is equalized or exceeded. An annual FDC can reflect the variability of daily streamflow during a typical period. The FDC plots can be calculated as follows:

$$p_i = i \,/\, (n + 1) \tag{8}$$

where i is the rank and n is the total number of days.

On the basis of flow duration curve (FDC), Vogel et al. (2007) proposed the concepts of eco-surplus and eco-deficit, which are the eco-flow metrics represent the amount of water shortage (eco-deficit) or excess (eco-surplus) in the river ecosystem requirement at different time scales. Eco-surplus manifests the altered "with dam" median annual flow duration curve above the natural "without dam" flow duration curve. Eco-deficit is where the altered median annual FDC below the natural median yearly FDC (Vogel et al., 1995). The eco-surplus and eco-deficit were defined as eco-flow indicators which can inspect the overall gain or loss of water flow in a dam-effected river (Figure 7).
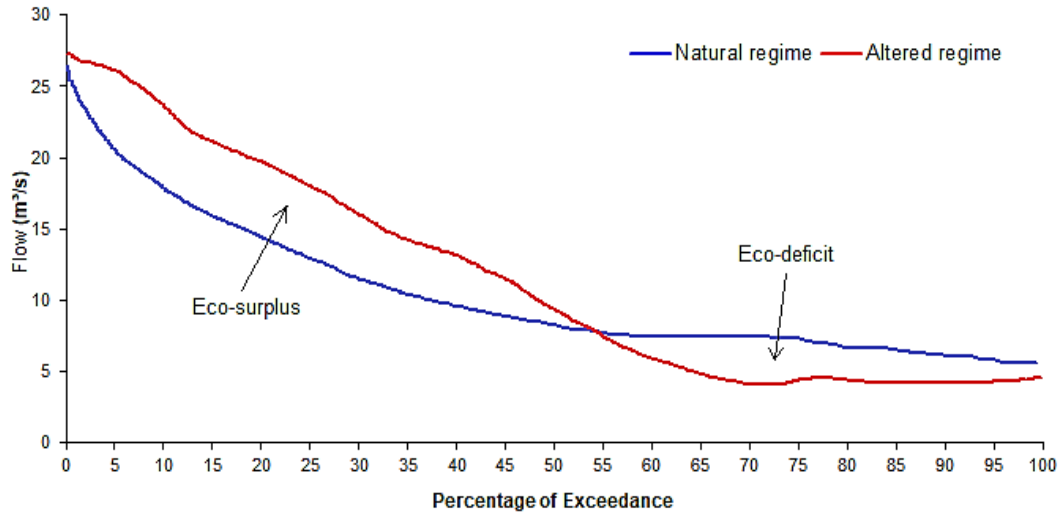
Figure 7. Definition of eco-surplus and eco-deficit in the flow duration curve (FDC)

Vogel et al. (2007) also introduced the range of variability method for assessing river flow regime changes via IHA measures. The 25th and 75th percentile ranges of these metrics being indicated as river management targets. According to some study, the terms eco-surplus and eco-deficit can be revised, and the 75th and 25th percentiles FDC should be utilized as the upper and lower bounds of the river ecosystem conservation target downstream, respectively (Gao B. et al., 2012). The area between the 25th percentile FDC and the annual or seasonal FDC was classified as eco-deficit if the annual or seasonal FDC of a given year was below the 25th percentile FDC. This value shows the level of water shortage compared to the river ecosystem's needs. If a given year's annual or seasonal FDC is higher than the 75th percentile FDC, the area between the 75th percentile FDC and the annual or seasonal FDC is referred as the eco-surplus.

IV – PUBLICATIONS

IV- **PUBLICATIONS**

This chapter presented the summary of the publications that make up this PhD Thesis. The thesis was organized into three sections, each of which included a research article published in an indexed scientific journal. The application of the SWAT model for evaluating water resources in the two studied basins was a common denominator in these three articles.

- **Publication 1:** Climate change and land-use/land-cover changes (LULC) caused by human activities are significant contributors to ecosystem degradation and the availability of a basin's water resources. It's critical to understand how these activities affect the quantity of water resources in basins such as the Segura River Basin. This article used the Soil and Water Assessment Tool (SWAT) to investigate the aforementioned implications in the Headwater Segura River Basin. SWAT was validated with a Nash-Sutcliffe efficiency (NSE) and a percent bias (PBIAS), showing that it accurately matched monthly streamflow. Land-use maps of 1956 and 2007 were used to create a set of scenarios that allowed us to evaluate the effects of these activities on both joint and individual water resources. Since the 1970s, a reforestation plan implemented in the basin increased the forest cover while reducing rainfed agriculture and shrubland areas. A drop of 26.3 percent in the quantity of produced water resources was resulted by climate change and the expansion of forest land.

- **Publication 2:** The second part of the research combined the Soil and Water Assessment Tool (SWAT) Model and the Chloride Mass Balance (CMB) Method to improve the modelling of streamflow in high–permeability bedrock basins receiving Interbasin Groundwater Flow (IGF). IGF refers to naturally occurring groundwater flow under a topographic divide, implying that the baseflow estimated by typical rainfall–runoff models may be significantly lower than the actual amount. Most hydrological models overlook the IGF with simple

simplifications because identifying and quantifying it is so challenging. The Castril River Basin (CRB) headwater was selected to demonstrate the issue and to suggest the CMB method suitability for determining the magnitude of the IGF contribution to baseflow. The CMB method demonstrates that IGF varies neither annually nor seasonally in this headwater basin with negligible groundwater exploitation, and constitutes around 51% of mean yearly baseflow. Simulated streamflow was modified based on this external IGF evaluation, resulting in a reduction in the percent bias (PBIAS) of the SWAT model from 52.29 to 22.40. During the calibration and validation phases of the SWAT model, corrected simulated streamflow was used. The total SWAT model performance was measured using the Nash–Sutcliffe Efficiency (NSE) Coefficient and its logarithmic values (lnNSE). This methodological framework provides a new formulation of system conceptualization and a repeatable method for dealing with similar basins, demonstrating that IGF has a major influence on the baseflow components.

- **Publication 3:** The hydrological situation is the basic attribute and important driving force of the river ecosystem, and changes in the morphology of rivers and riparian zones, flow patterns, water quality, flora and fauna, and riparian vegetation will affect the normal structure and function of the river ecosystem, and may even result in an irreversible ecological crisis. We offer a paradigm for assessing the effects of dam construction on flow regime and ecosystem in the final section of the study. The flow regime data with and without dam influence were compared in this study. In this work, IAHRIS (Indicators of Hydrologic Alteration in RIverS) was used, which is a free Spanish software based on the IHA approach for assessing hydrologic alteration in rivers. The findings revealed that alteration for usual values remained between excellent and good, whereas drought and flood values shifted from good to moderate. The river's flow regime was adjusted by the dam according to the current situation. The river's overall hydrological seasonality was preserved. Extreme flows were managed at different times, with high flows

being reduced during floods and low flows being increased during dry periods. Due to the dam's high flow control, there was primarily an eco-deficit between 4% and 26% of the Flow duration curve. In other intervals, the eco-surplus increased. The dam's regulation of high and low streamflows can be considered as the cause of variations in the river's biological influence. This research can help decision-makers identify methods to mitigate the negative effects of dam construction.

IV.1 PUBLICATION 1: ASSESSING IMPACTS OF CLIMATE VARIABILITY AND REFORESTATION ACTIVITIES ON WATER RESOURCES IN THE HEADWATERS OF THE SEGURA RIVER BASIN (SE SPAIN)

Senent-Aparicio, J.; Liu, S.; Pérez-Sánchez, J.; López-Ballesteros, A., Jimeno-Sáez, P. Assessing Impacts of Climate Variability and Reforestation Activities on Water Resources in the Headwaters of the Segura River Basin (SE Spain). *Sustainability*, **2018**, 10, 3277.

https://www.mdpi.com/2071-1050/10/9/3277

sustainability

MDPI

Article

Assessing Impacts of Climate Variability and Reforestation Activities on Water Resources in the Headwaters of the Segura River Basin (SE Spain)

Javier Senent-Aparicio *[ID], **Sitian Liu, Julio Pérez-Sánchez**[ID], **Adrián López-Ballesteros and Patricia Jimeno-Sáez**

Department of Civil Engineering, Catholic University of San Antonio, Campus de los Jerónimos s/n, 30107 Guadalupe, Murcia, Spain; sliu@alu.ucam.edu (S.L.); jperez058@ucam.edu (J.P.-S.); alopez976@alu.ucam.edu (A.L.-B.); pjimeno@ucam.edu (P.J.-S.)
* Correspondence: jsenent@ucam.edu; Tel.: +34-968-278-818

check for updates

Abstract: Climate change and the land-use and land-cover changes (LULC) resulting from anthropic activity are important factors in the degradation of an ecosystem and in the availability of a basin's water resources. To know how these activities affect the quantity of the water resources of basins, such as the Segura River Basin, is of vital importance. In this work, the Soil and Water Assessment Tool (SWAT) was used for the study of the abovementioned impacts. The model was validated by obtaining a Nash–Sutcliffe efficiency (NSE) of 0.88 and a percent bias (PBIAS) of 17.23%, indicating that SWAT accurately replicated monthly streamflow. Next, land-use maps for the years of 1956 and 2007 were used to establish a series of scenarios that allowed us to evaluate the effects of these activities on both joint and individual water resources. A reforestation plan applied in the basin during the 1970s caused that the forest area had almost doubled, whereas the agricultural areas and shrubland had been reduced by one-third. These modifications, together with the effect of climate change, have led to a decrease of 26.3% in the quantity of generated water resources, not only due to climate change but also due to the increase in forest area.

Keywords: SWAT; trend analysis; land-use change; climate variability; reforestation; Segura River Basin

1. Introduction

Water resources have suffered an important decrease in recent decades due to the effects of human activities and climate change [1]. This is especially the case in semi-arid regions, where water resources have become a critical element of socioeconomic development [2]. Many recent studies have studied the driving factors of the hydrological cycle, reaching the conclusion that climate and land-use/land-cover changes (LULC) are two critical factors that affect the hydrological processes in the basin [3]. On the one hand, climate change projections during this century in the Mediterranean region reveal a rise in temperature accompanied by a decrease in precipitation, resulting in a decrease of the water resources by over 20% [4]. In fact, recent studies in the headwaters of the Segura River Basin (HWSRB) [5] predicted a decrease of over 50% by the end of the century. Furthermore, human activities such as agricultural irrigation expansion or urbanization affect the availability of water resources through their influence on runoff. This is especially true in Mediterranean Europe, where human activities have modified the landscape [6–8]. Developing a better understanding of the influence of LULC on the hydrological processes of a watershed is essential for sustainable water resource management. This is particularly true in the Segura River Basin, which is located in a semi-arid region of southeast Spain, and where we can find the most water-stressed basin in Western Europe [9].

The HWSRB are relevant due to its 9% water resource contribution, in spite of the fact that it covers only 1.2% of the area over the total watershed [5].

The use of a physically based distributed hydrological model is a common approach to evaluating the impact of LULC changes on water resources [10]. From the hydrological models available, we chose the Soil and Water Assessment Tool (SWAT) model due to the fact that this model has been used worldwide to simulate the hydrological cycle and has been used extensively to evaluate the impacts of LULC changes on watershed hydrology [11]. Likewise, a multitude of studies have addressed separating the influences of human activities and climate variability on water resources using the SWAT model [3,11–13]. However, only two references have been found on the application of the SWAT model to assess the impacts of LULC changes in Spain. Molina-Navarro et al. [14] analyzed the potential effects of climate change and land-use management scenarios on water discharge and the water quality of the Pareja Reservoir located in the upper Tagus River Basin. Salmoral et al. [15] assessed the water-related impacts of land-use changes and agricultural practices, combining the use of the SWAT model and a water footprint assessment in the Genil River Basin (southern Spain).

Significant LULC have occurred in the southeastern part of Spain since the 1970s as a result of the progressive abandonment of dryland agricultural activities and the implementation of reforestation plans increasing forest cover [16]. The strategy for reforesting the HWSRB was to introduce pine species; *pinus nigra* was used in upper parts of the basin, whereas *pinus pinaster* and *pinus halepensis* were used in the intermediate and lower parts of the basin [17]. This increase of vegetation cover leads not only to a decrease in sediment yield [18] but also to a decrease in runoff generation. Several studies have analysed the potential water yield reduction due to forestation activities. Bosch and Hewlett [19] studied the effect of vegetation changes on the water yield on 94 different basins. They concluded that eucalypt and pine forest types cause a reduction of 40 mm in water yield per 10% change in cover, but in the case of shrubland, this reduction is four times lower (10 mm). Other authors added new basins in addition to those reviewed by Bosch and Hewlett; for example, Sahin and Hall [20] analysed 145 basins using a fuzzy linear regression analysis reaching similar conclusions, whereas Brown et al. [21] reviewed 166 basins focusing not only on water yield but also on low flows. Sun et al. [22] analysed the potential magnitude of annual water yield to forestation across China, suggesting that this reduction can vary from 30% in tropical regions to 50% in semiarid regions. Llorens et al. [23] studied a Mediterranean mountain basin showing a reduction in runoff up to 18% due to the reforestation activities using pine trees.

Due to the high water stress suffered in the Segura River Basin, the impact of forest restoration on water yield must be evaluated. Therefore, the objectives of this study were as follows: (1) to determine trends in the annual and monthly precipitation and temperature; (2) to calibrate and validate the SWAT model in a data-scarce river basin with a Mediterranean climate, such as the HWSRB; and (3) to analyze the impact of climate variability and reforestation activities on runoff and evapotranspiration (ET).

2. Materials and Methods

2.1. Study Area Description

The Segura River Basin represents one of the most arid zones of the Mediterranean area, presenting great heterogeneity in its flow regimes [24]. It is located in the southeastern part of Spain (Figure 1). The SWAT model was applied to the 235 km^2 of the HWSRB that flow into the Anchuricas Reservoir, which has a capacity of 6 hm^3 and exists to generate electricity. As the terrain is mountainous, it presents steep slopes with an elevation range from 898 to 1912 m. According to data from 1951 to 2015, the average annual precipitation is above 800 mm, ranging from 381 mm to 1447 mm. As a typical Mediterranean climate, precipitation is received mainly during spring and autumn while it is insignificant during summer. The average annual temperature was 11.8 °C.

The mean monthly flow of this river leaving the mountains varies between 0.74 m^3/s in August to 4.82 m^3/s in February. Land cover in the watershed is mostly a forest-dominated area and features

Mediterranean shrubland vegetation, which covers about 81% of the basin. The rest of the land is mainly used for range purposes. The main soil type is Rendzic Leptosol, which presents a variable depth but always less than 50 cm, abundant stoniness, high carbon levels and good drainage [5]. The study area is characterized by the fundamental role of the groundwater in the surface hydrology due to the fact that a significant part of the streamflow comes from groundwater sources. The large volume of precipitations and the abundance of outcropping carbonate rocks have caused the formation of karstic systems [25].
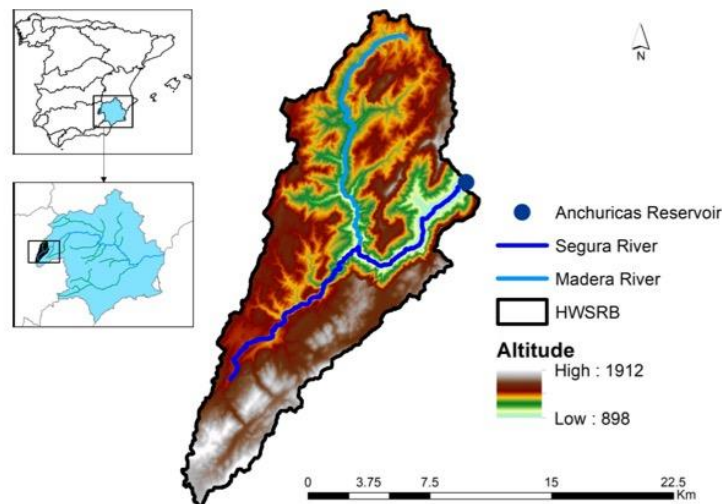
Figure 1. Location of the headwaters of the Segura River Basin (HWSRB) and its digital elevation model (DEM).

2.2. The Precipitation and Temperature Trend Analysis

In this study, Microsoft Excel template application MAKESENS (Version 1.0) was used to calculate the trends and changing rates of temperature and precipitation. This application includes the non-parametric Mann–Kendall (MK) test for the trend and Sen's non-parametric method for the magnitude of the trend. More details regarding the MAKESENS model can be found in Salmi et al. [26]. The MK test was used to detect the change in the annual and monthly temperature and precipitation. The advantage of the MK test, which is one of the most widely used nonparametric tests for detecting trends in hydroclimatic series [27], is that it does not require the data to be distributed normally and it has a low sensitivity to abrupt peaks due to inhomogeneous time series [28]. The complete description and formulae of the MK test can be obtained from Partal and Kahya [29]. The magnitudes of the estimated changes in the trend of temperature and precipitation were estimated by using a simple non-parametric procedure that Sen developed. The Sen [30] method alleviates the consequences of anomalous trends by using the median of the series of slopes as the judgmental foundation [13]. The Q_i is given by the following:

$$Q_i = median\left(\frac{x_j - x_k}{j - k}\right) \forall k \leq j \qquad (1)$$

where x_j and x_k are data values at times j and k, respectively. Estimator Q_i is the median over all combinations of record pairs for the entire dataset. A positive slope magnitude indicates an increasing tendency, whereas a negative slope magnitude indicates a decreasing tendency in the time series.

2.3. Description of SWAT Model

Hydrological modeling was performed using the SWAT extension for the QGIS interface, called QSWAT [31]. SWAT is a continuous-time, long-term, semi-distributed and physically based model. SWAT considers the heterogeneity of a watershed by dividing it into multiple sub-watersheds based on the river network and topography; subsequently, sub-watersheds are divided into hydrologic response units (HRUs) consisting of homogeneous land use, land management, and soil characteristics. These HRUs represent percentages of the sub-watershed area and are not identified spatially within a SWAT simulation [32]. SWAT was designed to predict the impact of land management practices on the hydrology of agricultural watersheds as well as on sediment and contaminant transport in these watersheds [33]. This model can simulate surface and subsurface flows, sediment generation and deposition, and nutrient fate and movement through rivers and landscapes. The hydrologic routines within SWAT account for unsaturated zone processes (i.e., infiltration, evaporation, plant uptake, lateral flow, and percolation), groundwater flows and snow accumulation and melt [34]. SWAT simulates the hydrologic cycle based on water balance, which is controlled by climate, moisture, and energy inputs, such as daily precipitation, the maximum/minimum air temperatures, solar radiation, the wind speed, and the relative humidity [35]. The water balance equation that governs the hydrological components of the SWAT model [36] is as follows:

$$SW_t = SW_0 + \sum_{i=1}^{t} \left(R_{day} - Q_{surf} - ET_i - W_{seep} - Q_{gw} \right)_i \tag{2}$$

where SW_t is the final water–soil content (mm), SW_0 is the initial water–soil content (mm), t is the time in days, R_{day} is the amount of precipitation on day i (mm), and Q_{surf} is the amount of surface runoff on day i (mm); ET_i is the actual evapotranspiration on day i (mm); W_{seep} is the percolation on day i; and Q_{gw} is the amount of baseflow on day i (mm).

The SWAT model offers three options to calculate potential evapotranspiration: Priestley–Taylor, Hargreaves, and Penman–Monteith. In this study, potential evapotranspiration was simulated using the Hargreaves method due to the fact that it requires only maximum and minimum temperatures. Actual evapotranspiration is calculated as the sum of actual plant transpiration, actual soil evaporation, and interception. Firstly, SWAT evaporates any precipitation intercepted by the plant canopy and then calculates the transpiration, sublimation, and soil evaporation using an approach similar to that of Ritchie [37].

2.3.1. Input Data for Hydrological Modelling

To study the effect of climate variability and reforestation activities, land-use data in 1956 and 2007 at a scale of 1:25,000 were provided by the Andalusian Network of Environmental Information (REDIAM) belonging to the Regional Government of Andalusia [38]. In addition to land cover, a 25 m resolution digital elevation model from the National Geographic Institute [39] was used. The soil data were obtained from the Harmonized World Soil Map [40] with a spatial resolution of about 1 km. The SWAT model was driven by meteorological data, including precipitation and temperature data, from various sources. The precipitation was obtained from the Spanish National Meteorological Agency (AEMET) grid, version 1.0, which provides daily rainfall in Spain for the period of 1951 to 2016 with a spatial resolution of 5 km. More information about this dataset can be found in Peral-García et al. [41]. Temperature data were collected from the fifth version of the high-resolution (approximately 10 km) gridded dataset called SPAIN02, where data are available from 1951 to 2016. Detailed documentation of the development and analysis of the SPAIN02 dataset can be found in Herrera et al. [42]. The discharge data at the catchment outlet were available on the Hydrographical Study Centre website [43].

2.3.2. Model Setup

The subdivision into hydrologic response units (HRUs, unique computational units of land coverage and soil types with homogeneous hydrologic responses) was performed with the land use, soil, and slope maps. Threshold levels of 10% were established to eliminate minor land uses, soils and slopes in each sub-basin and to facilitate model processing, and the SWAT interface identified 44 HRUs. These threshold values are used by the interface to eliminate minor land uses, soil types or slopes in each sub-basin.

To assess the impacts of reforestation activities, the parameters we calibrated were based on land-use data in 1956 that belonged to the natural period of 1951–1970. Discharge data from 1 January 1964 to 31 December 1970 and from 1 January 1954 to 31 December 1963 were selected to run the model validation and calibration respectively. Three first years (1951–1953) were used to allow the model parameters to reach equilibrium as a warm-up period. The sensitivity analysis and automatic calibration was done in this study using the sequential uncertainty fitting program (SUFI-2) in the SWAT Calibration and Uncertainty Programs [44]. First, a global sensitivity analysis was performed to identify the most influential parameters in governing the streamflow. A ranking of parameter sensitivities was obtained after 500 model runs to see the impact of each parameter on the objective function [45]. The automatic calibration procedure was used to determine the best parameter values based on the observed discharge, and using the Nash–Sutcliffe coefficient (NSE) as the objective function. A total of 1000 simulations were run in two steps of 500 simulations, with the parameters adjusted after the first 500 simulations.

2.3.3. Performance Evaluation Criteria

Model performance was assessed quantitatively using the NSE, the root mean square error (RMSE), the observations standard deviation ratio (RSR), and the percent bias (PBIAS), and qualitatively using graphical time series plots.

The RSR standardizes the RMSE using the RSR (STDEV$_{obs}$). The RSR is calculated as follows:

$$\text{RSR} = \frac{\text{RMSE}}{\text{STDEV}_{obs}} = \frac{\sqrt{\sum_{i=1}^{n}\left(Q_{\text{obs } i} - Q_{\text{sim } i}\right)^2}}{\sqrt{\sum_{i=1}^{n}\left(Q_{\text{obs } i} - \overline{Q}\right)^2}} \tag{3}$$

where n is the total number of observations, $Q_{\text{obs } i}$ and $Q_{\text{sim } i}$ are the observed and simulated discharges at ith observation, respectively, and $\overline{Q}$ is the mean of the observed data over the simulation period. The RSR varies from the optimal value of 0 to a large positive value. The lower the RSR, the lower the RMSE, and the better the model simulation performance.

The NSE [46] is a normalized statistic that determines the relative magnitude of the residual variance compared with the measured data variance. The NSE is dimensionless, and its values range from negative infinity to 1, with an optimal value of 1 [47]. It indicates a 1:1 line fit between observed and simulated data and is computed as follows:

$$\text{NSE} = 1 - \frac{\sum_{i=1}^{n}\left(Q_{\text{obs } i} - Q_{\text{sim } i}\right)^2}{\sum_{i=1}^{n}\left(Q_{\text{obs } i} - \overline{Q}\right)^2} \tag{4}$$

The PBIAS [48] measures the average tendency of the simulated data to be larger or smaller than their observed counterparts [47] and is calculated as:

$$\text{PBIAS} = \frac{\sum_{i=1}^{n}\left(Q_{\text{obs } i} - Q_{\text{sim } i}\right)\cdot 100}{\sum_{i=1}^{n}\left(Q_{\text{obs } i}\right)} \tag{5}$$

where the PBIAS is the deviation of data being evaluated, expressed as a percentage. The optimal value of the PBIAS is 0.0, with low-magnitude values indicating an accurate model simulation. Positive values indicate model underestimation bias, and negative values indicate model overestimation bias.

For model evaluation, we used the criteria that Moriasi et al. [49] proposed about the performance rating for the described statistics for a monthly time step. According to these criteria, the calibration/validation performance can be considered satisfactory when the NSE is greater than 0.5, the RSR is less than 0.5, and the PBIAS range is ±25%.

2.4. Framework for Separating Effects of Climate Change and LULC

As can be seen in Figure 2, to study climatic and land uses' impacts on water resources in the HWSRB, three simulation experiments were set up as follows: scenario A used land use and climate conditions around the 1950s and 1960s (land use in 1956 and weather/climate for 1951–1970); scenario B fixed land use in 1956 and actual weather conditions for 1996–2015; and scenario C used land use in 2007 and actual climate conditions for 1996–2015. Based on these scenarios, we analyzed the impacts on water resources due to climate variability (the differences between B and A), reforestation (the difference between C and B), and all factors (the difference between C and A) respectively. This approach of "one factor at a time" has been successfully applied in many studies to evaluate the effects of land-use change and climate variability on hydrology [11,12,50].
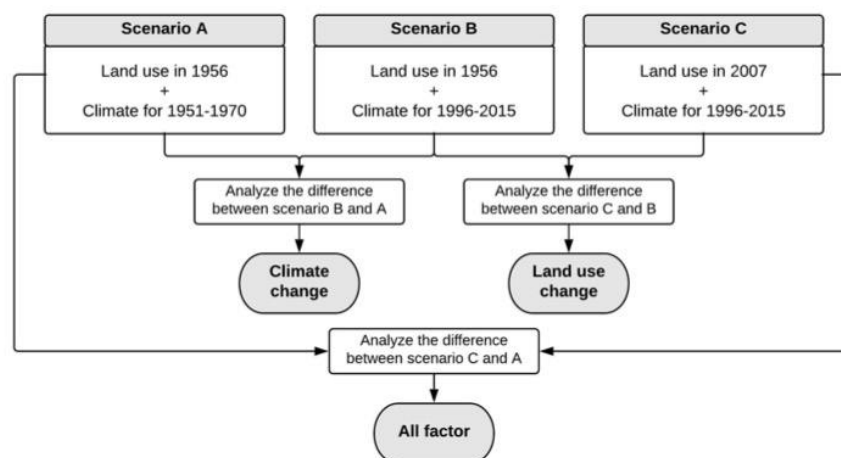
Figure 2. Scenarios setup and research framework.

3. Results

3.1. Climate Variability in the HWSRB

Climate trend analysis requires a minimum of 15–30 years for accurate results [51]. In this study, the annual and monthly precipitation, temperature, and streamflow trended for the period 1951–2015 were analyzed using the MK test. The values of the MK test statistic (Test Z) and Sen's slope for various months are provided in Table 1. In terms of precipitation, it can be seen that the greatest slope was in the months of December, March, and June. According to Paredes et al. [52], the strong decrease of rainfall in March is mostly associated with a positive trend of the North Atlantic oscillation (NAO) index. It is observed that eight of the 12 months revealed a decreasing trend. On a seasonal timescale, the most important decreases take place in the summer and winter. Del Río et al. [53] previously suggested these trends. The annual precipitation decreased across the study area with a

slope of 2.22 mm/year. Streamflow and precipitation show a similar decreasing trend in the study area. Influenced by the interaction between reforestation and climate variability factors, a large decrease in streamflow is occurring between October and April.

Table 1. Trend analysis results.

Month	Precipitation			Maximum Temperature			Minimum Temperature			Streamflow		
	Test Z	Sig.	Q_i	Test Z	Sig.	Q_i	Test Z	Sig.	Q_i	Test Z	Sig.	Q_i
January	−0.42		−0.19	−0.53		−0.01	−1.74	a	−0.02	−0.98		−0.03
February	0.06		0.03	−0.42		−0.01	−1.78	a	−0.02	−1.12		−0.03
March	−1.46		−0.51	1.00		0.02	−2.78	c	−0.02	−1.32		−0.05
April	−0.70		−0.17	1.22		0.02	−1.14		−0.01	−1.14		−0.03
May	0.59		0.17	1.27		0.02	−0.12		0.00	0.30		0.00
June	−2.26	b	−0.33	3.95	d	0.06	1.55		0.01	1.13		0.01
July	−1.48		−0.04	3.43	d	0.04	−0.43		−0.01	1.61		0.01
August	0.03		0.00	3.39	d	0.04	1.03		0.01	1.83	d	0.01
September	0.43		0.07	−0.29		0.00	−0.35		0.00	0.23		0.00
October	−0.41		−0.12	0.43		0.01	−0.39		0.00	−0.79		−0.01
November	−0.50		−0.17	−1.39		−0.02	−1.52		−0.02	−1.15		−0.02
December	−1.54		−0.67	−0.59		−0.01	−1.47		−0.02	−1.93	d	−0.05
Annual	−1.59		−2.22	2.16	b	0.02	−1.35		−0.01	−0.67		−0.12

Test Z is the Mann–Kendall (MK) test statistic; Q_i is the Sen's slope estimator; [a] indicates a significance level of 0.1; [b] indicates a significance level of 0.05; [c] indicates a significance level of 0.01; [d] indicates a significance level of 0.001.

Annual maximum air temperature indicated a significant upward trend at the 5% significant level. In addition, the highest magnitude of the trend was found in June. This result is in accordance with those that Del Río et al. [54] proposed. With the exception of winter months, the maximum air temperature showed a rising trend during the remaining months. The decreasing magnitude of the minimum air temperature was smaller compared with the increasing magnitude of the maximum air temperature. Compared with their monthly changes, the decreasing magnitudes in the cold months were larger than they were in warm months. The decrease of the minimum air temperature was especially significant in March (0.01 level of significance).

In summary, compared with the baseline period of time (1951–1970), the mean annual rainfall in the recent period (1996–2015) decreased by 81 mm, whereas the mean annual temperature in the HWSRB increased by 0.13 °C, indicating that the climate was getting warmer and drier. Both climate change and intensive human activities have contributed to a reduction of the mean annual streamflow in the recent period of about 16%.

3.2. Land-Use Change in the HWSRB

Table 2 shows the land uses in the HWSRB in 1956 and 2007. Two main trends of LULC existed from 1956 to 2007: the decrease of shrubland and agricultural land and the increase of forests. Compared with 1956, agricultural land, shrubland, and woodland-shrub transitions decreased in areal extent by respective amounts of 11.56, 14.79, and 15.60 km². In contrast, during the period of 1956−2007, the forest area showed an increase of 34.26 km². Urban areas, water bodies, grassland, and barren land changed little compared with their baselines of 1956.

Table 2. The conversion percentage (%) of each land-use type from 1956 to 2007.

Land Cover Type	Area Coverage (km²)		Area Coverage (%)		1956–2007	
	1956	2007	1956	2007	Change (km²)	Change (%)
Urban Areas	0.16	0.21	0.07	0.09	0.05	+0.02
Water Bodies	0.00	0.44	0.00	0.19	0.44	+0.19
Agricultural Land	17.04	5.48	7.23	2.32	−11.56	−4.91
Grassland	30.96	36.52	13.13	15.49	+5.56	+2.36
Forests	54.91	89.17	23.29	37.82	+34.26	+14.53
Shrubland	82.16	67.37	34.85	28.57	−14.79	−6.28
Transitional Woodland/Shrub	50.06	34.46	21.23	14.62	−15.6	−6.61
Barren Land	0.49	2.13	0.21	0.90	1.64	0.69

3.3. Validation of the SWAT model

The global sensitivity analysis found that the most influential parameters were the effective hydraulic conductivity in tributary channel alluvium (CH_K1), the U.S. Soil Conservation Service curve number (CN2), the moist bulk density (SOL_BD), the saturated hydraulic conductivity (SOL_K), the groundwater delay (GW_DELAY), the maximum canopy storage (CANMX), the lateral flow travel time (LAT_TTIME), and the available water capacity of the soil layer (SOL_AWC). Similar parameters were chosen for calibration in basins with similar characteristics [55]. Even the sensitivity analysis did not give the soil evaporation compensation factor (ESCO) as one of the most sensitive parameters, but it was considered to be a significant parameter because it is highlighted in the literature and in previous work made for this basin [5,56]. Sensitivity analysis was followed by automatic calibration. The optimal values and range of parameters are presented in Table 3.

Table 3. Calibration parameters.

Parameter	Description	Value Range	Adjusted Value
CH_K1	Effective hydraulic conductivity in tributary channel alluvium	0–300	17.94
LAT_TTIME	Lateral flow travel time	0–180	109.95
CN2	SCS runoff curve number	−20%–+20%	+8.75%
SOL_K	Saturated hydraulic conductivity	0–2000	0.054
GW_DELAY	Groundwater delay (days)	0–500	242.46
CANMX	Maximum canopy storage	0–100	8.65
SOL_AWC	Available water capacity of the soil layer	0–1	0.0567
SOL_BD	Moist bulk density	0.9–2.5	2.40
ESCO	Soil evaporation compensation factor	0–1	0.5725

According to Table 4, the SWAT model performed well in both the calibration and the validation period, accurately simulating the discharge after the sensitive parameters were optimized. The R, NSE, PBIAS, and RSR of the calibration period (1954–1963) for monthly runoff were 0.87, 0.86, −14.11%, and 0.38 respectively. Overall, the model had good performance not only during the calibration period but also during the validation period. This is not usual because parameters are optimized during calibration, and better performance is expected during this period [57,58]. The results suggest that the SWAT model performed well and can be used for further analysis in the HWSRB.

Table 4. Performance of Soil and Water Assessment Tool (SWAT) model during calibration and validation periods in the HWSRB.

Period	R	NSE	PBIAS	RSR
Calibration (1954–1963)	0.87	0.86	−14.11	0.38
Validation (1964–1970)	0.93	0.88	−17.23	0.35

NSE: Nash-Sutcliffe coefficient; PBIAS: percent bias; RSR: RMSE-observations standard deviation ratio.

To illustrate the model calibration and validation, observed and simulated monthly discharge data in the Anchuricas Reservoir for the calibration (1954–1963) and validation (1964–1970) periods are plotted in Figure 3.

As can be seen in Figure 4, we have also validated the model by comparing the simulated results using the 2007 land-use map (scenario C) with observed streamflows during the period 1996–2015. The values of model evaluation statistics such as NSE, R, PBIAS, and RSR were 0.72, 0.85, 21.93, and 0.53, respectively. These values indicate that the calibrated model satisfactorily simulates the monthly runoff.
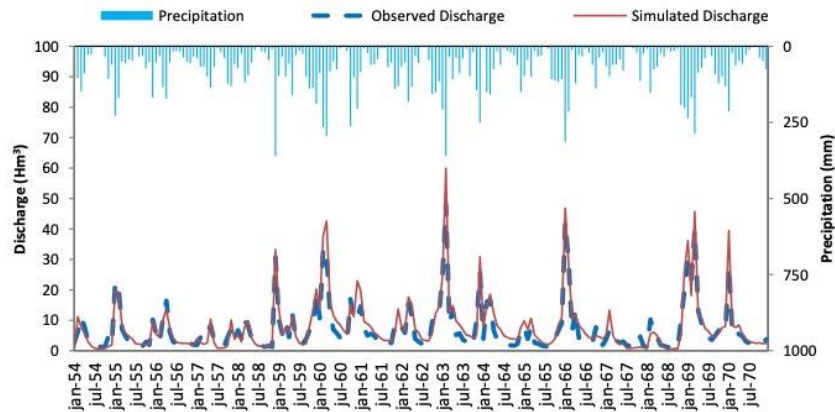
Figure 3. Calibration (1954–1963) and validation (1964–1970) results of SWAT model in Anchuricas Reservoir.
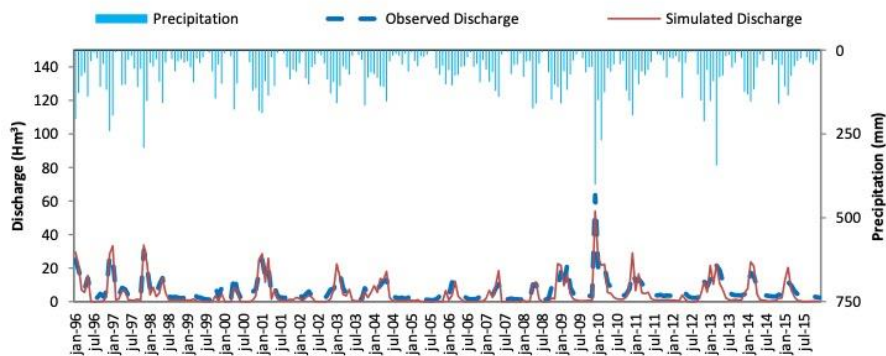
Figure 4. Observed and simulated monthly discharge data for the period 1996—2015 (scenario C) in Anchuricas Reservoir.

3.4. Impacts of Land-Use Change and Climate Variability on Runoff and ET at HWSRB

Table 5 shows the annual mean runoff and ET simulated by SWAT under the three different scenarios analyzed in this study. Following the recommendation of Li et al. [59], the simulated data rather than observed data were used to compare the hydrological effects under the three hypothetical scenarios presented in Section 2.4. Compared with the baseline scenario (Scenario A), simulated runoff in Scenario C decreased by 95.8 mm. This reduction is due to the combined effects of climate variability and the reforestation plan. The contrast between Scenarios A and B showed the influence of the climate variability. Surface runoff decreased significantly by 61.7 mm due to climate variation, which accounted for 64.4% of the total runoff reduction. The results revealed that the reforestation plan and climate variability both decreased the runoff. It should be noted that the contribution of climate variability (61.7 mm) is almost two times greater than that of the reforestation plan (34.1 mm). In terms of ET, the combined effect of land-use change and climate variation increased ET by 31.8 mm. The climate variation caused a decrease of 13.2 mm in the ET mainly due to the significant decrease in the precipitation shown in the trend analysis, and in spite of the slight temperature increase. It should also be noted that the reforestation plan contributed to an increase in the ET values by about 45 mm,

exceeding by far the impact of climate variability on ET. These results are consistent with those of previous studies [22,23].

Table 5. Simulated average annual runoff and ET under various scenarios (mm).

Scenarios	Climate	LUCC	P	Runoff	ET	Runoff Change	ET Change
A	1951–1970	1956	895.4	363.7	493.1		
B	1996–2015	1956	814.1	302.0	479.9	−61.7	−13.2
C	1996–2015	2007	814.1	267.9	524.9	−95.8	+31.8

LUCC: land-use land-cover changes; ET: evapotranspiration.

4. Conclusions

Considering the HWSRB, as a case study, the aim of this study was to distinguish the influences of human activities and climate variability on water resources by using the SWAT model. From the results of this study, the following conclusions can be stated:

1.   The SWAT model was able to reproduce the hydrological conditions of the HWSRB. The statistical results of calibration were NSE = 0.86, RSR = 0.38, and PBIAS = −14.11. The validation results were NSE = 088, RSR = 0.35, and PBIAS = −17.23. These results are indicative of the SWAT model's good performance.
2.   The main trend in land cover change was the conversion of agricultural areas and shrubland to forest, both of which are a result of the reforestation plan carried out during the 1970s.
3.   In general, climate change and reforestation activities tend to decrease the streamflow of the HWSRB. The contributions of climate change (64.4%) were larger than that of the reforestation plan (35.6%).
4.   The results also revealed that the reforestation plan had a higher impact than climate variability did on ET in the HWSRB.
5.   Although reforestation plans can result in decreased soil erosion rates, runoff is also reduced. The results obtained from this study may have strong implications for a basin that is already suffering from high water stress. The impacts of the reforestation plan should be incorporated into water resource management plans to develop sustainable strategies.
6.   Future reforestation plans in this area should strengthen the native shrub type of vegetation instead of increasing the forested area in order to preserve the water yield.

References

1.   Li, Y.Y.; Chang, J.X.; Wang, Y.M.; Jin, W.T.; Guo, A.J. Spatiotemporal impacts of climate, land cover change and direct human activities on runoff variations in the Wei River Basin, China. *Water* **2016**, *8*, 220. [CrossRef]
2.   Li, Z.; Deng, X.; Wu, F.; Hasan, S.S. Scenario analysis for water resources in response to land use change in the middle and upper reaches of the Heihe River Basin. *Sustainability* **2015**, *7*, 3086–3108. [CrossRef]
3.   Yang, L.; Feng, Q.; Yin, Z.; Wen, X.; Si, J.; Li, C.; Deo, R.C. Identifying separate impacts of climate and land use/cover change on hydrological processes in Upper Stream of Heihe River, northwest China. *Hydrol. Process.* **2017**, *31*, 1100–1112. [CrossRef]
4.   Giorgi, F.; Lionello, P. Climate change projections for the Mediterranean region. *Glob. Planet. Chang.* **2008**, *63*, 90–104. [CrossRef]

5. Senent-Aparicio, J.; Pérez-Sánchez, J.; Carrillo-García, J.; Soto, J. Using SWAT and Fuzzy TOPSIS to assess the impact of climate change in the headwaters of the Segura River Basin (SE Spain). *Water* **2017**, *9*, 149. [CrossRef]

6. Serra, P.; Pons, X.; Sauri, D. Land-cover and land-use change in a Mediterranean landscape: A spatial analysis of driving forces integrating biophysical and human factors. *Appl. Geogr.* **2008**, *28*, 189–209. [CrossRef]

7. Morán-Tejeda, E.; Ceballos-Barbancho, A.; Llorente-Pinto, J.; López-Moreno, J.I. Land-cover changes and recent hydrological evolution in the Duero Basin (Spain). *Reg. Environ. Chang.* **2012**, *12*, 17–33. [CrossRef]

8. García, C.; Amengual, A.; Homar, V.; Zamora, A. Losing water in temporary streams on a Mediterranean island: Effects of climate and land-cover changes. *Glob. Planet. Chang.* **2017**, *148*, 139–152. [CrossRef]

9. Senent-Aparicio, J.; Pérez-Sánchez, J.; Bielsa-Artero, A.M. Assessment of Sustainability in Semiarid Mediterranean Basins: Case Study of the Segura Basin, Spain. *Water Technol. Sci.* **2016**, *7*, 67–84.

10. Woldesenbet, T.A.; Elagib, N.A.; Ribbe, L.; Heinrich, J. Hydrological responses to land use/cover changes in the source region of the Upper Blue Nile Basin, Ethiopia. *Sci. Total Environ.* **2017**, *575*, 724–741. [CrossRef] [PubMed]

11. Zhang, L.; Karthikeyan, R.; Bai, Z.K.; Srinivasan, R. Analysis of streamflow responses to climate variability and land use change in the Loess Plateau region of China. *Catena* **2017**, *154*, 1–11. [CrossRef]

12. Zhao, A.Z.; Zhu, X.F.; Liu, X.F.; Pan, Y.Z.; Zuo, D.P. Impacts of land use change and climate variability on green and blue water resources in the Weihe River Basin of northwest China. *Catena* **2016**, *137*, 318–327. [CrossRef]

13. Yin, Z.; Feng, Q.; Yang, L.; Wen, X.; Si, J.; Zou, S. Long Term Quantification of Climate and Land Cover Change Impacts on Streamflow in an Alpine River Catchment, Northwestern China. *Sustainability* **2017**, *9*, 1278. [CrossRef]

14. Molina-Navarro, E.; Trolle, D.; Martínez-Pérez, S.; Sastre-Merlín, A.; Jeppesen, E. Hydrological and water quality impact assessment of a Mediterranean limno-reservoir under climate change and land use management scenarios. *J. Hydrol.* **2014**, *509*, 354–366. [CrossRef]

15. Salmoral, G.; Willaarts, B.A.; Garrido, A.; Guse, B. Fostering integrated land and water management approaches: Evaluating the water footprint of a Mediterranean basin under different agricultural land use scenarios. *Land Use Policy* **2017**, *61*, 24–39. [CrossRef]

16. Boix-Fayos, C.; de Vente, J.; Martinez-Mena, M.; Barbera, G.G.; Castillo, V. The impact of land use change and check-dams on catchment sediment yield. *Hydrol. Process.* **2008**, *22*, 4922–4935. [CrossRef]

17. Araque Jiménez, E. Forest landscapes in the Prebetic Arc. The Segura and Cazorla Mountains. *Rev. Estud. Reg.* **2013**, *96*, 321–344. (In Spanish)

18. Quiñonero-Rubio, J.M.; Nadeu, E.; Boix-Fayos, C.; de Vente, J. Evaluation of the effectiveness of forest restoration and check-dams to reduce catchment sediment yield. *Land Degrad. Dev.* **2016**, *27*, 1018–1031. [CrossRef]

19. Bosch, J.M.; Hewlett, J.D. A review of catchment experiments to determine the effects of vegetation changes on water yield and evapotranspiration. *J. Hydrol.* **1982**, *55*, 3–23. [CrossRef]

20. Sahin, V.; Hall, M.J. The Effects of Afforestation and Deforestation on Water Yields. *J. Hydrol.* **1996**, *178*, 293–309. [CrossRef]

21. Brown, A.E.; Zhang, L.; McMahon, T.A.; Western, A.W.; Verstessy, R.A. A review of paired catchment studies for determining changes in water yield resulting from alteration in vegetation. *J. Hydrol.* **2005**, *310*, 28–61. [CrossRef]

22. Sun, G.; Zhou, G.; Zhang, Z.; Wei, X.; McNulty, S.G.; Vose, J.M. Potential water yield reduction due to forestation across China. *J. Hydrol.* **2006**, *328*, 548–558. [CrossRef]

23. Llorens, P.; Latron, J.; Oliveras, I. Modelización del efecto del Cambio Global en la hidrología superficial. Ejemplo de aplicación a una cuenca Mediterránea de montaña. In Proceedings of the 3rd Asamblea Hispano-Portuguesa de Geodesia y Geofísica, Valencia, Spain, 4–7 February 2002; García, F., Berné, J.L., Eds.; Universidad Politécnica de Valencia: Valencia, Spain, 2003; Volume 3, pp. 1679–1681. (In Spanish)

24. Belmar, O.; Velasco, J.; Martinez-Capel, F. Hydrological classification of natural flow regimes to support environmental flow assessments in intensively regulated Mediterranean rivers, Segura River Basin (Spain). *Environ. Manag.* **2011**, *47*, 992. [CrossRef] [PubMed]

25. Moral, F.; Cruz-Sanjulian, J.J.; Olias, M. Geochemical evolution of groundwater in the carbonate aquifers of Sierra de Segura (Betic Cordillera, Southern Spain). *J. Hydrol.* **2008**, *360*, 281–296. [CrossRef]

26. Salmi, T.; Maatta, A.; Anttila, P.; Airola, T.R.; Amnell, T. *Detecting Trends of Annual Values of Atmospheric Pollutants by the Mann–Kendal Test and Sen's Slope Estimates—The Excel Template Application MAKESENS*; User Manual; Air Quality, Finish Meteorological Institute: Helsinki, Finland, 2002; p. 35.

27. Tesemma, Z.K.; Mohamed, Y.A.; Steenhuis, T.S. Trends in rainfall and runoff in the Blue Nile Basin: 1964–2003. *Hydrol. Process.* **2010**, *24*, 3747–3758. [CrossRef]

28. Jaagus, J. Climatic changes in Estonia during the second half of the 20th century in relationship with changes in large-scale atmospheric circulation. *Theor. Appl. Climatol.* **2006**, *83*, 77–88. [CrossRef]

29. Partal, T.; Kahya, E. Trend analysis in Turkish precipitation data. *Hydrol. Process.* **2006**, *20*, 2011–2026. [CrossRef]

30. Sen, P.K. Estimates of the regression coefficient based on Kendall's tau. *J. Am. Stat. Assoc.* **1968**, *63*, 1379–1389. [CrossRef]

31. Dile, Y.; Daggupati, P.; George, C.; Srinivasan, R.; Arnold, J. Introducing a new open source GIS user interface for the SWAT model. *Environ. Model. Softw.* **2016**, *85*, 129–138. [CrossRef]

32. Narsimlu, B.; Gosain, A.K.; Chahar, B.R. Assessment of future climate change impacts on water resources of upper Sind River basin, India using SWAT model. *Water Resour. Manag.* **2013**, *27*, 3647–3662. [CrossRef]

33. Arnold, J.G.; Srinivasan, R.; Muttiah, R.S.; Williams, J.R. Large area hydrologic modeling and assessment Part I: Model development. *J. Am. Water Resour. Assoc.* **1998**, *34*, 73–89. [CrossRef]

34. Zhang, X.; Srinivasan, R.; Hao, E. Predicting hydrologic response to climate change in the Luohe River basin using the SWAT model. *Trans. ASABE* **2007**, *50*, 901–910. [CrossRef]

35. Abbaspour, K.C.; Rouholahnejad, E.; Vaghefi, S.; Srinivasan, R.; Yang, H.; Klove, B. A continental-scale hydrology and water quality model for Europe: Calibration and uncertainty of a high-resolution large-scale SWAT model. *J. Hydrol.* **2015**, *524*, 733–752. [CrossRef]

36. Neitsch, S.; Arnold, J.; Kiniry, J.; Williams, J.; King, K. *Soil and Water Assessment Tool*, Theoretical Documentation, version 2009; Texas Water Resources Institute: College Station, TX, USA, 2005.

37. Ritchie, J.T. Model for predicting evaporation from a row crop with incomplete cover. *Water Resour. Res.* **1972**, *8*, 1204–1213. [CrossRef]

38. Andalusian Network of Environmental Information (REDIAM). Comparador WMS Ortofotos; Cartografía de Inundaciones en Febrero-Marzo 2010 en las Cuencas de los ríos Guadalquivir y Guadalete; Mapa de usos y Coberturas Vegetales Multitemporal. Available online: http://www.juntadeandalucia.es/medioambiente/site/rediam (accessed on 11 January 2018). (In Spanish)

39. Spanish National Geographic Institute (IGN). Plan Nacional de Ortofotografía Aérea. Available online: http://pnoa.ign.es/ (accessed on 3 January 2018). (In Spanish)

40. Nachtergaele, F.O.; Van Velthuizen, H.; Verelst, L.; Wiberg, D. *Harmonized World Soil Database*, version 1.2; IIASA: Laxenburg, Austria, 2012.

41. Peral García, C.; Navascués Fernández-Victorio, B.; Ramos Calzado, P. *Serie de Precipitación Diaria en Rejilla Con Fines Climáticos. Nota Técnica 24 de AEMET*; Spanish Meteorological Agency (AEMET): Madrid, Spain, 2017. (In Spanish)

42. Herrera, S.; Fernández, J.; Gutiérrez, J.M. Update of the Spain02 gridded observational dataset for EURO-CORDEX evaluation: Assessing the effect of the interpolation methodology. *Int. J. Climatol.* **2016**, *36*, 900–908. [CrossRef]

43. MAGRAMA (Ministerio de Agricultura y Pesca, Alimentación y Medio Ambiente). Sistema de Información del Anuario de Aforo. Available online: http://sig.magrama.es/aforos (accessed on 1 February 2018). (In Spanish)

44. Abbaspour, K.C. *SWAT Calibration and Uncertainty Program—A User Manual*; SWAT-CUP-2012; Swiss Federal Institute of Aquatic Science and Technology: Dubendorf, Switzerland, 2012.

45. Abbaspour, K.; Vaghefi, S.; Srinivasan, R. A guideline for successful calibration and uncertainty analysis for soil and water assessment: A review of papers from the 2016 International SWAT Conference. *Water* **2018**, *10*, 6. [CrossRef]

46. Nash, J.E.; Sutcliffe, J.V. River flow forecasting through conceptual models. Part I: A discussion of principles. *J. Hydrol.* **1970**, *10*, 282–290. [CrossRef]

47. Gupta, H.V.; Sorooshian, S.; Yapo, P.O. Status of automatic calibration for hydrologic models: Comparison with multilevel expert calibration. *J. Hydrol. Eng.* **1999**, *4*, 135–143. [CrossRef]

48. Legates, D.R.; McCabe Jr, G.J. Evaluating the use of "goodness-of-fit" measures in hydrological and hydroclimatic model validation. *Water Resour. Res.* **1999**, *35*, 233–241. [CrossRef]

49. Moriasi, D.N.; Arnold, J.G.; Van Liew, M.W.; Bingner, R.L.; Harmel, R.D.; Veith, T.L. Model evaluation guidelines for systematic quantification of accuracy in watershed simulations. *Trans. ASABE* **2007**, *50*, 885–900. [CrossRef]

50. Zang, C.; Liu, J.; Gerten, D.; Jiang, L. Influence of human activities and climate variability on green and blue water provision in the Heihe River Basin, NW China. *J. Water Clim. Chang.* **2015**, *6*, 800–815. [CrossRef]

51. Anil, A.P.; Ramesh, H. Analysis of climate trend and effect of land use land cover change on Harangi streamflow, South India: A case study. *Sustain. Water Resour. Manag.* **2017**, *3*, 257–267. [CrossRef]

52. Paredes, D.; Trigo, R.M.; Garcia-Herrera, R.; Trigo, I.F. Understanding precipitation changes in Iberia in early spring: Weather typing and storm-tracking approaches. *J. Hydrometeorol.* **2006**, *7*, 101–113. [CrossRef]

53. Río, S.D.; Herrero, L.; Fraile, R.; Penas, A. Spatial distribution of recent rainfall trends in Spain (1961–2006). *Int. J. Climatol.* **2011**, *31*, 656–667. [CrossRef]

54. Rio, S.D.; Herrero, L.; Pinto-Gomes, C.; Penas, A. Spatial analysis of mean temperature trends in Spain over the period 1961–2006. *Glob. Planet. Chang.* **2011**, *78*, 65–75.

55. Jimeno-Sáez, P.; Senent-Aparicio, J.; Pérez-Sánchez, J.; Pulido-Velazquez, D. A Comparison of SWAT and ANN models for daily runoff simulation in different climatic zones of peninsular Spain. *Water* **2018**, *10*, 192. [CrossRef]

56. De Almeida Bressiani, D.; Srinivasan, R.; Jones, C.A.; Mendiondo, E.M. Effects of spatial and temporal weather data resolutions on streamflow modeling of a semi-arid basin, northeast Brazil. *Int. J. Agric. Biol. Eng.* **2015**, *8*, 125–139.

57. Gassman, P.W.; Reyes, M.R.; Green, C.H.; Arnold, J.G. The soil and water assessment tool: Historical development, applications, and future directions. *Trans. ASABE* **2007**, *50*, 1211–1250. [CrossRef]

58. Molina-Navarro, E.; Martínez-Pérez, S.; Sastre-Merlín, A.; Bienes-Allas, R. Hydrologic modeling in a small mediterranean basin as a tool to assess the feasibility of a limno-reservoir. *J. Environ. Qual.* **2014**, *43*, 121–131. [CrossRef] [PubMed]

59. Li, Z.; Liu, W.; Zhang, X.; Zheng, F. Impacts of land use change and climate variability on hydrology in an agricultural catchment on the Loess Plateau of China. *J. Hydrol.* **2009**, *377*, 35–42. [CrossRef]

IV.2 Publication 2: Coupling SWAT Model and CMB Method for 3 Modelling of High–Permeability Bedrock Basins 4 Receiving Interbasin Groundwater Flow

Senent- Aparicio, J.; Alcalá, F.J.; Liu, S.; Jimeno- Sáez, P. Coupling SWAT Model and CMB Method for Modelling of High–Permeability Bedrock Basins Receiving Interbasin Groundwater Flow. *Water,* **2020**, *12*, 657.

https://doi.org/10.3390/w12030657

water

MDPI

Coupling SWAT Model and CMB Method for Modeling of High-Permeability Bedrock Basins Receiving Interbasin Groundwater Flow

Javier Senent-Aparicio [1,*], **Francisco J. Alcalá [2,3]**, **Sitian Liu [1]** and **Patricia Jimeno-Sáez [1]**

[1] Department of Civil Engineering, Universidad Católica San Antonio de Murcia,
    Campus de los Jerónimos s/n, Guadalupe, 30107 Murcia, Spain; sliu@alu.ucam.edu (S.L.);
    pjimeno@ucam.edu (P.J.-S.)
[2] Geological Survey of Spain, Ríos Rosas, 23 28003 Madrid, Spain; fj.alcala@igme.es
[3] Instituto de Ciencias Químicas Aplicadas, Facultad de Ingeniería, Universidad Autónoma de Chile,
    7500138 Santiago, Chile
* Correspondence: jsenent@ucam.edu; Tel.: +34-968-278-818

check for updates

Abstract: This paper couples the Soil and Water Assessment Tool (SWAT) model and the chloride mass balance (CMB) method to improve the modeling of streamflow in high-permeability bedrock basins receiving interbasin groundwater flow (IGF). IGF refers to the naturally occurring groundwater flow beneath a topographic divide, which indicates that baseflow simulated by standard hydrological models may be substantially less than its actual magnitude. Identification and quantification of IGF is so difficult that most hydrological models use convenient simplifications to ignore it, leaving us with minimal knowledge of strategies to quantify it. The Castril River basin (CRB) was chosen to show this problematic and to propose the CMB method to assess the magnitude of the IGF contribution to baseflow. In this headwater area, which has null groundwater exploitation, the CMB method shows that yearly IGF hardly varies and represents about 51% of mean yearly baseflow. Based on this external IGF appraisal, simulated streamflow was corrected to obtain a reduction in the percent bias of the SWAT model, from 52.29 to 22.40. Corrected simulated streamflow was used during the SWAT model calibration and validation phases. The Nash–Sutcliffe Efficiency (NSE) coefficient and the logarithmic values of NSE (lnNSE) were used for overall SWAT model performance. For calibration and validation, monthly NSE was 0.77 and 0.80, respectively, whereas daily lnNSE was 0.81 and 0.64, respectively. This methodological framework, which includes initial system conceptualization and a new formulation, provides a reproducible way to deal with similar basins, the baseflow component of which is strongly determined by IGF.

Keywords: SWAT model; CMB method; interbasin groundwater flow; Castril River; baseflow filter

1. Introduction

Hydrological models have become essential tools for water management issues due to their ability to simulate the hydrological cycle through integrated and multidisciplinary approaches, along with their skills to simulate climate change scenarios, land use, and water management [1]. Reliability of such models depends on the spatial and temporal scales covered, as well as the capacity to conceptualize the system functioning [2–4]. Those hydrological models operating at a basin scale are powerful decision support tools because they can provide insights into water resource management [5]. Among them, the SWAT (Soil and Water Assessment Tool) model, a physically-based and semi-distributed eco-hydrological open access model [6] stands out. SWAT can simulate the quality and quantity of surface water and groundwater balance components at different catchment scales to predict the impact

of climate change on the water balance of large watersheds [7,8] and deduce the effect of human-induced actions on water resources, such as irrigation practices and land-use changes [9]. A recent review of water quality and erosion models reveals that SWAT is, by far, the most used model [10]. However, a downside of SWAT is related to the simplified groundwater concept [11]. The simplified representation of the groundwater discharge and aquifer storage processes has been highlighted by several authors as something that may lead to a misunderstanding of the hydrological processes that occur in groundwater dominated watersheds [12].

One of these limitations is SWAT's inability to consider interbasin groundwater flow (IGF). IGF can be defined as the naturally occurring groundwater flow beneath the topographic divide that defines the basin boundary introduced in the SWAT model and in other hydrological models. It contributes to the baseflow of another basin different from that from which it was generated [13]. The magnitude of IGF may be especially relevant in high-permeability bedrock areas, such as steep karst areas. IGF maintains permanent streamflow in dry seasons, thus significantly altering the water balance of a region [14]. Despite the fact that IGF is a common hydrological process in large karst areas, it is often difficult to estimate, even tentatively [15]. Methodologies to identify and quantify IGF have traditionally relied on physical techniques, including the soil–water budget and water fluctuation, when there are sufficient data [16,17], tracer techniques measuring mostly environmental chemicals and stable isotope contents of precipitation and stream water [18,19], and groundwater modeling tools for indirect evaluations [20,21]. Some studies have aimed to assess IGF using the SWAT model. More specifically, Palanisamy and Workman (2014) [22] developed the KarstSWAT model to simulate IGF in watersheds dominated by typical karst features, determining input (recharge in sinkholes) and output (discharge in springs) water component dynamics. Malagó et al. (2016) [23] developed the KSWAT model, which was based on a combination of two previous SWAT applications: (1) a SWAT model adaptation to consider fast infiltration through caves and sinkholes up to the deep aquifers developed by Baffaut and Benson (2009) [24] and (2) a karst flow model in Excel to simulate spring flow discharge developed by Nikolaidis et al. (2013) [25]. More recently, Nguyen et al. (2020) [14] proposed a two linear reservoir model to represent the duality of aquifer recharge and discharge processes in a karst-dominated area in Germany. However, this interest is ongoing and, to our knowledge, the SWAT model has yet to be combined with the CMB method to improve hydrological cycle simulation in those basins where there is a difference between groundwater flow divides and surface topographic divides.

The evaluation of IGF is a complex, uncertain task when groundwater system functioning is partially unknown and the spatiotemporal coverage of data is too low to implement suitable evaluation techniques. In general, spatiotemporal coverage of environmental variables decreases in mountainous areas, thereby limiting the range of suitable techniques to assess IGF and other water balance components. In ungauged areas, IGF can be indirectly assessed when enough is known about groundwater system functioning to assert that IGF equals net aquifer recharge, which is the typical circumstance in most mountainous karst areas in a natural regime. In steep basins with gaining streams under a natural (undisturbed) regime, long-term net aquifer recharge (R) and discharge can be equated when groundwater abstraction, direct evapotranspiration from shallow aquifers, and underflow to deep aquifers are virtually null [26,27]. In such undisturbed hydrological functioning, net aquifer discharge equals the baseflow component of streamflow [28–31], and the problem shrinks to a matter of implementing suitable and viable techniques to determine R. Note that R is the infiltration amount that effectively contributes to the aquifer storage after some delay, smoothing out the variability inherent to precipitation events [32,33]. To assess renewable groundwater resources that finally reach streambeds, R is the governing variable [4,34].

Different methods can be used for R [35,36]. An independent, well-known method to determine R is the atmospheric Chloride Mass Balance (CMB) method [37–41]. The CMB method has been widely applied in different orographic, climatic, and geological contexts to yield mostly long-term (steady) R estimates when recharge water salinity can be attributed to the atmospheric salinity that reaches the water table. The CMB method was recently used to assess distributed mean R from precipitation and its uncertainty over continental Spain by verifying that the CMB variables were steady long-term [34,42].

This data availability was the reason the CMB method was chosen to assess IGF in areas with no human activities. In other territories, other techniques strictly intended for regional R can be selected for IGF evaluations when there are available data sets of similarly sufficient confidence.

This paper aims to evaluate the reliability of coupling the SWAT model and the CMB method to improve the modeling of streamflow in high-permeability bedrock basins receiving IGF. To that end, two main methodological steps are introduced. The first conceptualizes the hydrogeological functioning to confidently estimate IGF from existing CMB datasets for a control period and introduces a new formulation to generate a long-term baseflow series. The second step integrates corrected baseflow series into the SWAT model to improve the streamflow simulation. This methodology has been applied to the Castril River basin (CRB), which is an undisturbed, high-permeability bedrock area, characterized by the strong contribution of IGF to streamflow, as evidenced by a preliminary surface runoff coefficient greater than one.

2. Materials and Methods

2.1. Study Area

The Castril River is an aquifer-fed mountain stream located 37°47'–37°59' north and 2°40'–2°50' west at the headwater of the Guadalquivir River watershed (GRW) in the province of Granada in southern Spain, adjacent to the Segura River watershed (SRW) (Figure 1a). The Castril River basin (CRB) headwater extends from the GRW-SRW divide (peak elevation is 2130 m a.s.l. in the north) to the Portillo Reservoir (outlet is 837 m a.s.l. in the south), covers an area of about 120 km^2, and flows southward among the Sierra de Castril (west) and Sierra Seca (east) Mountains [43] (Figure 1b).

The climate is comparable to the continental Mediterranean, according to the Köppen classification [44]. Average annual precipitation is about 770 mm, with a coefficient of variation of 0.31 over the period 1951–2017. Precipitation is generated by Atlantic weather fronts coming in from the west and by short, intense Mediterranean convective storms. Most precipitation occurs during the autumn and spring. In winter, wet westerly and cold northerly winds predominate, whilst in summer and autumn, wet easterly and warm southerly winds blow [45]. Based on the period 1951–2016, the average annual temperature is about 8 °C, with the lowest temperatures in January and the highest in August. Average annual potential evapotranspiration is about 800 mm [46].

Geologically, the area belongs to the inner Prebetic domain of the external zone of the Alpine Betic Chain, which includes the following synthetic succession from bottom to top [47,48]: (1) Triassic gypsum-rich marls and clays (Keuper facies) with occasional limestones (Muschelkalk facies); (2) Lower and Middle Jurassic dolomites and oolitic limestones; (3) Upper Jurassic nodule limestones, calcareous marls, and marls; (4) Lower Cretaceous dolomites, dolomitic limestones, and marls; (5) Upper Cretaceous calcareous marls, marls, and dolomitic limestones; and (6) Paleocene to Middle Miocene limestones, marls, and calcarenites [48,49]. Small Late Quaternary alluvial deposits intermittently fill the valleys (Figure 1c).

From a hydrogeological point of view, geological materials can be classified into four groups, attending to the permeability type and storage capacity reported by the Geological Survey of Spain (IGME) (1988, 1995, 2001) [50–52]: (1) Triassic marls and clays are low-permeability materials that form the impervious boundary of local aquifers; (2) Jurassic and Cretaceous carbonate materials form highly permeable aquifers as thick as 300 m and have manifest karst features; (3) Jurassic and Cretaceous marls and calcareous marls are low-permeability materials, often confining the above Jurassic and Cretaceous carbonate materials; and (4) Late Quaternary alluvial deposits form temporary unconfined aquifers (Figure 1c).
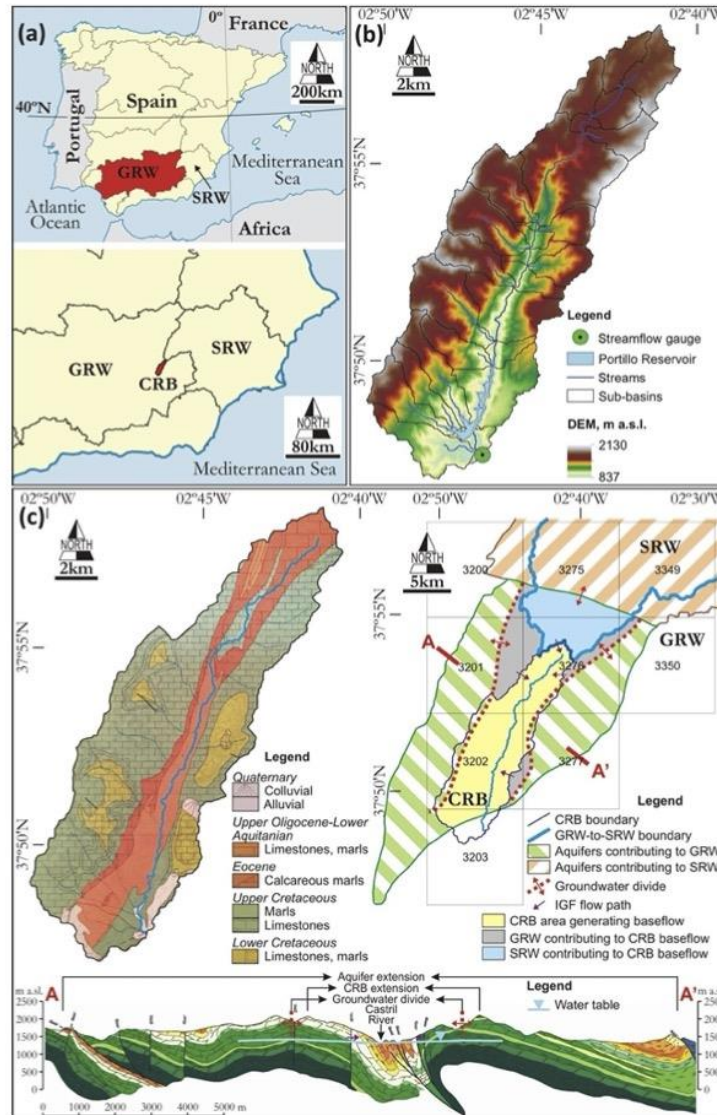
Figure 1. (a) Location of the Castril River basin (CRB) within the Guadalquivir River watershed (GRW) in southern Spain, adjacent to the Segura River watershed (SRW). (b) Discretization of the CRB and 29 sub-basins using the 25 m resolution Digital Elevation Model (DEM) from the Spanish National Geographic Institute, showing other features cited in the text. (c) After the Geological Survey of Spain (IGME) (1988, 1995, 2001) [50–52] and direct field observations, a hydrogeological map of the CRB (scale 1:200,000), the schematic hydrogeological functioning of the CRB and the hydraulically connected upstream GRW and SRW contributing areas, a hydrogeological cross-section A–A′ showing aquifer dimensions, CBR location, groundwater divides and flow paths, and the 10 km × 10 km cells for distributed net aquifer recharge (R) in the part of continental Spain [34,42] covered in the study area was developed.

Hydrogeological functioning of the area was defined by IGME (1988, 1995, 2001) [50–52]. Aquifer boundaries, groundwater divides, and groundwater flow paths were established from hydrogeological maps, piezometry, and chemical and isotopic data. These hydrogeological criteria enabled experts to identify preferred areas for aquifer recharge in summits and for aquifer discharge, at the precise place where the incisive valley topography intersects the piezometry of Cretaceous carbonate aquifers to generate intermittent (upstream) and permanent (downstream) springs (Figure 1c). Downstream, outside the study area, Pliocene and Quaternary alluvial formations fill the Castril River valley and form an unconfined aquifer that hydraulically connects to the stream [43].

The study area is within the Sierra de Castril Natural Park, which has been an environmentally protected space since 1989, and is catalogued as a zone of special conservation for wildlife by the European Natura 2020 network. With respect to land use, forest, grassland, woodland and shrubland, sparsely vegetated areas, bare areas, and marginal rain-fed crops occupy most of the basin surface (Figure 2). Other marginal uses are seasonal livestock (sheep and goats), irrigated traditional crops, and riverine forest of *Pinus nigra* and *Pinus Halepensis* [53]. Neither permanent human settlements nor relevant water uses exist.
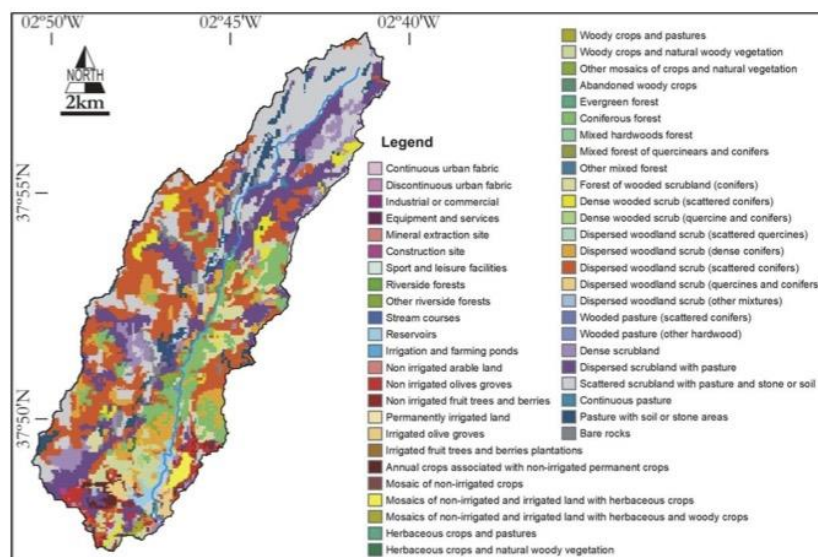
Figure 2. Land-use map (scale 1:25,000) from the Andalusian Environmental Information Network (REDIAM).

2.2. Overall Model Description

A coupled application of the SWAT model and the CMB method to improve streamflow simulation by considering IGF is introduced. This application includes four steps, shown as bulleted lists (Figure 3). The first step uses the CMB method to assess the magnitude of IGF contributing to the CRB baseflow from another upstream GRW and SRW areas, as described in Section 2.3. The second step uses the automated digital filter program BFLOW to split daily streamflow records into baseflow and surface runoff components, as a prerequisite to correct streamflow records by adding IGF to the baseline component, as described in Section 2.4. The third step uses the SWAT model to compare simulated streamflow with and without IGF, as described in Section 2.5. The fourth step uses the SWAT model for standard calibration and validation of simulated streamflow by considering the IGF correction, as described in Section 2.5.
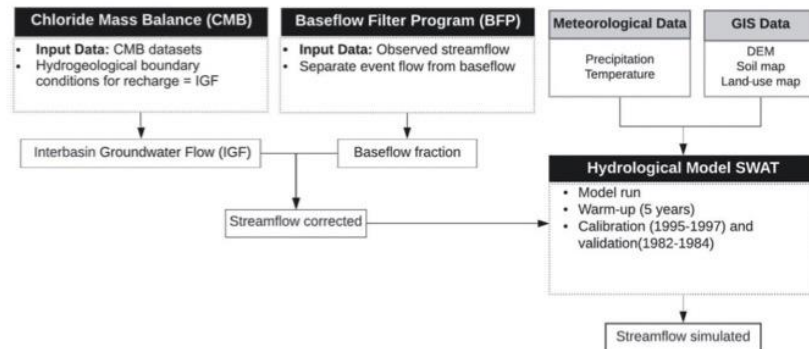
Figure 3. Flow diagram for the coupled Soil and Water Assessment Tool (SWAT) model and chloride mass balance (CMB) method application to model streamflow of hydrological basins subjected to interbasin groundwater flow (IGF).

2.3. CMB Method

2.3.1. CMB Method Application for Aquifer Recharge over Continental Spain

The atmospheric chloride mass balance (CMB) is one of the most widely used methods to estimate net aquifer recharge (R) from precipitation in different orographic, climatic, and geological contexts [35,36]. The CMB is a global method based on the principle of mass conservation of a conservative tracer, in this case the chloride ion, atmospherically contributing to the land surface. This technique yields mostly long-term (steady) R estimations when recharge water salinity can be attributed to the atmospheric salinity that reaches the water table [37–41].

The CMB method was recently applied to estimate distributed spatial mean R and its natural uncertainty (standard deviation) over continental Spain. For a confident application, the long-term steady condition of the CMB variables: atmospheric chloride bulk deposition, chloride export flux by surface runoff, and recharge water chloride content was verified [34,42,54]. This evaluation examined the influence of hydraulic properties (mostly permeability and storability) of different aquifer lithologies on R estimates, as well as the potential contribution of non-atmospheric sources of chloride [55]. For local usage, the reliability and hydrological meaning of distributed R were evaluated by comparing them with local, presumably trustworthy R estimates; one of these local cases was the CRB. Ordinary kriging was used to regionalize the CMB variables at the same 4976 nodes of a 10 km × 10 km grid. In each grid node a mean R value was estimated. Nodal R values were affected by two main types of uncertainty, the natural variability of the CMB variables and the error from its mapping. These uncertainties were identified and estimated [34,42].

The evaluation covered a 10-year period, which represented the critical balance period for the CMB variables to reach comparable steady means and standard deviations. This 10-year period matches the decadal global climatic cycles acting on the Iberian Peninsula, with irregular ~5-year positive and negative phases that follow the North Atlantic Oscillation trend [45,56]. Considering that (1) at least a 10-year balance period is required for reliably steady R evaluations in continental Spain and (2) the CMB datasets preferably spanned the period 1994–2007, the control period (1996–2005), which span a full 10-year long NAO climatic cycle, was chosen to estimate R in this work. Other authors have also implemented these CMB datasets for reliable local R evaluations in different climatic and geological settings, such as Andreu et al. (2011) [27] in Sierra de Gádor karst Massif in Southern Spain, Raposo et al. (2013) [57] in varied geological contexts in Galicia, on the coast of Northern Spain, and Barberá et al. (2018) [58] in the high-mountain, weathered-bedrock Bérchules basin in Southern Spain.

2.3.2. IGF Series Generation

As introduced in Section 1, long-term steady R and IGF can be made equivalent in steep basins with gaining stream under natural (undisturbed) regime when groundwater abstractions, direct evapotranspiration from shallow aquifers, and underflow to deep aquifers are virtually null, and the hydrogeological functioning is well-defined [28–31]. This is the case of the CRB, as described in Section 2.1, because human water use is virtually null and there is enough hydrogeological information. The fraction of R produced in upstream contributing areas can be used as a reliable proxy for the additional baseflow fraction contributing to the CRB baseline [26,27]. To assess the IGF, R is the significant factor [4,34].

As described above, several cells, each one yielding a nodal mean R value and its standard deviation for the control period (1996–2005) instead of a yearly R series, cover the CRB and upstream contributing areas. Adapted from Pulido-Velázquez et al. (2018) [59], a procedure is introduced to obtain the yearly R series by adopting the temporal structure of the yearly P series for the control period (1996–2005). This model uses a correction function that forces the control R series to have the same relative deviation as the control P series, while maintaining the magnitude of its initial mean and standard deviation. The calibrated function is applied to obtain a yearly R series, presuming the correction function does not change. The calculation includes the following steps:

Average change in mean and standard deviation of P and R for the same control period (1996–2005):

$$\Delta m = \frac{m(R) - m(P)}{m(P)} \tag{1a}$$

$$\Delta \sigma = \frac{\sigma(R) - \sigma(P)}{\sigma(P)} \tag{1b}$$

where Δm is the change in mean and $\Delta \sigma$ is the change in standard deviation.

Normalization of the yearly P series:

$$Pn_i = \frac{P_i - \overline{P}}{\sigma_R} \tag{2}$$

where P_i is i–year P and Ps_i is its normalized value, $\overline{P}$ is mean P, and σ_R is standard deviation of mean R.

Generation of yearly R series from yearly P series:

$$R_i = m_C + \sigma_C \cdot Ps_i \tag{3}$$

where R_i is i–year R, and m_C and σ_C are expressed as:

$$m_C = m(P) \cdot (1 + \Delta m) \tag{4a}$$

$$\sigma_C = \sigma(P) \cdot (1 + \Delta \sigma) \tag{4b}$$

When Equation (4) is applied to the control yearly P series, the generated yearly R series adopts the same mean and standard deviation as the control R series from Alcalá and Custodio (2014, 2015) [34,42]. When this procedure is applied to the full yearly P series, the equivalent yearly R series is obtained by assuming that the bias correction remains invariant over the full observation period.

2.4. BFLOW Program

The automated digital filter program (BFLOW) to split daily streamflow records into the baseflow and surface runoff components was used. Nathan and McMahon (1990) [60] were the first to implement this recursive digital filter technique for baseflow analysis. The hypothesis of BFLOW is that low-frequency signals represent the baseflow component while high-frequency signals represent the runoff component [61]. This technique gives results similar to those obtained using other automated

models or manual techniques despite having no physical basis. BFLOW has been used in many studies related to the SWAT model [30,62]; see Arnold and Allen (1999) [63] for more details about this technique. The baseflow obtained by BFLOW was increased by adding IGF, calculated in previous section.

2.5. SWAT Model

2.5.1. Description of the SWAT Model

The Soil and Water Assessment Tool (SWAT) is a long-term watershed hydrological model with strong physical mechanisms, developed jointly in 1994 by the Agricultural Research Service of the United States Department of Agriculture (USDA-ARS) and Texas A&M AgriLife Research, part of the Texas A&M University System. The SWAT model simulation includes atmospheric precipitation, surface runoff, subsurface flow, evapotranspiration, groundwater flow, river network flow concentration, and other intermediate water balance components subjected to variable delays [6]. The SWAT model first divides the study area into several hydrological response units (HRUs) based on the digital elevation model (DEM), land use, soil type, and meteorological data. Then, SWAT establishes a hydrophysical conceptual model of each HRU, calculates runoff in each HRU, and finally connects the entire set of the HRU runoff responses through the river network of the study area toward the basin outlet. The hydrological processes simulated by the SWAT model are based on the following water balance equation:

$$SW_t = SW_0 + \sum_{i=1}^{t} \left(P_{day} - E_{day} - Q_{surf} - W_{seep} - Q_{gw} \right)_i \tag{5}$$

where SW_t is final soil–water content (mm H_2O), SW_0 is initial soil–water content (mm H_2O), t is time (days), P_{day} is precipitation on day i (mm H_2O), ET_{day} is evapotranspiration on day i (mm H_2O), Q_{surf} is surface runoff on day i (mm H_2O), W_{seep} is water amount that enters the vadose zone from the soil profile on day i (mm H_2O), and Q_{gw} is groundwater return flow on day i (mm H_2O).

2.5.2. Data, Model Set-Up, Calibration, and Validation

Datasets used to implement the SWAT model were: (1) the 25-m resolution DEM from the Spanish National Geographic Institute (IGN); (2) the land-use map (scale 1:25,000) from the Andalusian Environmental Information Network (REDIAM); (3) the 1-km resolution georeferenced soil data from the World Soil Coordination Map; (4) the 5-km resolution nodal daily precipitation series in Spain from the Spanish National Weather Service (AEMET) grid version 1.0, which cover the period 1951–2017; (5) the 10-km resolution nodal daily temperature series in Spain from the fifth version of the high-resolution SPAIN02 grid, which cover the period 1951–2016; and (6) the 24-h streamflow records downloaded from the Spanish Centre for Public Works Studies and Experimentation (CEDEX) website. The open source QGIS interface for SWAT (QSWAT 1.8) was used to set up the SWAT model.

The SUFI-2 algorithm of SWAT-CUP (Calibration and Uncertainty Programs) to calibrate and validate the SWAT model was used. Based on our previous modeling experiences [64,65], twenty-one widely used flow calibration parameters and their ranges were initially selected. Aimed at reaching an acceptable calibration, two iterations (representing 500 simulations each) were performed; the first included 13 parameters on a monthly scale, the latter included 8 parameters on a daily scale. To mitigate the effect of initial soil–water condition, a five-year warm-up period was imposed [66]. The periods 1995–1997 and 1982–1984 were, respectively, selected for the calibration and validation phases. As the downloaded daily streamflow (discharge) series was discontinuous, time intervals for calibration and validation were carefully selected to minimize the effect of existing data gaps.

As the CRB is a singular aquifer-fed mountain stream, some quantitative information to cross-validate the SWAT model results were used. For model efficiency criteria, Nash-Sutcliffe efficiency coefficient (NSE), logarithmic form of the NSE (lnNSE), coefficient of determination (R^2), percent bias (PBIAS), Root Mean Square Error (RMSE), and RMSE relative to standard deviation of the observed data (RSR) were used (Table 1).

Table 1. Equations, ranges, and optimal values for SWAT model performance statistics, after Moriasi et al. (2012) [67].

Statistic and Equation [1]	Description
NSE : Nash–Sutcliffe Efficiency Coefficient $$= 1 - \frac{\sum_{i=1}^{n}(Q_{obs\,i}-Q_{sim\,i})^2}{\sum_{i=1}^{n}(Q_{obs\,i}-\overline{Q})^2}$$	NSE indicates a perfect match between observed and simulated data, and ranges from $-\infty$ to 1. Higher than 0.5 is considered satisfactory.
lnNSE$= 1 - \frac{\sum_{i=1}^{n}(ln(Q_{obs\,i})-ln(Q_{sim\,i}))^2}{\sum_{i=1}^{n}(ln(Q_{obs\,i})-ln(\overline{Q}))^2}$	lnNSE is the logarithmic form of the model efficiency coefficient. NSE emphasizes the high flows, and lnNSE emphasizes the low flows.
R^2 : Coefficient of Determination $$= \left(\frac{\sum_{i=1}^{n}(Q_{obs\,i}-\overline{Q})(Q_{sim\,i}-\overline{Q_{sim}})}{\sqrt{\sum_{i=1}^{n}(Q_{obs\,i}-\overline{Q})^2}\sqrt{\sum_{i=1}^{n}(Q_{sim\,i}-\overline{Q_{sim}})^2}} \right)^2$$	R^2 indicates the degree of linear relationship between simulated and observed data, and ranges from 0 to 1. Higher than 0.5 is considered a satisfactory result.
PBIAS : Percent Bias $$= \frac{\sum_{i=1}^{n}(Q_{obs\,i}-Q_{sim\,i})\Delta 100}{\sum_{i=1}^{n}(Q_{obs\,i})}$$	PBIAS calculates the average tendency of the simulated data to be higher or lower than their observed counterparts. The optimal value is 0, and an acceptable one is between ±25.
RMSE : Root Mean Square Error $$= \sqrt{\sum_{i=1}^{n}(Q_{obs\,i}-Q_{sim\,i})^2}$$	RMSE = 0 indicates a perfect match between observed and simulated data. Increasing RMSE values indicate that matching is getting worse.
RSR : Root Mean Square Error relative to standard deviation of the observed data $$= \frac{RMSE}{STDEV_{obs}} = \frac{\sqrt{\sum_{i=1}^{n}(Q_{obs\,i}-Q_{sim\,i})^2}}{\sqrt{\sum_{i=1}^{n}(Q_{obs\,i}-\overline{Q_{obs\,i}})^2}}$$	RSR is RMSE relative to standard deviation of the observed data, and ranges from 0 to ∞. The lower the RSR, the lower the RMSE and the better the model performance. Lower than 0.7 is acceptable.

[1] n is the total number of observations, $Q_{obs\,i}$ and $Q_{sim\,i}$ are observed and simulated streamflow at observation i, $\overline{Q}$ is the mean of the observed data over the simulation period, and $\overline{Q_{sim\,i}}$ is the mean of the simulated data over the simulation period.

3. Results and Discussion

3.1. Using the CMB Datasets to Estimate IGF

As shown in Figure 1c, the entire hydrogeological system that contributes to streamflow at the CRB outlet covers the CRB surface itself and some hydraulically connected adjacent areas from GRW and SRW. The methodology described in Section 2.3 was applied to the nodal R values gathered from those 10 km × 10 km cells covering the CRB and those contributing to upstream GRW and SRW areas. Attending to the hydrogeological functioning (Figure 1c) and existing land and water uses (Figure 2), nodal mean values and standard deviations of R and baseflow can be assumed to be equal.

In this area, for the control period (1996–2005), nodal mean R varied within the range 143–332 mm year^{-1}, which means recharge–precipitation ratios were in the 0.29–0.37 range; the standard deviation of mean R varied within the 39–90 mm year^{-1} range, which placed the given coefficients of variation of mean annual R (mean value-to-standard deviation ratio) in the 0.27–0.30 range (Table 2). For the control period (1996–2005), fitting parameters were calculated to generate the yearly R data series in the CRB and upstream GRW and SRW contributing areas, which are in Table 3, whereas the generated surface-weighted yearly P and R series are in Table 4. In each area, yearly R and P series for the control period (1996–2005) were compared. The resulting parametric functions allowed for the extension of the calculated yearly R series to cover the yearly P full record (1951–2016) (Figure 4). Figure 5 shows the full yearly baseflow series generated within the CBR, as well as the yearly surface-weighted IGF series contributed by upstream GRW and SRW areas. As observed, IGF is somewhat higher than baseflow, generated within the CRB. IGF is about 51% of total CRB baseflow.

Table 2. For the 10 km × 10 km cells covering the CRB and upstream GRW and SGW contributing areas, the CMB datasets gathered from Alcalá and Custodio (2014, 2015) [34,42].

Cell [1]	CRB					GRW					SRW				
	S	P [2]	CVP	R	CVR	S	P	CVP	R	CVR	S	P	CVP	R	CVR
3200						3.2	894	0.31	315	0.27	0.8	894	0.31	315	0.27
3201	10.4	909	0.33	332	0.27	20.2	909	0.33	332	0.27					
3202	60.6	693	0.34	229	0.28	4.8	693	0.34	229	0.28					
3203	7.1	486	0.35	143	0.27										
3275						1.0	813	0.32	276	0.27	21.7	813	0.32	276	0.27
3276	22.0	668	0.33	206	0.29	14.5	668	0.33	206	0.29	25.0	668	0.33	206	0.29
3277	1.8	517	0.35	153	0.30	1.1	517	0.35	153	0.30					
3349						0.1	687	0.32	212	0.27	0.5	687	0.32	212	0.27
3350						2.0	612	0.33	186	0.28	0.5	612	0.33	186	0.28
Sum	101.9					46.9					48.4				
SWA [3]		692	0.34	227	0.28		787	0.33	269	0.28		736	0.32	239	0.28

[1] Cell ID as in Figure 1c. [2] S is surface in km^2, P and R are, respectively, mean precipitation and mean net aquifer recharge over the control period (1996–2005) in mm year^{-1}; and CVP and CVR are the dimensionless coefficients of variation of mean P and R over the control period (1996–2005) as fractions. [3] SWA is surface-weighted average.

Table 3. Fitting parameters for the CRB and upstream GRW and SGW areas.

Parameter [1]	CRB	GRW	SRW
Δm	−0.67	−0.66	−0.67
$\Delta \sigma$	−0.73	−0.71	−0.72
m_C	227	269	239
σ_C	63.1	74.9	66.8

[1] Δm and $\Delta \sigma$ are dimensionless, and m_C and σ_C are in mm year^{-1}.

Table 4. For the control period (1996–2005), surface-weighted yearly series of (i) P and R in the CRB and in upstream GRW and SRW areas, and (ii) IGF from the GRW and SRW area contributing to CRB.

Year	P [1]	Psi [1]	R, CRB [1]	R, GRW	R, SRW	IGF, GRW+SRW [2]
1996	1037.9	1.76	338.5	401.4	357.1	378.9
1997	978.9	1.47	319.8	379.2	337.3	357.9
1998	472.3	−1.08	159.2	188.7	167.4	177.9
1999	575.4	−0.56	191.9	227.5	202.0	214.6
2000	669.5	−0.09	221.7	262.9	233.6	248.0
2001	742.6	0.28	244.9	290.4	258.1	274.0
2002	616.8	−0.35	205.0	243.1	215.9	229.3
2003	723.7	0.19	238.9	283.3	251.8	267.3
2004	641.5	−0.23	212.9	252.4	224.2	238.1
2005	406.9	−1.40	138.5	164.1	145.5	154.7
Mean [3]	686.6		227.1	269.3	239.3	240.1
SD	199.2		63.1	74.9	66.8	66.8
CV	0.29		0.28	0.28	0.28	0.28

[1] P and R are, respectively, annual precipitation and net aquifer recharge in mm year^{-1}, and Psi is dimensionless normalized yearly P. [2] IGF is interbasin groundwater flow in mm year^{-1}. [3] Mean and SD are mean and standard deviation over the control period (1996–2005) in mm year^{-1}, and CV is dimensionless coefficient of variation as a fraction.
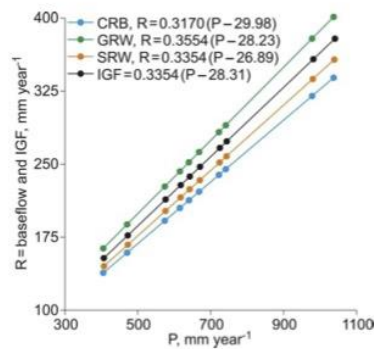

Figure 4. For the control period (1996–2005), parameterization of yearly P–R functions in the CRB and upstream GRW and SRW contributing areas; yearly R equals yearly baseflow. Yearly IGF series refers to the surface-weighed sum of upstream R = baseflow from GRW and SRW areas contributing to the CRB streamflow. In all cases, the Pearson coefficient of correlation is 1.

3.2. Comparison of SWAT Model Results with and without IGF

Based on DEM analysis and after SWAT model implementation, the CRB was discretized into 29 sub-basins. Based on the combination of land uses, soil types, and slope ranges (<2%, 2%–8%, >8%), 149 HRUs were defined. The thresholds for defining HRUs were set to 5% to optimize model processing. The Hargreaves non-global method was used to simulate potential evapotranspiration [68]. As a result, only precipitation and temperature data to run the SWAT model were needed.

As described in Section 3.1, the IGF from upstream GRW and SRW areas greatly contributes to the Castril River streamflow. For the period 1995–1997, the SWAT model was doubly implemented on a monthly scale with and without IGF. The result was a large difference between observed and initial simulated streamflow when IGF was omitted (Figure 6). When IGF was included as an additional baseflow fraction, the difference between observed and corrected simulated streamflow clearly narrowed. This preliminary trial at model performance showed that the statistics NSE and PBIAS improve when IGF was included (Figure 6). Overall model performance increased about 80% in absolute terms.
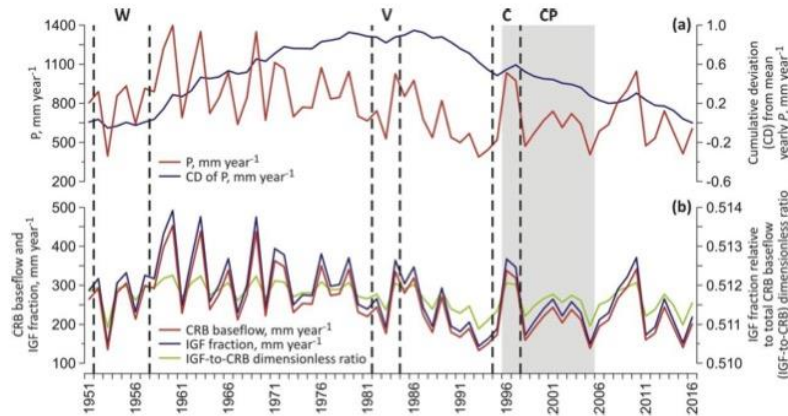
Figure 5. For the full period (1951–2016), (**a**) surface-weighted yearly P series in the area compiled from the Spanish National Weather Service (AEMET) grid version 1.0 and cumulative deviation (CD) from mean yearly P in mm year^{-1}; and (**b**) generated yearly baseflow series in the CRB and yearly surface-weighed IGF series from upstream GRW and SRW contributing areas in mm year^{-1}, and IGF fraction relative to total CRB baseflow (IGF–CRB) dimensionless ratio. The control period (1996–2005) is grey shallowed (CP). Vertical dotted lines indicate selected time intervals for the SWAT model warm-up (W), calibration (C), and validation (V) phases.
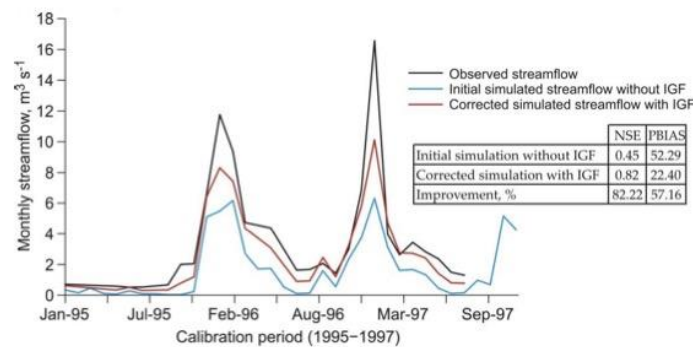
Figure 6. For the selected calibration period (1995–1997) and on a monthly scale, observed streamflow compared to (i) initial simulated streamflow without IGF and (ii) corrected simulated streamflow with IGF. The statistics NSE and PBIAS show the model performance achieved in each simulation.

3.3. Calibration and Validation of SWAT Model Including IGF

A total of 21 SWAT parameters were optimized using the SUFI-2 algorithm from SWAT-CUP. As described in Section 2.5.2, parameter selection was based on our previous research experiences in similar basins in Southern Spain [64,65]. The SWAT calibration phase covered a 3-year period (1995–1997). The final ranges used and the final fitted values of these parameters are given in Table 5.

The magnitude of calibrated GW_REVAP, ESCO, LAT_TTIME, GWQMN, and ALPHA_BF parameters is quite similar to those obtained with similar orography, geology, climate, and land use [64,65]. The ESCO is also similar to that fitted in other Mediterranean karst areas, where yearly actual evapotranspiration is typically 0.7–0.9 fold yearly precipitation [26,27,46]. The low value of ALPHA_BF indicates a slow aquifer response [69]. This is corroborated by the long-delayed responses to recharge events in similar karst aquifers in the region, reported by Moral et al. (2008) [70].

Table 5. Description of parameters used for SWAT model calibration in the CRB.

Parameter [1]	Description	Range Used in Calibration	Fitted Value
r_CN2.mgt	Soil Conservation Service (SCS) runoff curve number	−0.1 to 0.1	0.08
v_ALPHA_BF.gw	Baseflow alpha factor (day^{-1})	0 to 1	0.11
a_GW_DELAY.gw	Groundwater delay time (day)	0 to 60	2.82
a_GWQMN.gw	Threshold depth of water in the shallow aquifer for return flow to occur (mm)	−200 to 1000	898.00
v_GW_REVAP.gw	Groundwater revap coefficient	0.02 to 0.1	0.09
a_RCHRG_DP.gw	Deep aquifer percolation fraction	−0.05 to 0.05	0.04
a_REVAPMN.gw	Threshold depth of water in shallow aquifer for revap or percolation to deep aquifer to occur (mm)	−500 to 500	−61.00
v_CANMX.hru	Maximum canopy storage (mm)	0 to 8	0.47
v_EPCO.bsn	Plant uptake compensation factor	0.5 to 1	0.56
v_ESCO.bsn	Soil evaporation compensation factor	0.3 to 0.8	0.61
r_SOL_AWC.sol	Available water capacity of the soil layer (mm H_2O/mm soil)	−0.02 to 0.02	−0.02
v_LAT_TTIME.hru	Lateral flow travel time (day)	0 to 180	76.50
v_SLSOIL.hru	Slope length for lateral subsurface flow (m)	0 to 150	1.35
r_SLSUBBSN.hru	Average slope length (m)	−0.5 to 0.5	0.08
r_HRU_SLP.hru	Average slope steepness (m/m)	−0.5 to 0.5	0.40
v_OV_N.hru	Manning's 'n' value for overland flow	0.01 to 1	0.61
r_CH_S1.sub	Average slope of tributary channels (m/m).	−0.5 to 0.5	0.26
v_CH_N1.sub	Manning's 'n' value for the tributary channels	0.01 to 30	1.68
r_CH_S2.rte	Average slope of main channel along the channel length (m/m)	−0.5 to 0.5	−0.04
v_CH_N2.rte	Manning's 'n' value for the main channel	0.01 to 0.3	0.04
v_SURLAG.bsn	Surface runoff lag coefficient	0.05 to 24	20.71

[1] (r_) refers to relative change, i.e., the current parameter must be multiplied by (1 + the value obtained in calibration), (v_) means that the existing parameter value must be replaced by the value obtained in calibration, and (a_) refers to absolute change, i.e., the fitted value must be added to the existing value of the parameter.

Corrected streamflow records with IGF were used for model calibration (1995–1997) and validation (1982–1984) phases. Observed streamflow was compared to corrected simulated streamflow on monthly (Figure 7) and daily (Figure 8) scales during the calibration and validation periods. In the CRB, the fitted SWAT model replicated, almost identically, the trend of the streamflow hydrograph. The higher fluctuations in the simulated peaks and the lower ones in low flows were found, both in monthly and daily streamflow simulations.
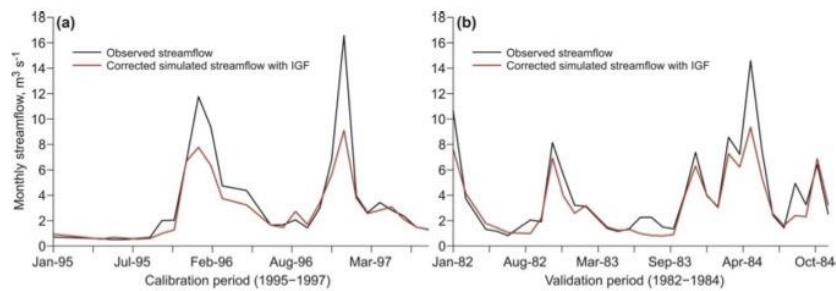
Figure 7. On a monthly scale, observed streamflow compared to corrected simulated streamflow with SWAT model for the (**a**) calibration and (**b**) validation phases.
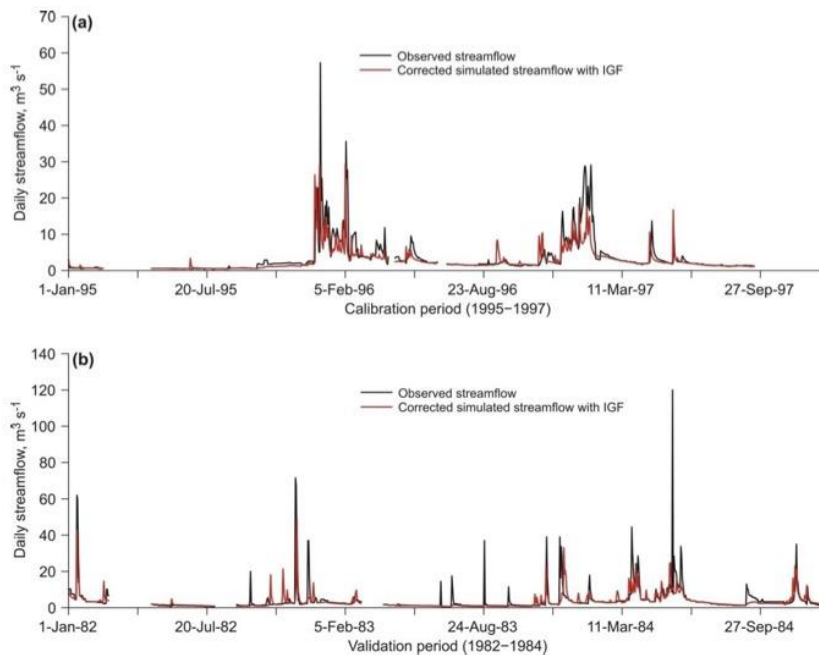
Figure 8. On a daily scale, observed streamflow compared to corrected simulated streamflow with SWAT model for the (**a**) calibration and (**b**) validation phases.

As observed in Figure 8, low flows predominate in the CRB daily streamflow record. As many other SWAT models reported for other similar aquifer-fed karst areas, the SWAT model performance for high and normal flows decreased in the face of predominant low flows [65,71]. Therefore, following the

suggestion of Krause et al. (2005) [72], NSE and lnNSE were used to measure, respectively, the high and the low flows, to reduce the problem of the squared differences and the resulting sensitivity to extreme values of NSE. Calibration and validation of monthly corrected streamflow showed good agreement of simulated and observed data, as indicated by the model performance statistics for monthly and daily simulations given in Table 6.

Table 6. SWAT model performance statistics for corrected simulated monthly and daily streamflow during calibration and validation phases.

Statistic	Time Step	Calibration	Validation
NSE	Monthly	0.77	0.8
R^2	Monthly	0.92	0.89
PBIAS	Monthly	19.82	17.25
RSR	Monthly	0.48	0.44
lnNSE	Daily	0.81	0.64

As finally deduced, the SWAT model performs well and can be used for further analysis in the CRB and in other similar high-permeability bedrock basins, the baseflow of which is strongly determined by IGF. For this, there must be a confident evaluation of IGF or, at minimum, a reliable external evaluation available. In this paper, the CMB method and the available CMB datasets in continental Spain [34,42] were used for this purpose. However, as described for other groundwater and surface water coupling models, the SWAT-CMB application presented here reveals the following overall problems: (1) the spatial (size and volume) and temporal (renovation rate) scales of groundwater and surface water bodies differ, whereas the coupling model can only simulate the same spatial and temporal scale in both types of bodies; (2) the coupling models had defects in the coupling mechanism processing, which demanded substantial simplification of the coupling process, thereby causing model distortion; and (3) this coupling model was established for a certain region or a specific problem and, although good results have been achieved, there is no general adaptability, so additional hydrogeological knowledge of local applications is needed to consider the changes in scale effects and actual flow conditions.

4. Conclusions

This paper presents the combined application of the SWAT model and the CMB method to model streamflow in the CRB, a representative high-permeability bedrock basin where the streamflow is significantly determined by IGF from upstream contributing areas. The CMB method and available CMB datasets in continental Spain were used for the IGF that adds to the baseflow generated within the CRB. The SWAT model performance improved noticeably when simulated streamflow with IGF was used. Using the CMB datasets for streamflow correction, the SWAT model showed good performance both in daily and monthly simulations. Some overall remarks from this research are highlighted below.

The influence of IGF on basins like the CRB is remarkable. Therefore, IGF must be considered to improve water resource evaluation and management in this kind of basin located in the headwater of large river watersheds. In the CRB, IGF means about 51% of total baseflow. We do not suggest using the SWAT model alone for modeling of these aquifer-fed mountain basins. It must be coupled with other specific methods to accurately assess IGF. The CMB was revealed to be a suitable method for IGF, because of the favorable hydrogeological setting and the negligible groundwater abstraction, which allowed for equivalent net aquifer recharge to the baseflow contributing to streamflow in the headwater of large river watersheds. In other areas that reflect different patterns of groundwater use and hydrogeological features, assessment of IGF must rely on other techniques coupled with the SWAT model.

References

1. Trolle, D.; Hamilton, D.P.; Hipsey, M.R.; Bolding, K.; Bruggeman, J.; Mooij, W.M.; Janse, J.H.; Nielsen, A.; Jeppesen, E.; Elliott, A.; et al. A community–based framework for aquatic ecosystem models. *Hydrobiologia* **2012**, *683*, 25–34. [CrossRef]

2. Hojberg, A.L.; Refsgaard, J.C. Model uncertainty-parameter uncertainty versus conceptual models. *Water Sci. Technol.* **2005**, *52*, 177–186. [CrossRef] [PubMed]

3. Beven, K. Towards integrated environmental models of everywhere: Uncertainty, data and modelling as a learning process. *Hydrol. Earth Syst. Sci.* **2007**, *11*, 460–467. [CrossRef]

4. Alcalá, F.J.; Martínez-Valderrama, J.; Robles-Marín, P.; Guerrera, F.; Martín-Martín, M.; Raffaelli, G.; Tejera de León, J.; Asebriy, L. A hydrological-economic model for sustainable groundwater use in sparse-data drylands: Application to the Amtoudi Oasis in southern Morocco, northern Sahara. *Sci. Total Environ.* **2015**, *537*, 309–322. [CrossRef]

5. Francesconi, W.; Srinivasan, R.; Pérez-Miñana, E.; Willcock, S.P.; Quintero, M. Using the Soil and Water Assessment Tool (SWAT) to model ecosystem services: A systematic review. *J. Hydrol.* **2016**, *535*, 625–636. [CrossRef]

6. Arnold, J.G.; Srinivasan, R.; Muttiah, R.S.; Williams, J.R. Large area hydrologic modeling and assessment Part I: Model development. *J. Am. Water Resour. Assoc.* **1998**, *34*, 73–89. [CrossRef]

7. Molina-Navarro, E.; Andersen, H.E.; Nielsen, A.; Thodsen, H.; Trolle, D. Quantifying the combined effects of land use and climate changes on stream flow and nutrient loads: A modelling approach in the Odense Fjord catchment (Denmark). *Sci. Total Environ.* **2018**, *621*, 253–264. [CrossRef]

8. Blanco-Gómez, P.; Jimeno-Sáez, P.; Senent-Aparicio, J.; Pérez-Sánchez, J. Impact of Climate Change on Water Balance Components and Droughts in the Guajoyo River Basin (El Salvador). *Water* **2019**, *11*, 2360. [CrossRef]

9. Senent-Aparicio, J.; Liu, S.; Pérez-Sánchez, J.; López-Ballesteros, A.; Jimeno-Sáez, P. Assessing Impacts of Climate Variability and Reforestation Activities on Water Resources in the Headwaters of the Segura River Basin (SE Spain). *Sustainability* **2018**, *10*, 3277. [CrossRef]

10. Fu, B.; Merritt, W.S.; Croke, B.F.W.; Weber, T.R.; Jakeman, A.J. A review of catchment-scale water quality and erosion models and a synthesis of future prospects. *Environ. Model. Softw.* **2019**, *114*, 75–97. [CrossRef]

11. Luo, Y.; Arnold, J.; Allen, P.; Chen, X. Baseflow simulation using SWAT model in an inland river basin in Tianshan Mountains, Northwest China. *Hydrol. Earth Syst. Sci.* **2012**, *16*, 1259–1267. [CrossRef]

12. Ficklin, D.L.; Luo, Y.; Zhang, M. Watershed Modelling of Hydrology and Water Quality in the Sacramento River Watershed, California. *Hydrol. Process.* **2012**, *27*, 236–250. [CrossRef]

13. Genereux, D.P.; Jordan, M.T.; Carbonell, D. A pired-watershed budget study to quantify interbasin groundwater flow in a lowland rain forest. Costa Rica. *Water Resour. Res.* **2005**, *41*, W04011. [CrossRef]

14. Nguyen, V.T.; Dietrich, J.; Uniyal, B. Modeling interbasin groundwater flow in karst areas: Model development, application, and calibration strategy. *Environ. Modell. Softw.* **2020**, *124*, 104606. [CrossRef]

15. Zanon, C.; Genereux, D.P.; Oberbauer, S.F. Use of a watershed hydrologic model to estimate interbasin groundwater flow in a Costa Rican rainforest. *Hydrol. Process.* **2014**, *28*, 3670–3680. [CrossRef]

16. Rahayuningtyas, C.; Wu, R.S.; Anwar, R.; Chiang, L.C. Improving avswat stream flow simulation by incorporating groundwater recharge prediction in the upstream Lesti watershed, East Java, Indonesia. *Terr. Atmos. Ocean. Sci.* **2014**, *25*, 881–892. [CrossRef]

17. Han, M.; Zhao, C.Y.; Šimůnek, J.; Feng, G. Evaluating the impact of groundwater on cotton growth and root zone water balance using Hydrus-1D coupled with a crop growth model. *Agric. Water Manag.* **2015**, *160*, 64–75. [CrossRef]

18. Obuobie, E. Estimation of Groundwater Recharge in the Context of Future Climate Change in the White Volta River Basin, West Africa. Germany. Ph.D. Thesis, Rheinischen Friedrich-Wilhelms-Universität, Bonn, Germany, 2008; 165p.

19. Alcalá, F.J.; Martín-Martín, M.; Guerrera, F.; Martínez-Valderrama, J.; Marín, P.R. A feasible methodology for groundwater resource modelling for sustainable use in sparse-data drylands: Application to the Amtoudi Oasis in the northern Sahara. *Sci. Total Environ.* **2018**, *630*, 1246–1257. [CrossRef]

20. Kim, N.W.; Chung, I.M.; Won, Y.S.; Arnold, J.G. Development and application of the integrated SWAT-MODFLOW model. *J. Hydrol.* **2008**, *356*, 1–16. [CrossRef]

21. Bouaziz, L.; Weerts, A.; Schellekens, J.; Sprokkereef, E.; Stam, J.; Savenije, H.; Hrachowitz, M. Redressing the balance: Quantifying net intercatchment groundwater flows. *Hydrol. Earth Syst. Sci.* **2018**, *22*, 6415–6434. [CrossRef]

22. Palanisamy, B.; Workman, S.R. Hydrologic modeling of flow through sinkholes located in streambeds of Cane Run stream, Kentucky. *J. Hydrol. Eng.* **2014**, *20*, 04014066. [CrossRef]

23. Malagó, A.; Efstathiou, D.; Bouraoui, F.; Nikolaidis, N.P.; Franchini, M.; Bidoglio, G.; Kritsotakis, M. Regional scale hydrologic modeling of a karst-dominant geomorphology: The case study of the island of Crete. *J. Hydrol.* **2016**, *540*, 64–81. [CrossRef]

24. Baffaut, C.; Benson, V.W. Modeling flow and pollutant transport in a karst watershed with SWAT. *Trans. ASABE* **2009**, *52*, 469–479. [CrossRef]

25. Nikolaidis, N.P.; Bouraoui, F.; Bidoglio, G. Hydrologic and geochemical modeling of a karstic Mediterranean watershed. *J. Hydrol.* **2013**, *477*, 129–138. [CrossRef]

26. Alcalá, F.J.; Cantón, Y.; Contreras, S.; Were, A.; Serrano-Ortiz, P.; Puigdefábregas, J.; Solé-Benet, A.; Custodio, E.; Domingo, F. Diffuse and concentrated recharge evaluation using physical and tracer techniques: Results from a semiarid carbonate massif aquifer in southeastern Spain. *Environ. Earth Sci.* **2011**, *63*, 541–557. [CrossRef]

27. Andreu, J.M.; Alcalá, F.J.; Vallejos, Á.; Pulido-Bosch, A. Recharge to aquifers in SE Spain: Different approaches and new challenges. *J. Arid Environ.* **2011**, *75*, 1262–1270. [CrossRef]

28. Rutledge, A.T.; Mesko, T.O. *Estimated Hydrologic Characteristics of Shallow Aquifer Systems in the Valley and Ridge, the Blue Ridge, and the Piedmont Physiographic Provinces Based on Analysis of Streamflow Recession and Base Flow*; U.S. Geological Survey: Reston, VA, USA, 1996; 58p.

29. Lim, K.J.; Engel, B.A.; Tang, Z.; Choi, J.; Kim, K.S.; Muthukrishnan, S.; Tripathy, D. Automated web GIS based hydrograph analysis tool, WHAT. *J. Am. Water Resour. Assoc.* **2005**, 1407–1416. [CrossRef]

30. Plesca, I.; Timbe, E.; Exbrayat, J.-F.; Windhorst, D.; Kraft, P.; Crespo, P.; Vaché, K.B.; Frede, H.-G.; Breuer, L. Model intercomparison to explore catchment functioning: Results from a remote montane tropical rainforest. *Ecol. Model.* **2012**, *239*, 3–13. [CrossRef]

31. Lee, J.; Kim, J.; Jang, W.S.; Lim, K.J.; Engel, B.A. Assessment of Baseflow Estimates Considering Recession Characteristics in SWAT. *Water* **2018**, *10*, 371. [CrossRef]

32. Lerner, D.N.; Issar, A.S.; Simmers, I. Groundwater recharge. A guide to understanding and estimating natural recharge. In *IAH International Contributions to Hydrogeology*; Heise: Hannover, Germany, 1990; 345p.

33. Batelaan, O.; De Smedt, F. GIS-based recharge estimation by coupling surface-subsurface water balances. *J. Hydrol.* **2007**, *337*, 337–355. [CrossRef]

34. Alcalá, F.J.; Custodio, E. Spatial average aquifer recharge through atmospheric chloride mass balance and its uncertainty in continental Spain. *Hydrol. Process.* **2014**, *28*, 218–236. [CrossRef]

35. Scanlon, B.R.; Healy, R.W.; Cook, P.G. Choosing appropriate techniques for quantifying groundwater recharge. *Hydrogeol. J.* **2002**, *10*, 18–39. [CrossRef]

36. McMahon, P.B.; Plummer, L.N.; Bohlke, J.K.; Shapiro, S.D.; Hinkle, S.R. A comparison of recharge rates in aquifers of the United States based on groundwater-based data. *Hydrogeol. J.* **2011**, *19*, 779–800. [CrossRef]

37. Claasen, H.C.; Reddy, M.M.; Halm, D.R. Use of the chloride ion in determining hydrologic-basin water budgets: A 3-year case study in the San Juan Mountains, Colorado, USA. *J. Hydrol.* **1986**, *85*, 49–71. [CrossRef]

38. Dettinger, M.D. Reconnaissance estimates of natural recharge to desert basins in Nevada, USA, by using chloride-balance calculations. *J. Hydrol.* **1989**, *106*, 55–78. [CrossRef]

39. Wood, W.W.; Sanford, W.E. Chemical and isotopic methods for quantifying ground-water recharge in a regional, semiarid environment. *Ground Water* **1995**, *33*, 458–468. [CrossRef]

40. Sami, K.; Hughes, D.A. A comparison of recharge estimates to a fractured sedimentary aquifer in South Africa from a chloride mass balance and an integrated surface-subsurface model. *J. Hydrol.* **1996**, *179*, 111–136. [CrossRef]

41. Scanlon, B.R.; Keese, K.E.; Flint, A.L.; Flint, L.E.; Gaye, C.B.; Edmunds, W.M.; Simmers, I. Global synthesis of groundwater recharge in semiarid and arid regions. *Hydrol. Process.* **2006**, *20*, 3335–3370. [CrossRef]

42. Alcalá, F.J.; Custodio, E. Natural uncertainty of spatial average aquifer recharge through atmospheric chloride mass balance in continental Spain. *J. Hydrol.* **2015**, *524*, 642–661. [CrossRef]

43. Paz, C.; Alcalá, F.J.; Carvalho, J.M.; Ribeiro, L. Current uses of ground penetrating radar in groundwater-dependent ecosystems research. *Sci. Total Environ.* **2017**, *595*, 868–885. [CrossRef]

44. Capel-Molina, J.J. *Los Climas de España*; Oikos-Tau: Barcelona, Spain, 1981; 403p.

45. Trigo, R.; Pozo-Vázquez, D.; Osborn, T.; Castro-Díez, Y.; Gámiz-Fortis, S.; Esteban-Parra, M. North Atlantic oscillation influence on precipitation, river flow and water resources in the Iberian peninsula. *Int. J. Climatol.* **2004**, *24*, 925–944. [CrossRef]

46. Vanderlinden, K.; Giraldez, J.V.; Van Meirvenne, M. Assessing Reference Evapotranspiration by the Hargreaves Method in Southern Spain. *J. Irrig. Drain. Eng.* **2004**, *130*, 184–191. [CrossRef]

47. Azéma, J.; Foucault, A.; Fourcade, E.; García–Hernández, M.; González–Donoso, J.M.; Linares, D.; López–García, A.C.; Rivas, P.; Vera, J.A. *Las Microfacies del Jurásico y Cretácico de las Zonas Externas de las Cordilleras Béticas*; Servicio de Publicaciones de la Universidad de Granada: Granada, Spain, 1979.

48. Vera, J.A. *Geología de España*, 1st ed.; Sociedad Geológica de España e Instituto Geológico y Minero de España, Ministerio de Educación y Ciencia: Madrid, Spain, 2004; 884p.

49. Sanz de Galdeano, C.; Peláez, J.A. *La Cuenca de Guadix–Baza. Estructura, Tectónica Activa, Sismicidad, Geomorfología y Dataciones Existentes*; Universidad de Granada–CSIC: Granada, Spain, 2007; 351p.

50. IGME. Hydrogeological Map of Spain, Scale 1:200,000; Sheet nº 78, Baza; Geological Survey of Spain, Memory and Maps. 1988. Available online: http://info.igme.es/cartografiadigital/tematica/Hidrogeologico200.aspx (accessed on 20 January 2020).

51. IGME. *Hydrogeological Map of Spain, Scale 1:200,000*. Sheet nº 71, Villacarrillo; Geological Survey of Spain, Memory and Maps. 1995. Available online: http://info.igme.es/cartografiadigital/tematica/Hidrogeologico200.aspx (accessed on 20 January 2020).

52. IGME. *Proyecto para la actualización de la infraestructura hidrogeológica de las Unidades 05.01 Sierra de Cazorla, 05.02 Quesada-Castril, 07.07 Sierras de Segura-Cazorla y el Carbonatado de la Loma de Úbeda*; Geological Survey of Spain and General Directorate for Water Planning; Ministry of Industry: Madrid, Spain, 2001. (In Spanish)

53. Peralta-Maraver, I.; López-Rodríguez, M.J.; de Figueroa, J.T. Structure, dynamics and stability of a Mediterranean river food web. *Mar. Freshwater Res.* **2017**, *68*, 484–495. [CrossRef]

54. Alcalá, F.J.; Custodio, E. Atmospheric chloride deposition in continental Spain. *Hydrol. Process.* **2008**, *22*, 3636–3650. [CrossRef]

55. Alcala, F.J.; Custodio, E. Using the Cl/Br ratio as a tracer to identify the origin of salinity in aquifers in Spain and Portugal. *J. Hydrol.* **2008**, *359*, 189–207. [CrossRef]

56. Hurrell, J.W. Decadal trends in the North Atlantic Oscillation, regional temperatures and precipitation. *Nature* **1995**, *269*, 676–679. [CrossRef]

57. Raposo, J.R.; Dafonte, J.; Molinero, J. Assessing the impact of future climate change on groundwater recharge in Galicia-Costa, Spain. *Hydrogeol. J.* **2013**, *21*, 459–479. [CrossRef]

58. Barberá, J.A.; Jódar, J.; Custodio, E.; González-Ramón, A.; Jiménez-Gavilán, P.; Vadillo, I.; Pedrera, A.; Martos-Rosillo, S. Groundwater dynamics in a hydrologically-modified alpine watershed from an ancient managed recharge system (Sierra Nevada National Park, Southern Spain): Insights from hydrogeochemical and isotopic information. *Sci. Total Environ.* **2018**, *640–641*, 874–893. [CrossRef]

59. Pulido-Velazquez, D.; Collados-Lara, A.J.; Alcalá, F.J. Assessing impacts of future potential climate change scenarios on aquifer recharge in continental Spain. *J. Hydrol.* **2018**, *567*, 803–819. [CrossRef]

60. Nathan, R.J.; McMahon, T.A. Evaluation of automated techniques for base-flow and recession analyses. *Water Resour. Res.* **1990**, *26*, 1465–1473. [CrossRef]

61. Arnold, J.G.; Allen, P.M.; Muttiah, R.; Bernhardt, G. Automated Base Flow Separation and Recession Analysis Techniques. *Ground Water* **1995**, *33*, 1010–1018. [CrossRef]

62. Meaurio, M.; Zabaleta, A.; Angel, J.; Srinivasan, R.; Antigüedad, I. Evaluation of SWAT models performance to simulate streamflow spatial origin. The case of a small forested watershed. *J. Hydrol.* **2015**, *525*, 326–334. [CrossRef]

63. Arnold, J.G.; Allen, P.M. Automated Methods for Estimating Baseflow and Ground Water Recharge from Streamflow Records. *JAWRA J. Am. Water Resour. Assoc.* **1999**, *35*, 411–424. [CrossRef]

64. Senent-Aparicio, J.; Pérez-Sánchez, J.; Carrillo-García, J.; Soto, J. Using SWAT and Fuzzy TOPSIS to Assess the Impact of Climate Change in the Headwaters of the Segura River Basin (SE Spain). *Water* **2017**, *9*, 149. [CrossRef]

65. Jimeno-Sáez, P.; Senent-Aparicio, J.; Pérez-Sánchez, J.; Pulido-Velazquez, D. A Comparison of SWAT and ANN models for daily runoff simulation in different climatic zones of peninsular Spain. *Water* **2018**, *10*, 192. [CrossRef]

66. Abbaspour, K.C.; Rouholahnejad, E.; Vaghefi, S.; Srinivasan, R.; Yang, H.; Kløve, B. A continental-scale hydrology and water quality model for Europe: Calibration and uncertainty of a high-resolution large-scale SWAT model. *J. Hydrol.* **2015**, *524*, 733–752. [CrossRef]

67. Moriasi, D.N.; Wilson, B.N.; Douglas-Mankin, K.R.; Arnold, J.G.; Gowda, P.H. Hydrologic and water quality models: Use, calibration, and validation. *Trans. ASABE* **2012**, *55*, 1241–1247. [CrossRef]

68. Hargreaves, G.H.; Samani, Z.A. Estimating potential evapotranspiration. *J. Irrig. Drain. Div. ASCE* **1982**, *108*, 225–230.

69. Arnold, J.G.; Kiniry, J.R.; Srinivasan, R.; Williams, J.R.; Haney, E.B.; Neitsch, S.L. Soil and Water Assessment Tool—Input/Output Documentation—Version 2012. Available online: http://swat.tamu.edu/documentation/ (accessed on 20 December 2019).

70. Moral, F.; Cruz-Sanjulian, J.J.; Olias, M. Geochemical evolution of groundwater in the carbonate aquifers of Sierra de Segura (Betic Cordillera, Southern Spain). *J. Hydrol.* **2008**, *360*, 281–296. [CrossRef]

71. Senent-Aparicio, J.; Jimeno-Sáez, P.; Bueno-Crespo, A.; Pérez-Sánchez, J.; Pulido-Velazquez, D. Coupling machine-learning techniques with SWAT model for instantaneous peak flow prediction. *Biosyst. Eng.* **2019**, *177*, 67–77. [CrossRef]

72. Krause, P.; Boyle, D.P.; Base, F. Comparison of different efficiency criteria for hydrological model assessment. *Adv. Geosci.* **2005**, *5*, 89–97. [CrossRef]

IV.3   PUBLICATION 3: A NOVEL APPROACH TO ASSESSING THE IMPACTS OF DAM
         CONSTRUCTION ON ECOHYDROLOGICAL CONDITIONS IN THE CASTRIL RIVER

Liu, S.; Pérez-Sánchez, J.; Jimeno-Sáez, P.; Alcalá, F.J.; Senent-Aparicio, J. A
novel approach to assessing the impacts of dam construction on ecohydrological
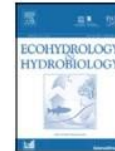conditions in the Castril River basin. *Ecohydrology & Hydrobiolog*, **22(2022)**, *598-608.*
https://doi.org/10.1016/j.ecohyd.2022.08.004

Original Research Article

A novel approach to assessing the impacts of dam construction on hydrologic and ecosystem alterations. Case study: Castril river basin, Spain

Sitian Liu[a], Julio Pérez-Sánchez[b], Patricia Jimeno-Sáez[a], Francisco Javier Alcalá[c,d], Javier Senent-Aparicio[a,*]

[a] Department of Civil Engineering, Catholic University of San Antonio, Campus de los Jerónimos s/n, 30107, Guadalupe, Murcia, Spain
[b] Department of Civil Engineering, Universidad de Las Palmas de Gran Canaria, Campus de Tafira, 35017 Las Palmas de Gran Canaria, Spain
[c] Departamento de Desertificación y Geo-Ecología, Estación Experimental de Zonas Áridas (EEZA–CSIC), 04120 Almeria, Spain
[d] Instituto de Ciencias Químicas Aplicadas, Facultad de Ingeniería, Universidad Autónoma de Chile, 7500138, Santiago, Chile

ARTICLE INFO

ABSTRACT

The hydrological situation of rivers, the fundamental driving force of river ecosystems, has continued to change due to the impact of human activities on water environments. Intra- and inter-annual variation also causes alterations in morphology, water quality, flora, and fauna in riparian zones. In this study, we present a novel approach to assessing the impacts of dam construction on flow river regimes and associated ecosystems in the Castril River (Spain). We compared the altered flows recorded from 2000 to 2018 with those of the natural regime of the river obtained from a previously calibrated hydrological model after the dam was put into operation in 2000. The Indicators of Hydrologic Alteration in RIverS (IAHRIS) method was used because it considers the inter- and intra-annual variabilities of Mediterranean climates. The results showed that the average differences in annual volumes between the natural and altered regimes were below 10% for normal and wet years but decreased to 20.49% in dry years. Thus, the alteration of usual values remained between excellent and good. In droughts and floods, values were from good to moderate, respectively. The flow rate control reduced flow peaks downstream from the dam, decreasing hydrological connectivity of river-riverine-flood plains. This decrease may reduce the transportation of sediment and organic resources, threatening habitat rejuvenation and floodplain biodiversity. This study provides a valuable tool to monitor the impacts of existing dams' regulated regimes, allowing decision makers to develop flow management strategies and adaptation measures to meet ecological water requirements.

© 2022 European Regional Centre for Ecohydrology of the Polish Academy of Sciences. Published by Elsevier B.V. All rights reserved.

1. Introduction

With economic and societal development, the impact of human activities on the ecosystems of rivers and lakes is continually increasing, and the hydrological situation of rivers is constantly changing (Dong et al., 2017). The hydrological situation is the river ecosystem's fundamental at-

* Corresponding author. Tel.: +34 968 278 818.
   E-mail addresses: julio.sanchez@ulpgc.es (J. Pérez-Sánchez), pjimeno@ucam.edu (P. Jimeno-Sáez), fjalcala@eeza.csic.es (F.J. Alcalá), jsenent@ucam.edu (J. Senent-Aparicio).

tribute and an important driving force of its environmental status (Jiang et al., 2014). Its intra- and inter-annual variations cause changes in the morphology and biota of rivers and riparian zones, affecting the normal structure and function of the river ecosystem and even potentially leading to an irreversible ecological crisis (Zuo and Liang, 2015). In recent decades, the intensification of human activities has profoundly impacted rivers and altered most of their original biodiversity (Gierszewski et al., 2020). Therefore, analysing the characteristics of changes in hydrological conditions before and after human interference and assessing their impacts on river ecosystems are important research issues for river health assessment.

There are more than 1,200 large dams in Spain, most of which were constructed during the mid-20th century. They have significantly contributed to the country's socio-economic development (Mezger et al., 2021). This large number of dams positions Spanish rivers as among the most regulated worldwide. Several studies have recently been published analysing the hydrologic alteration caused by dams in Spanish rivers. Vicente-Serrano et al. (2017) studied highly regulated basins, such as the Segre River basin in Northeastern Spain, highlighting the significant impact of existing dams on the frequency, duration and severity of hydrological droughts. Peñas and Barquín (2019) evaluated the degree of hydrological alteration at 139 gauging stations located below dams, concluding that the most significant hydrological impact was the modification of the intra-annual variability of daily flows. García de Jalón et al. (2019) classified the natural variability of rivers in different basins in Northern Spain according to their variability from the pre-dam to the post-dam period. Mezger et al. (2021) investigated hydrological alteration in 22 Spanish rivers under altered hydrological regimes and analysed the impact of the implementation of ecological flows on correcting this alteration. While these studies are of considerable interest, they all use different methodologies based on observed flow data, making it difficult to separate the effects of dam construction from those of climate change. In addition, most of these studies have focused on rivers in the country's northern half; few studies have been undertaken in the southeast of peninsular Spain.

A literature review of previous studies (do Vasco et al., 2019; Gunawardana et al., 2021; Yan et al., 2021; Zhang et al., 2016) shows that the most common method of assessing the hydrological impacts of dam construction is a comparison of the indicators of hydrological alteration (IHA) calculated for different periods before and after dam construction (pre-impact and post-impact periods). Based on observed data, this methodology requires fewer data and is easy to implement (Lu et al., 2018), but it does not permit a separate analysis of the impacts of climate change and dam construction. In the case of the Spanish Mediterranean, where the effects of climate change on water resources are particularly severe (Senent-Aparicio et al., 2018), differentiating between the two factors is necessary. Accordingly, a previously calibrated hydrological model was used to simulate the post-impact period, which allowed for an analysis of the influence of dam construction without the influence of climate change on the flow series. Previous works using this framework are scarce (Brouziyne et al., 2022; Zhang et al., 2020; Lu et al., 2018; Mittal et al., 2014).

The Portillo Dam is located in Southern Spain and began operation in 1999. It is located inside a nature preserve whose main environmental value is the river and its surrounding ecosystems. The dam has received fierce opposition from ecologists and conservationists due to its negative environmental effects on the Castril River (Hervás-Gámez and Delgado-Ramos, 2019). This study compared the natural flow regime data (without the dam effect) and the altered flow regime data (with the dam effect) from 2001 to 2018. Therefore, this study's objectives were as follows: (a) to present a framework to assess the impacts of dam construction on the flow regime and watershed ecosystem; (b) to explore the long-term trend of hydrologic metrics; (c) to analyse the possible causes of flow changes and the potential ecological and morphological impacts in downstream reaches; and (d) to provide several recommendations for management strategies to improve the hydrological conditions of the river, which can significantly affect ecological sustainability.

2. Materials and methods

2.1. Study area and data

The Castril River is a mountain stream located at the headwater of the Guadalquivir River Basin in the province of Granada, Andalusia, in Southern Spain (Figure 1). The high-permeability bedrock basin causes a large infiltration and an important interbasin groundwater flow in its water balance (Senent-Aparicio et al., 2020). The GRB is adjacent to the Segura River Basin. The study area of the watershed is 120 km² with altitudes varying from 2,130 m.a.s.l. in the north to 837 m.a.s.l. in the reservoir in the south. The dam and reservoir were built to regulate the river's flow, with a capacity of 34.50 hm³ and a surface of 143 ha. The Spanish government commissioned it, and it came into operation in 1999. It is a rockfill dam with an impervious core of 82.40 m above the foundation and a coronation length of 369 m. It was designed for a maximum peak flow of 529 m³/s, with a spillway lip fixed at 500 m³/s of capacity and a bottom outlet of 35 m³/s. Furthermore, a hydroelectric plant uses a 72-metre waterfall at the base of the dam with a flow of 4.50 m³/s and a total capacity of 2,958 kW.

The climate is continental Mediterranean (Capel-Molina, 1981), with dry summers and cold winters. The annual average temperature is about 8° C, the winter temperature is lower than 0° C, and the highest temperature in summer is over 40° C. The average annual potential evapotranspiration is about 800 mm (Vanderlinden et al., 2004), and the average annual precipitation is about 770 mm. The most rainfall occurs from autumn to spring. Winter is characterized by a cold north wind and humid west wind, while summer and autumn are dominated by southeast winds, high temperatures and less rainfall than in the other seasons (Trigo et al., 2004).

The Castril River Basin is located within Sierra de Castril Natural Park, which the European Natura 2020
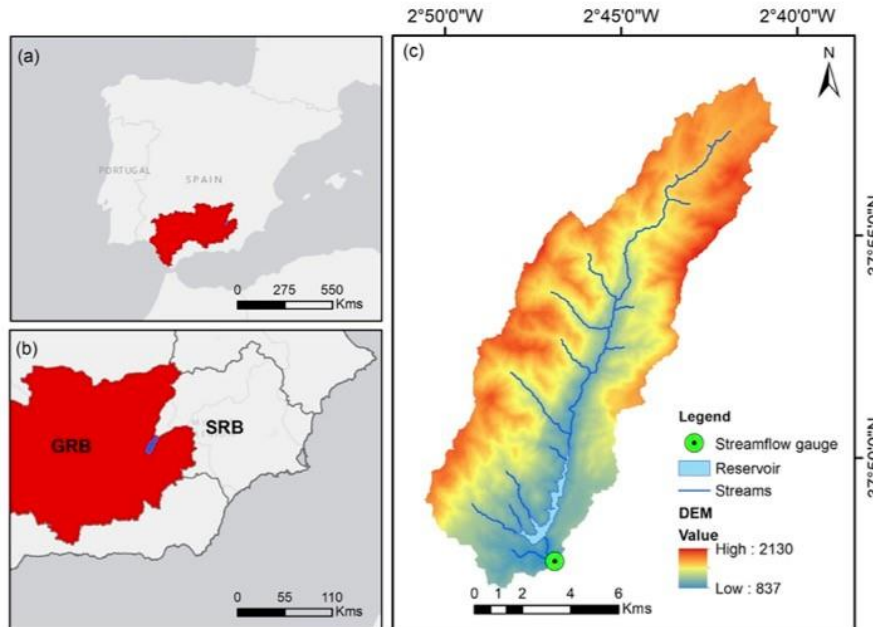
Figure 1. (a) Situation of Guadalquivir River Basin (GRB). (b) Location of the Castril River Basin (CRB). (c) Digital Elevation Model (DEM) of the CRB.

network catalogued as a special wildlife conservation site. The river is the park's core value and is responsible for the environment's morphology and singularity. It is also home to an interesting population of brown trout (*Salmo trutta*), with unique genetic varieties (Gortázar et al., 2007). Additionally noteworthy is the presence of the otter (*Lutra lutra*), the barbel (*Luciobarbus sclateri*) and the boga (Pseudochondrostoma willkommii). Birds in this area include the dipper, the grey heron and the martin fisherman. Numerous amphibians, reptiles and other organisms and more than 150 taxa of aquatic macroinvertebrates are protected by the European Habitats Directive 92/43/CEE (MITECO, 2020). Black pines and junipers are found in mountainous areas, while poplars, willows and ash trees alternate with rushes (Scirpus holoschoenus) and herbs (*Ranunculaceae Umbelliferae and Compositae*) in the riverine (Peralta-Maraver et al., 2016).

The input data used for the implementation of the model were a 25-metre resolution Digital Elevation Model (DEM) obtained from the Spanish Instituto Geográfico Nacional (IGN), the Harmonized World Soil Database (HWSD) soil map and a land use map downloaded from the Andalusia Environmental Information Network (REDIAM). The meteorological data were extracted from the precipitation grid available from the Spanish Meteorological State Agency (AEMET) and the temperature data from the SPAIN02 dataset (Herrera et al., 2016). In addition, observed pre- and post-impact daily flows were downloaded

from the Centre for Public Works Studies and Experimentation (CEDEX) website. Table 1 shows the main characteristics of these datasets. More details on this model can be found in Senent–Aparicio et al. (2020).

2.2. Methodological approach

From a methodological perspective, the vast majority of recent studies on the influence of dams on a river's ecohydrological conditions have used the set of IHA developed by Richter et al. (1996). In this work, though, we have used the indicators included in the IAHRIS free software designed specifically for the climatic conditions of Spain, as they consider the pronounced inter- and intra-annual variability characteristic of Mediterranean climates. Although their use in the recent literature is scarce, there are some examples of their successful application (Aznarez et al., 2021; López-Ballesteros et al., 2020; Pérez-Sánchez et al., 2020; Magdaleno et al., 2018).

Furthermore, a novel approach was applied to quantify the hydrological impact of the start-up of the Portillo Dam without considering the climate change impact. Instead of directly comparing the observed flows before and after the dam began operation, the natural regime of the Castril River was simulated using a previously calibrated hydrological model (Senent-Aparicio et al., 2020). Given the complexity of the case study, this model was developed by the combined application of the SWAT hydrological

Table 1
Main characteristics of the input data sources used.

Variable	Source	Resolution	Link
DEM	IGN	25 m	http://centrodedescargas.cnig.es/CentroDescargas/index.jsp
Soil	HWSD	1 km^2	https://www.fao.org/soils-portal/soil-survey/soil-maps-and-databases/harmonized-world-soil-database-v12/ru/
Land use	REDIAM	1:25000	https://www.juntadeandalucia.es/medioambiente/portal/acceso-rediam
Precipitation	AEMET	5 km	https://www.aemet.es/es/serviciosclimaticos/cambio_climat/datos_diarios
Temperature	SPAIN02	10 km	http://www.meteo.unican.es/datasets/spain02
Streamflow	CEDEX	-	https://ceh.cedex.es/anuarioaforos/default.asp

model and the chloride mass balance method to quantify the amount of interbasin groundwater flow characteristic of high-permeability bedrock basins, such as the CRB. As can be deduced from an analysis of the model's goodness of fit, the statistics performed by the model provide an acceptable reflection of the natural hydrological regime of the Castril River. For calibration and validation, the monthly Nash–Sutcliffe Efficiency was 0.77 and 0.80, respectively, while its daily logarithmic values were 0.81 and 0.64, respectively (Senent-Aparicio et al., 2020).

The methodological approach followed in this work consisted of two main steps: (1) A previously calibrated model (Senent-Aparicio et al., 2020) was used to simulate the natural flow series from 2001 to 2018, and (2) simulated and observed daily flows were implemented using IAHRIS software to analyse the influence of the Portillo Dam on the Castril River's ecohydrological conditions.

2.3. IAHRIS

IAHRIS is free software developed by CEDEX, which evaluates the degree of hydrological and environmental changes through a series of indicators. IHARIS is suitable for Spain because hydrological alteration is assessed according to the criteria established by the Spanish Hydrological Planning Instruction. In IAHRIS, the IHA value is obtained by comparing 19 parameters (Table 2) of the natural and altered regimes. Three are derived from annual flow, six from monthly flow and the rest from daily flow. These indicators are divided into usual values, maximum extreme values (floods) and minimum extreme values (droughts). Five aspects of the impact on the ecosystem are considered: magnitude, variability, seasonality, duration and frequency at each level.

With these parameters, 21 IAH values can be obtained (Table 3). Each IAH value corresponds to a comparison of natural and altered hydrological conditions. The ratio between the natural and altered parameter values ranges from 0 to 1, where 1 means no alteration and 0 means total alteration. When the IAH is higher than 1, the obtained value is replaced by its inverse, thus ensuring the proportionality in the variation of both regimes (natural versus altered) and avoiding the compensations that would result in global alteration index calculus if there were indices lower and higher than 1. A detailed description of the IAHRIS method is found in Fernández et al. (2012) and Pérez-Sánchez et al. (2020).

Mediterranean rivers are characterised by important inter-annual and seasonal variability and frequent floods (Fernández et al., 2012); therefore, the study and discretisation of inter-annual usual values were necessary previous stages. This discretisation aimed to determine the streamflow thresholds that allow years to be classified as wet, medium or dry. It was considered a wet year if the annual volume in the natural regime was higher than the 25th percentile. If the annual volume was lower than the 75th percentile, that year was considered dry, and the years between the 25th and 75th percentiles were catalogued as normal years. Thus, an indicator was obtained for each type, and finally, a weighted year indicator was calculated according to Equation 1.

$$\text{Indicator weighted year} = 0.25\,\text{Indicator wet year}$$
$$+ 0.5\,\text{Indicator normal year} + 0.25\,\text{Indicator dry year}$$
$$(1)$$

IAHRIS uses the colours recommended by Ecological Quality Ratios (WFD, 2003) to classify IAH into five hydrologic states (Table 4). The higher the index's value, the lower the hydrological alteration. Blue indicates excellent ecological status. Green, yellow, orange and red indicate good, moderate, deficient and very deficient status, respectively.

IAHRIS also provides two types of results for each of the three groups (usual, droughts and floods). On one side is a spider chart that shows the similarities and differences between natural and altered regime indicators (Figure 2). On the other side, an index of global alteration (IAG) is calculated for usual values, droughts and floods. The IAG is quantified by the ratio between the areas of the natural and altered polygons of the spider chart. A colour code was established to present the hydrologic states (Table 5).

3. Results

3.1. Characterisation of the inter-annual variability during the period 2001-2018

The IAHRIS divided the 17 years of the studied period (2001–2018) into wet, normal and dry years according to the 25th and 75th percentile of the annual volume of the natural regime. These values resulted in 41,902 hm^3 and 103,627 hm^3, respectively. As shown in Fig. 3, the two series performed similarly, although the dry and normal year volumes were almost always higher in a regulated regime than in a natural regime. Two years considered dry in the natural regime (2001–02 and 2005–06) were considered normal in the regulated regime, thus halving the years considered dry. In wet years, the opposite is true, with an average decrease in peak volume of 7.72% except for the last year of the studied period (2017–18), when there was an increase of 20.39% in annual volume, changing from normal to wet year in the altered regime. The inter-annual

Table 2
Parameters of IAHRIS.

Group	Aspect		Description	Parameter
Usual values	Annual and monthly volumes	Magnitude	Mean of annual volumes	P1
		Variability	Difference between maximum and minimum volume in the year	P2
		Seasonality	Months of maximum and minimum volume in the year	P3
	Daily flows	Variability	Differences between average flows of 10% and 90% percentiles	P4
Extreme values	Maximum daily flow (floods)	Magnitude and frequency	Average of annual maximum daily flow	Qc (P5)
			Effective discharge	Q_{GL} (P6)
			Connectivity flow	Q_{CONEC} (P7)
			Usual flow in flooding (5% exceedance percentile)	Q5% (P8)
		Variability	Coefficient of variation of annual maximum daily flow	Cv (Qc) (P9)
				Cv (Q5%) (P10)
			Coefficient of variation of usual flow in flooding	
		Duration	Consecutive days in a year with exceedance percentile below 5%	Duration of flooding (P11)
		Seasonality	Average number of days per month with exceedance percentile above 5%	One value per month (P12)
	Minimum daily flow (droughts)	Magnitude and frequency	Average annual minimum	Qs (P13)
			Usual flow in droughts (95% exceedance percentile)	Q95% (P14)
		Variability	Coefficient of variation of annual minimum daily flow	Cv (Qs) (P15)
				Cv (Q95%) (P16)
			Coefficient of variation of usual flow in droughts	
		Duration	Consecutive days in a year with exceedance percentile below 95%	Duration of droughts (P17)
			Average number of days per month with null flow	One value per month (P18)
		Seasonality	Average number of days per month with exceedance percentile below 95%	One value per month (P19)

Table 3
Indicators of hydrological alteration.

Group	Aspect	IAH indicator	Description	Parameter
Usual Values	Magnitude	IAH1	Magnitude of annual volume	P1
		IAH2	Magnitude of monthly volume	P1
	Variability	IAH3	Habitual variability	P4
		IAH4	Extreme variability	P2
	Seasonality	IAH5	Seasonality of maximums	P3
		IAH6	Seasonality of minimums	P3
Floods	Magnitude and Frequency	IAH7	Magnitude of maximum floods	P5
		IAH8	Magnitude of effective discharge	P6
		IAH9	Frequency of connectivity flow	P7
		IAH10	Magnitude of usual floods	P8
	Variability	IAH11	Variability of maximum floods	P9
		IAH12	Variability of usual floods	P10
	Duration	IAH13	Floods' duration	P11
	Seasonality	IAH14	Seasonality of floods (one for each month)	P12
Droughts	Magnitude and Frequency	IAH15	Magnitude of extreme droughts	P13
		IAH16	Magnitude of usual droughts	P14
	Variability	IAH17	Variability of extreme droughts	P15
		IAH18	Variability of usual droughts	P16
	Duration	IAH19	Duration of droughts	P17
		IAH20	Number of days of null flow (one for each month)	P18
	Seasonality	IAH21	Seasonality of droughts (one for each month)	P19

Table 4
Hydrologic states in IAHRIS.

Category	Level IExcellent	Level IIGood	Level IIIModerate	Level IVDeficient	Level VVery deficient
Range	$0.8 < \text{IAH} \leq 1$	$0.6 < \text{IAH} \leq 0.8$	$0.4 < \text{IAH} \leq 0.6$	$0.2 < \text{IAH} \leq 0.4$	$0 < \text{IAH} \leq 0.2$

Table 5
Hydrologic state of IAG in IAHRIS.

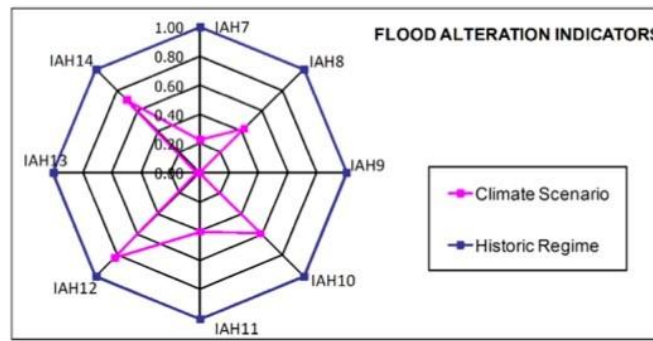| Category	Level IExcellent	Level IIGood	Level IIIModerate	Level IVDeficient	Level VVery deficient
Range	$0.64 < IAG \leq 1$	$0.36 < IAG \leq 0.64$	$0.16 < IAG \leq 0.36$	$0.04 < IAG \leq 0.16$	$0 < IAG \leq 0.04$

Figure 2. Example of spider chart of IAHRIS.
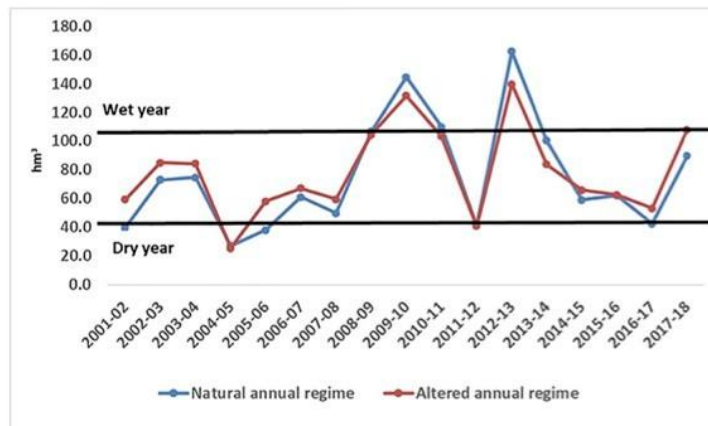
Figure 3. Comparison of natural and altered annual regime for the 2001-2018 period. The dry and the wet years correspond to 41,902 hm³ and 103,627 hm³, respectively.

water balance from 2001 to 2018 resulted in an increase in volume in the altered regime that was 9.64% over that of the modelled natural regime.

3.2. Characterisation of intra-annual variability

The average monthly volumes in the natural and altered regimes are shown in Figure 4. An analysis of intra-annual variability enabled the differentiation of two main seasonal periods: one from May to October (both included) of low flow and the other from November to April (both included), of higher water volume that reached its maxi-

mum in March. The tendencies in the three types of years (wet, normal and dry) generally follow similar patterns, but the differences in steepness and peaks are significant. The flow regime showed more significant changes in the autumn and winter. In October, the volume in the altered regime increased to over 100% (106.38%) more than in the natural regime in wet years and reached 122% in December in normal years and 77% in November in dry years. In fact, the volumes were generally higher in the altered regime, except in August, due to the scarce rainfall in the summer and spring for wet and normal years, when the maximum values were recorded. Nonetheless, the natural regime vol-

Figure 4. Monthly volumes in natural and altered regimes (by type of year).

umes were below the altered regime in normal and dry years for eight and nine months, respectively.
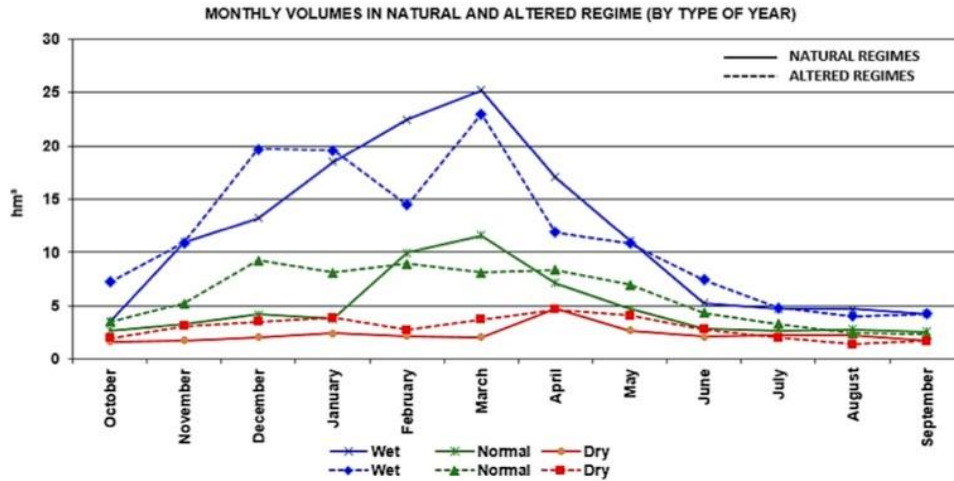
3.3. Indicators of hydrological alteration for the period 2001-2018

IHARIS parameters were used to assess hydrological changes in the Castril River during dam construction, comparing the regulated–altered and natural–modelled volumes from 2001 to 2018. Table 6 shows the usual values for the normal, wet and dry years and the weighted year, which was obtained using Eq. 1, based on the percentage of each type in the series. The average differences in annual volumes between the natural and altered regimes were below 10% in normal and wet years but decreased to 20.49% in dry years. However, due to dam regulation, the average annual volume of the weighted year was 3.76% higher than in the natural regime. March and April remained the months with maximum volumes in both regimes, but the months with minimum volumes moved forward from September and October in the natural regime to August in the altered regime.

As previously noted and shown in the spider charts, the factor showing the greatest change in all types of years was seasonality. Although in normal years it ranged from good (0.70) to excellent (0.91) levels, the seasonality of minimum values, mainly in dry years (0.33) but also in wet years (0.46), resulted in the moderate alteration of minimum values (0.55) in the weighted year. The average of days with a flow lower than the 95th percentile of the studied series increased in the regulated regime during the summer season, especially in August (5.2 days) and September (3.3 days). The inverse occurred, however, for the remainder of the year, with a decrease in the number of days with very low volumes (lower than the 95th per-

centile), especially in autumn, when the difference reached an average of 6.2 days in November. Despite this, the maximum number of consecutive days in the year with a volume lower than the 95th percentile remained similar, with 27.06 days in the natural regime and 26.47 days in the altered regime. Equally noteworthy is that the magnitude and variability in nearly half of the indicators for the three types of years showed inverse values, meaning that the altered volumes were higher than in the natural regime. Table 7 summarises the river's hydrological state. The usual values indicated a good hydrological state, with the IAG varying between 0.47 and 0.65 for dry and normal years, respectively. The latter value guaranteed excellent status for the river.

Tables 8 and 9 showed the calculated results of extreme values. The IAG value of droughts was 0.69, an excellent status, and the IAG value of floods was 0.35, a moderate status close to the threshold of good (0.36). The latter result indicated that the extreme values in floods were more deficient than the extreme values in droughts. As with normal values, the seasonality in droughts was the most affected parameter. Only IAH21 for droughts (seasonality) had a value of lower than 0.6, which lies between moderate and good status. The worst results were obtained from August to November at the end of the year's driest period. The rest of the indicators were good to excellent, thus not suggesting serious problems in drought periods that could affect the riverine ecosystem or hydraulic conditions. Spider charts for floods indicated the largest shrinkage in the studied area, as shown in Table 8. Regarding the IHA values of floods, the frequency of connectivity flow (IAH9) and flood duration (IAH13) were both deficient, with values of 0.28 and 0.37, respectively. The regulation of the magnitude (IAH7) and variability (IAH11) of maximum floods under the dam's influence was moderate,

Table 6
IHA of usual values for natural and altered regimes for the period 2001-2018 (* Inverse).

Group	Aspect	Code	Value	Spider Chart
Usual Values – Wet year	Magnitude	IAH1	0.92	
		IAH2	0.72*	
	Variability	IAH3	0.67*	
		IAH4	0.67	
	Seasonality	IAH5	0.88	
		IAH6	0.46	
Usual Values – Normal year	Magnitude	IAH1	0.87*	
		IAH2	0.71*	
	Variability	IAH3	0.83	
		IAH4	0.82*	
	Seasonality	IAH5	0.91	
		IAH6	0.70	
Usual Values – Dry year	Magnitude	IAH1	0.81	
		IAH2	0.68*	
	Variability	IAH3	0.81	
		IAH4	0.71*	
	Seasonality	IAH5	0.79	
		IAH6	0.33	
Usual Values – Weighted year	Magnitude	IAH1	0.87	
		IAH2	0.70	
	Variability	IAH3	0.77	
		IAH4	0.76	
	Seasonality	IAH5	0.87	
		IAH6	0.55	

Table 7
IAG of usual values for natural and altered regimes for the period 2001-2018.

Aspect	Value	Code	Level
Usual Values – Wet year	0.51	IAG$_{II}$ WET YEAR	
Usual Values – Normal year	0.65	IAG$_{II}$ NORMAL YEAR	
Usual Values – Dry year	0.47	IAG$_{II}$ DRY YEAR	
Usual Values – Weighted year	0.54	IAG$_{II}$ WEIGHTED YEAR	

with values of 0.55 and 0.53, respectively. The regulation of the magnitude (IAH7) and variability (IAH11) of maximum floods under the influence of the dam were moderate, with values of 0.55 and 0.53, respectively. The control of flow peaks downstream of the dam significantly reduced the risk of flood hazards, but it has also led to a decline in the hydrological connectivity of river-riverine-flood plains.

4. Discussion

Despite an increase of nearly 10% in volume in the altered regime over that of the modelled natural regime and, consequently, an overall positive inter-annual environmental outlook, intra-annual variations in stream flow are significant to riverine ecosystem conservation and livelihood development (Richter et al., 1996; Li et al., 2014). A regulated flow regime should reproduce a natural flow regime as much as possible, both in instream and out-of-stream conditions, to guarantee the river's health (IFC, 2004).

The analysis of the intra-annual variability also points in the same direction: the Portillo Dam has a significant regulating effect on the watershed's regime of volumes. After the dam's completion, the river's maximum flow regime decreased in high-volume periods due to flood retention and peak reduction in the wet years. On the other hand, the river's minimum flow increased in the

Table 8

IHA of extreme values for natural and altered regimes for the period 2001-2018 (* Inverse).

Group	Aspect	Code	Value	Spider Chart
Floods	Magnitude and frequency	IAH7	0.55*	
		IAH8	0.81*	
		IAH9	0.28	
		IAH10	0.92	
	Variability	IAH11	0.53	
		IAH12	0.72	
	Duration	IAH13	0.37	
	Seasonality	IAH14	0.86	
Droughts	Magnitude and frequency	IAH15	0.82*	
		IAH16	0.98*	
	Variability	IAH17	0.76	
		IAH18	0.74*	
	Duration	IAH19	0.98	
		IAH20	1.00	
	Seasonality	IAH21	0.56	

Table 9

IAG of extreme values for natural and altered regimes for the period 2001-2018.

Aspect	Aspect	Aspect	Level
Floods	0,35	IAG_F	
Droughts	0,69	IAG_D	

dry years to meet the downstream water requirements. Despite this, and even though the annual average volumes for all types of years were higher in altered regimens than in natural ones, the variations in seasonality, especially in wet years, could substantially modify the floodplain conditions (Zheng et al., 2019) and alter the river eco-environment (Ngor et al., 2018; Lin and Qi, 2017; Pool et al., 2017; Zhang et al., 2016; Arias et al., 2014; Junk et al. 1989). Notwithstanding, the increase in altered volumes in the natural regime ensures the necessary availability of habitat for aquatic and terrestrial organisms (Gonçalves, 2003), soil moisture in the riverine and access to spawning areas (Friday and Haxton, 2021; Hayes et al., 2018) It also ensures the heterogeneity and quality of the habitat and the non-exclusive competence between species (Arthington, 2012).

The relative modifications in seasonality during the driest periods can affect the quality of water, the synchronism of phenology of many vegetal and animal species (Naiman et al., 2002) and the colonisation of exotic species (Bunn and Arthington, 2002). Nevertheless, the moderate changes in droughts in the rest of the considered parameters because of the regulation of dams ensure the avail-

ability of habitats and the sustainability of aquatic habitats (Bae and Park, 2019, Aspin et al., 2019).

Floods experienced the largest alterations, with a significant reduction in connectivity flow (Q_{CONEC}) in the altered regime. This volume is particularly important for riparian habitat dynamics and periodic flood-dependent ecosystems. Connectivity flow guarantees accessibility to this band and adequate moisture, which is vital for the biota's different levels and the habitat's rejuvenation (Martínez and Fernández, 2010). Many studies have been carried out on the effects of modifications in flood regimes on fauna and vegetation in the river environment (Whipple et al., 2017; Richter and Richter, 2000; Hickey and Salas, 1995). Transversal connectivity is critical for maintaining the diversity and functionality of macroinvertebrate communities (Collier and Scarsbrook, 2000). Moreover, from a geomorphological point of view, processes of erosion and sedimentation could be altered as well as the lack of hydraulic variability in the riverbed and the floodplains (Guo et al., 2018; Wohl et al., 2015; Thoms and Sheldon, 2002).

5. Conclusions

In this study, the impact of the Portillo Dam on the hydrological status and ecological environment of the Castril River was assessed by comparing the altered flows recorded from 2000 to 2018 with those of the natural regime of the river obtained from the previously calibrated hydrological model. Significant results were obtained from this work and are as follows:

1. Regarding inter-annual variations, the trends of altered and natural regimes in normal and dry years were similar, although the number of the latter was halved. The peak volume in wet years decreased by 7.72% on average.

2. Intra-annual flow alterations were characterised by general volume increases in the regulated regime, especially in normal and dry years. Yet flood retention and peak reduction in the wet years reduced the maximum flow regime in high-volume periods.

3. The usual IAG values (0.47–0.65) and IAG values for droughts (0.69) indicated a lack of serious problems that could affect the riverine ecosystem or hydraulic conditions.

4. The IAG value for floods was 0.35, a moderate hydrological status with a relevant deficiency in the frequency of connectivity flow and flood duration.

5. The control of flow peaks downstream of the dam declined in terms of the hydrological connectivity of river-riverine-flood plains, thus reducing the transport of sediment and organic resources and threatening, for instance, the rejuvenation of the habitat and the floodplain biodiversity.

The sustainability of river ecosystems must be actively monitored to mitigate the negative impacts of the regulated regime of existing dams. This study methodology can significantly help practitioners implement integrated approaches in flow management strategies and develop adaptation measures to meet ecological water requirements.

Declaration of Competing Interest

The authors declare that they have no known competing financial interests or personal relationships that could have appeared to influence the work reported in this paper.

Acknowledgements

References

Arias, M.E., Piman, T., Lauri, H., Cochrane, T.A., Kummu, M., 2014. Dams on Mekong tributaries as significant contributors of hydrological alterations to the Tonlé Sap Floodplain in Cambodia Hydrology and Earth System Sciences 18 (12), 5303.

Arthington, A.H., 2012. Environmental flows: saving rivers in the third millennium. University of California Press, Berkeley, 424. USA.

Aspin, T.W.H., Khamis, K., Matthews, T.J., Milner, A.M., O'Callaghan, M.J., Trimmer, M., Ledger, M.E., 2019. Extreme drought pushes stream invertebrate communities over functional thresholds. Global Change Biology 25, 230–244. doi:10.1111/gcb.14495.

Aznarez, C., Jimeno-Sáez, P., López-Ballesteros, A., Pacheco, J.P., Senent-Aparicio, J., 2021. Analysing the impact of climate change on hydrological ecosystem services in Laguna del Sauce (Uruguay) using the SWAT model and remote sensing data. Remote Sensing 13 (10).

Bae, M.J., Park, Y.S., 2019. Evaluation of precipitation impacts on benthic macroinvertebrate communities at three different stream types. Ecological Indicators 102, 446–456. doi:10.1016/j.ecolind.2019.02.060.

Brouziyne, Y., Belaqziz, S., Benaabidate, L., Aboubdillah, A., El Bilali, A., El-beltagi, A., Tzoraki, O., Chehbouni, A., 2022. Modeling long term response of environmental flow attributes to future climate change in a North African watershed (Bouregreg watershed, Morocco). Ecohydrology & Hydrobiology 22 (1), 155–167.

Bunn, S., Arthington, A., 2002. Basic Principles and Ecological Consequences of Altered Flow Regimes for Aquatic Biodiversity. Environmental Management 30, 492–507. doi:10.1007/s00267-002-2737-0.

Capel-Molina, J.J., 1981. Los Climas de España, Oikos-Tau ed., Barcelona, Spain.

Collier, K.J., Sacrsbrook, M.K., 2000. Use of riparian and hyporheic habitats. New Zealand Stream Invertebrates: ecology and implications for management. New Zealand Limnological Society. NIWA.

Dong, Z, Zhang, J, Zhao, J., 2017. Comments upon progress of environmental flows assessments. Journal of Hydraulic Engineering 48 (6), 670–677.

do Vasco, A.N., Netto, A.D.O.A., da Silva, M.G., 2019. The influence of dams on ecohydrological conditions in the São Francisco River Basin. Brazil. Ecohydrology & Hydrobiology 19 (4), 556–565.

Fernández, J.A., Martínez, C., Magdaleno, F., 2012. Application of indicators of hydrologic alterations in the designation of heavily modified water bodies in Spain. Environmental Science & Policy 16, 31–43. doi:10.1016/j.envsci.2011.10.004.

Friday, M., Haxton, T., 2021. Evaluating the effects of controlled flows on historical spawning site access, reproduction and recruitment of lake sturgeon Acipenser fulvescens. Journal of Fish Biology 99 (6), 1940–1957. doi:10.1111/jfb.14900.

García de Jalón, S., González del Tánago, M., García de Jalón, D., 2019. A new approach for assessing natural patterns of flow variability and hydrological alterations: The case of the Spanish rivers. Journal of environmental management 233, 200–210.

Gonçalves Moreira De Jesús, M.T., 2003. Impacto de centrais mini-hídricas na qualidade biológica da água: a "Cascata"do Alva (Portugal). III Congreso Ibérico sobre gestión y planificación del agua. La Directiva Marco del Agua: realidades y futuros, Sevilla, Spain.

Gortázar, J., García de Jalón, D., Alonso-González, C., Vizcaino, P., Baeza, D., Marchamalo, M., 2007. Spawning period of a southern brown trout population in a highly unpredictable stream. Fish Ecology Journal 16, 515–527. doi:10.1111/j.1600-0633.2007.00246.x.

Gierszewski, P.J., Habel, M., Szmańda, J., Luc, M., 2020. Evaluating effects of dam operation on flow regimes and riverbed adaptation to those changes. Science of the Total Environment 710, 136202.

Gunawardana, S.K., Shrestha, S., Mohanasundaram, S., Salin, K.R., Piman, T., 2021. Multiple drivers of hydrological alteration in the transboundary Srepok River Basin of the Lower Mekong Region. Journal of Environmental Management 278, 111524.

Guo, L., Su, N., Zhu, C., He, Q., 2018. How have the river discharges and sediment loads changed in the Changjiang River basin downstream of the Three Gorges Dam? Journal of Hydrology 560, 259–274. doi:10.1016/j.jhydrol.2018.03.035.

Hayes, D.S., Brändle, J.M., Seliger, C., Zeiringer, B., Ferreira, T., Schmutz, S., 2018. Advancing towards functional environmental flows for temperate floodplain rivers. Science of the Total Environment 633, 1089–1104. doi:10.1016/j.scitotenv.2018.03.221.

Herrera, S., Fernández, J., Gutiérrez, J.M., 2016. Update of the Spain02 gridded observational dataset for EURO-CORDEX evaluation: assessing the effect of the interpolation methodology. International Journal of Climatology 36 (2), 900–908. doi:10.1002/joc.4391.

Hervás-Gámez, C., Delgado-Ramos, F., 2019. Critical Review of the Public Participation Process in Drought Management Plans, The Guadalquivir River Basin Case in Spain. Water Resources Management 33, 4189–4200. doi:10.1007/s11269-019-02354-0.

Hickey, J.T., Salas, J.D., 1995. Environmental effects of extreme floods in Proceedings of the Italy Research Workshop on the Hydrometeorology, Impacts, and Management of Extreme Floods. Perugia, Italy.

IFC, Instream Flow Council, 2004. Instream Flows for Riverine Resource Stewardship, revised ed., Cheyenne, Wyo.

Jiang, L., Ban, X., Wang, X., Cai, X., 2014. Assessment of hydrologic alterations Cased by Three Gorges Dam in the middle and lower reaches of Yangtze River, China. Water 6 (5), 1419–1434.

Junk, W.J., Bayley, P.B., Sparks, R.E., 1989. The flood pulse concept in river-floodplain systems. Canadian Special Publication of Fisheries and Aquatic Sciences 106, 110–127.

Li, F., Zhang, G., Xu, Y.J., 2014. Spatiotemporal variability of climate and streamflow in the Songhua River Basin, northeast China. Journal of Hydrology 514, 53–64.

Lin, Z., Qi, J., 2017. Hydro-dam – A nature-based solution or an ecological problem: The fate of the Tonlé Sap Lake. Environmental Research 158, 24–32. doi:10.1016/j.envres.2017.05.016.

López-Ballesteros, A., Senent-Aparicio, J., Martinez, C., Pérez-Sánchez, J., 2020. Assessment of future hydrologic alteration due to climate change in the Aracthos River basin (NW Greece). Science of The Total Environment 733, 139299.

Lu, W., Lei, H., Yang, D., Tang, L., Miao, Q., 2018. Quantifying the impacts of small dam construction on hydrological alterations in the Jiulong River basin of Southeast China. Journal of Hydrology 567, 382–392.

Magdaleno, F., Donadio, C., Kondolf, G.M., 2018. 30-year response to damming of a Mediterranean river in California, USA. Physical Geography 39 (3), 197–215.

Martínez, C., Fernández, J.A., 2010. IAHRIS 2.2 Indicators of Hydrologic Alteration in Rivers: Methodological Reference Manual.

Mezger, G., del Tánago, M.G., De Stefano, L., 2021. Environmental flows and the mitigation of hydrological alteration downstream from dams: The Spanish case. Journal of Hydrology 598, 125732.

MITECO, Ministerio para la Transición Ecológica y el Reto Demográfico, 2020. Evaluación y seguimiento del estado ecológico del río Castril y de los caudales ecológicos aguas abajo del embalse del portillo, online http://altiplanogranada.org/wp-content/uploads/2020/10/PRIMER-INFORME-PARCIAL-caudales-ecol%C3%B3gicos.pdf.

Mittal, N., Mishra, A., Singh, R., Bhave, A.G., van der Valk, M., 2014. Flow regime alteration due to anthropogenic and climatic changes in the Kangsabati River. India. Ecohydrology & Hydrobiology 14 (3), 182–191.

Naiman, R.J., Bunn, S.E., Nilsson, C., Petts, G.E., Pinay, G., Thompson, L.C., 2002. Legitimizing Fluvial Ecosystems as Users of Water: An Overview. Environmental Management 30 (4), 455–467.

Ngor, P.B., Oberdorff, T., Phen, C., Baehr, C., Grenouillet, G., Lek, S., 2018. Fish assemblage responses to flow seasonality and predictability in a tropical flood pulse system. Ecosphere 9 (11). doi:10.1002/e02366.10.1002/ecs2.2366.

Peñas, F.J., Barquín, J., 2019. Assessment of large-scale patterns of hydrological alteration caused by dams. Journal of Hydrology 572, 706–718.

Peralta-Maraver, I., López-Rodríguez, M.J., Tierno de Figueroa, J.M., 2016. Structure, dynamics and stability of a Mediterranean river food web. Marine and Freshwater Research 68 (3), 484–495. doi:10.1071/MF15154.

Pérez-Sánchez, J., Senent-Aparicio, J., Martínez Santa-María, C., López-Ballesteros, A., 2020. Assessment of Ecological and Hydro-Geomorphological Alterations under Climate Change Using SWAT and IAHRIS in the Eo River in Northern Spain. Water 12 (6), 1745. doi:10.3390/w12061745.

Pool, T., Holtgrieve, G., Elliott, V., McCann, K., McMeans, B., Rooney, N., Smits, A., Phanara, T., Cooperman, M., Clark, S., Phen, C., Chhuoy, S., 2017. Seasonal increases in fish trophic niche plasticity within a floodpulse river ecosystem (Tonle Sap Lake, Cambodia). Ecosphere 8 (7). doi:10.1002/ecs2.1881.

Richter, B.D., Baumgartner, J.V., Powell, J., Braun, D.P., 1996. A method for assessing hydrologic alteration within ecosystems. Conservation Biology 10 (4), 1163–1174.

Richter, B.D., Richter, H.E., 2000. Prescribing Flood Regimes to Sustain Riparian Ecosystems along Meandering Rivers. Conservation Biology 14, 1467–1478. doi:10.1046/j.1523-1739.2000.98488.x.

Senent-Aparicio, J., Liu, S., Pérez-Sánchez, J., López-Ballesteros, A., Jimeno-Sáez, P., 2018. Assessing impacts of climate variability and reforestation activities on water resources in the headwaters of the Segura River Basin (SE Spain). Sustainability 10 (9), 3277.

Senent-Aparicio, J., Alcalá, F.J., Liu, S., Jimeno-Sáez, P., 2020. Coupling SWAT Model and CMB Method for Modeling of High-Permeability Bedrock Basins Receiving Interbasin Groundwater Flow. Water 12, 657. doi:10.3390/w12030657.

Thoms, M.C., Sheldon, F., 2002. An ecosystem approach for determining environmental water allocations in Australian dryland river systems: the role of geomorphology. Geomorphology 47, 153–168.

Trigo, R., Pozo-Vázquez, D., Osborn, T., Castro-Díez, Y., Gámiz-Fortis, S., Esteban-Parra, M., 2004. North Atlantic oscillation influence on precipitation, river flow and water resources in the Iberian Peninsula. International Journal of Climatology 24, 925–944. doi:10.1002/joc.1048.

Vanderlinden, K., Giráldez, J.V., Van Meirvenne, M., 2004. Assessing Reference Evapotranspiration by the Hargreaves Method in Southern Spain. Journal of Irrigation and Drainage Engineering 130, 184–191. doi:10.1061/(ASCE)0733-9437(2004)130:3(184).

Vicente-Serrano, S.M., Zabalza-Martínez, J., Borràs, G., López-Moreno, J.I., Pla, E., Pascual, D., Savé, R., Biel, C., Funes, I., Azorin-Molina, C., Sanchez-Lorenzo, A., Martín-Hernández, N., Peña-Gallardo, M., Alonso-González, E., Tomas-Burguera, M., El Kenawy, A., 2017. Extreme hydrological events and the influence of reservoirs in a highly regulated river basin of northeastern Spain. Journal of Hydrology: Regional Studies 12, 13–32.

WFD, Water Framework Directive, 2003. Online: https://ec.europa.eu/environment/water/water-framework/facts_figures/guidance_docs_en.htm.

Whipple, A.A., Viers, J.H., Dahlke, H.E., 2017. Flood regime typology for floodplain ecosystem management as applied to the unregulated Cosumnes River of California. United States. Ecohydrology 10, e1817. doi:10.1002/eco.1817.

Wohl, E., Bledsoe, B.P., Jacobson, R.B., LeRoy Poff, N., Rathburn, S.L., Walters, D.M., Wilcox, A.C., 2015. The Natural Sediment Regime in Rivers: Broadening the Foundation for Ecosystem Management. BioScience 65 (4), 358–371. doi:10.1093/biosci/biv002.

Yan, M., Fang, G.H., Dai, L.H., Tan, Q.F., Huang, X.F., 2021. Optimizing reservoir operation considering downstream ecological demands of water quantity and fluctuation based on IHA parameters. Journal of Hydrology 600, 126647.

Zhang, Z., Huang, Y., Huang, J., 2016. Hydrologic alteration associated with dam construction in a medium-sized coastal watershed of southeast China. Water 8 (8), 317.

Zhang, Z., Liu, J., Huang, J., 2020. Hydrologic impacts of cascade dams in a small headwater watershed under climate variability. Journal of Hydrology 590, 125426.

Zheng, Y., Zhang, G., Wu, Y., Xu, Y.J., Dai, C., 2019. Dam Effects on Downstream Riparian Wetlands: The Nenjiang River, Northeast China. Water 11, 2038. doi:10.3390/w11102038.

Zuo, Q., Liang, S., 2015. Effects of dams on river flow regime based on IHA/RVA. Proceedings of the International Association of Hydrological Sciences 368, 275–280.

IV.4   SUMMARY OF RESULTS AND DISCUSSIONS

IV.4.1 Impact of climate variability and reforestation activities on the components of water balance

To investigate the effect of climate variability and reforestation activities, a 25-m resolution digital elevation model (DEM) from the National Geographic Institute (IGN, 2018) was used. The soil information was taken from the Harmonized World Soil Map (HWSM) (Nachtergaele F.O.; Van Velthuizen H.; Verelst L. and Wiberg D., 2012), which has a spatial resolution of about 1 km. The Andalusian Network of Environmental Information (REDIAM) of the Regional Government of Andalusia (REDIAM, 2010) provided the land use data in 1956 and 2007 at a scale of 1: 25,000. The SWAT model was driven by meteorological data from a variety of sources, including precipitation and temperature data. The precipitation data came from the AEMET grid, version 1.0, which offers daily rainfall in Spain for the 1951–2016 period with a spatial resolution of 5 km. More information about this dataset can be found in Peral-García et al. (Peral García C., Navascués Fernández-Victorio B., and Ramos Calzado P., 2017). Temperature data were gathered from the fifth version of the SPAIN02 high-resolution (approximately 10 km) gridded dataset, which covers the years 1951 to 2016. Herrera et al. (Herrera S., Fernández J. and Gutiérrez J.M., 2016) provided detail documentation of the development and analysis of the SPAIN02 dataset. The streamflow discharge data at the basin outlet were accessible on the Hydrographical Study Centre website (MAGRAMA, 2018).

IV.4.1.1 Model setup and research framework

The land use, soil, and slope maps were used to divide the data into hydrologic response units (HRUs, which are unique computational units of land coverage and soil types with uniform hydrologic responses, as defined above). To exclude minor land uses, soils, and slopes in each sub-basin and improve model processing, 10% threshold values were defined, and the SWAT interface identified 44 HRUs. The interface employed these threshold values to filter out minor land uses, soil types, and slopes in each sub-basin.

In this study, the calculated parameters to estimate the impacts of reforestation activities were based on the land use data of 1956 from the natural 1951–1970 period. The model validation and calibration were done by using streamflow discharge data from 1 January 1964 to 31 December 1970 and from 1 January 1954 to 31 December 1963, respectively. The first three years (1951–1953) as a warm-up period were employed to allow the model parameters to approach equilibrium. The sequential uncertainty fitting tool (SUFI-2) in the SWAT Calibration and Uncertainty Programs (Abbaspour K.C., 2012) was used for sensitivity analysis and automatic calibration. To begin, a global sensitivity analysis was used to determine the most important parameters in managing streamflow. After 500 model runs, a ranking of parameter sensitivities was created to see the impact of each parameter on the objective function (Abbaspour K., Vaghefi S. and Srinivasan R., 2018). The Nash–Sutcliffe coefficient (NSE) was employed as the goal function in an automatic calibration procedure to select the best parameter values based on the observed streamflow. A total of 1000 simulations were run, with the parameters revised after the first 500 simulations.

Three simulation experiments were set up at the HWSRB to study the impacts of climate and land use on water resources: scenario A used land use and climate conditions around the 1950s and 1960s (land use in 1956 and climate for the period 1951–1970); scenario B fixed land use in 1956 and actual weather conditions for the period 1996–2015; and scenario C used land use in 2007 and actual climate
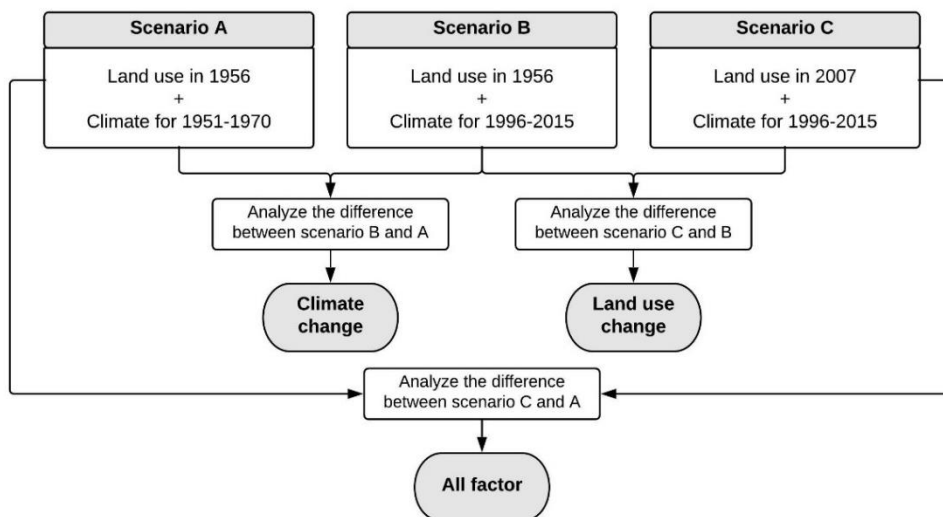

Figure 8. Flow diagram of the research framework.

conditions for the period 1996–2015. The effects of climate variability (the variations between B and A), reforestation (the difference between C and B), and all factors (the difference between C and A) on water resources were evaluated using these scenarios (Figure 8).

IV.4.1.2 Model setup and research framework

The MK test was used to evaluate the yearly and monthly trends in precipitation, temperature, and streamflow from 1951 to 2015. Table 8 showed the values of the MK test statistic (Test Z) and Sen's slope for various months.

Table 8. Trend analysis results.

Month	Precipitation			Maximum Temperature			Minimum Temperature			Streamflow		
	Test Z	Sig.	Q_i	Test Z	Sig.	Q_i	Test Z	Sig.	Q_i	Test Z	Sig.	Q_i
Jan	−0.42		−0.19	−0.53		−0.01	−1.74	a	−0.02	−0.98		−0.03
Feb	0.06		0.03	−0.42		−0.01	−1.78	a	−0.02	−1.12		−0.03
Mar	−1.46		−0.51	1.00		0.02	−2.78	c	−0.02	−1.32		−0.05
Apr	−0.70		−0.17	1.22		0.02	−1.14		−0.01	−1.14		−0.03
May	0.59		0.17	1.27		0.02	−0.12		0.00	0.30		0.00
Jun	−2.26	b	−0.33	3.95	d	0.06	1.55		0.01	1.13		0.01
Jul	−1.48		−0.04	3.43	d	0.04	−0.43		−0.01	1.61		0.01
Aug	0.03		0.00	3.39	d	0.04	1.03		0.01	1.83	d	0.01
Sep	0.43		0.07	−0.29		0.00	−0.35		0.00	0.23		0.00
Oct	−0.41		−0.12	0.43		0.01	−0.39		0.00	−0.79		−0.01
Nov	−0.50		−0.17	−1.39		−0.02	−1.52		−0.02	−1.15		−0.02
Dec	−1.54		−0.67	−0.59		−0.01	−1.47		−0.02	−1.93	d	−0.05
Annual	−1.59		−2.22	2.16	b	0.02	−1.35		−0.01	−0.67		−0.12

Test Z is the MK test statistic; Q_i is the Sen's slope estimator; [a] indicates a significance level of 0.1; [b] indicates a significance level of 0.05; [c] indicates a significance level of 0.01; [d] indicates a significance level of 0.001.

As shown in Table 8, the biggest slope in terms of precipitation can be noticed in March, June and December. It was found that eight of the twelve months had a downward trend. On a seasonal scale, the most significant reductions occur in the summer and winter months. With a slope of 2.22 mm/year, yearly precipitation dropped over the study area. Streamflow and precipitation were all on the decline. Between October and April, streamflow decreases dramatically due to the interplay of reforestation and climate variable factors.

At the 5% significant level, the annual maximum air temperature showed a significant rising trend. In June, the trend reached its peak magnitude. With the exception of the winter months, the maximum air temperature increased throughout the year. When compared to the increasing magnitude of the maximum air temperature, the decreasing magnitude of the minimum air temperature was smaller. The decreasing magnitudes in the cold months were larger than in the warm months when compared to the monthly changes. In March, the drop in minimum air temperature was very noticeable, with 0.01 level of significance.

In summary, the mean annual rainfall in the recent 1996–2015 period declined by 81 mm compared to the 1951–1970 period, while the mean annual temperature in the HWSRB increased by 0.13 °C, showing that the climate is becoming warmer and drier. Climate change and intensive human activities have both contributed to a 16 percent decline in mean annual streamflow in recent years.

The land uses in the HWSRB in 1956 and 2007 are showed in Table 9, which presented that the shrubland and rainfed agriculture areas decreased and the forests area increased. All the details of the land-cover type changes can be found in Table 9.

Table 9. The conversion percentage (%) of each land-use type from 1956 to 2007.

Land Cover Type	Area Coverage (km²)		Area Coverage (%)		Change (1956–2007)	
	1956	2007	1956	2007	By km²	By %
Urban Areas	0.16	0.21	0.07	0.09	0.05	+0.02
Water Bodies	0.00	0.44	0.00	0.19	0.44	+0.19
Agricultural Land	17.04	5.48	7.23	2.32	−11.56	−4.91
Grassland	30.96	36.52	13.13	15.49	+5.56	+2.36

Forests	54.91	89.17	23.29	37.82	+34.26	+14.53
Shrubland	82.16	67.37	34.85	28.57	−14.79	−6.28
Transitional Woodland/Shrub	50.06	34.46	21.23	14.62	−15.6	−6.61
Barren Land	0.49	2.13	0.21	0.90	1.64	0.69

IV.4.1.3 Sensitivity analysis, calibration and validation of the SWAT model

The global sensitivity analysis found that the most influential parameters were the effective hydraulic conductivity in tributary channel alluvium (CH_K1), the U.S. Soil Conservation Service curve number (CN2), the moist bulk density (SOL_BD), the saturated hydraulic conductivity (SOL_K), the groundwater delay (GW_DELAY), the maximum canopy storage (CANMX), the lateral flow travel time (LAT_TTIME) and the available water capacity of the soil layer (SOL_AWC). The soil evaporation compensation factor (ESCO) parameter was not considered in the sensitivity analysis, but it was still added as a significant parameter according to the earlier research for this basin (De Almeida Bressiani D., Srinivasan R. and Jones C.A., 2015; Senent-Aparicio J., et al., 2017). Table 10 shows the adjusted values and ranges for each parameter.

Table 10. Calibration parameters.

Parameter	Description	Value Range	Adjusted Value
CH_K1	Effective hydraulic conductivity in tributary channel alluvium.	0 to 300	17.94
LAT_TTIME	Lateral flow travel time.	0 to 180	109.95
CN2	SCS runoff curve number.	−20% to +20%	+8.75%
SOL_K	Saturated hydraulic conductivity.	0 to 2000	0.054
GW_DELAY	Groundwater delay (days).	0 to 500	242.46
CANMX	Maximum canopy storage.	0 to 100	8.65
SOL_AWC	Available water capacity of the soil layer.	0 to 1	0.0567
SOL_BD	Moist bulk density.	0.9 to 2.5	2.40
ESCO	Soil evaporation compensation factor.	0 to 1	0.5725

Table 11 shows the performance of SWAT model in calibration and validation periods. The R^2, NSE, PBIAS and RSR of the calibration period (1954–1963) for monthly runoff were 0.87, 0.86, −14.11% and 0.38 respectively. The R^2, NSE, PBIAS and RSR of the validation period (1964–1970) for monthly runoff were 0.93, 0.88, −17.23% and 0.35 respectively. The model had good performance both in the calibration and the validation period.

Table 11. Performance of SWAT model during calibration and validation periods in the HWSRB.

Period	R^2	NSE	PBIAS	RSR
Calibration (1954–1963)	0.87	0.86	−14.11	0.38
Validation (1964–1970)	0.93	0.88	−17.23	0.35
Scenario C	0.72	0.85	21.93	0.53

Figure 9 shows observed and simulated monthly streamflow discharge data in the Anchuricas Reservoir for the calibration (1954–1963) and validation (1964–1970) periods. In addition, this research also validated the model by comparing the simulated results using the 2007 land-use map (scenario C) with observed
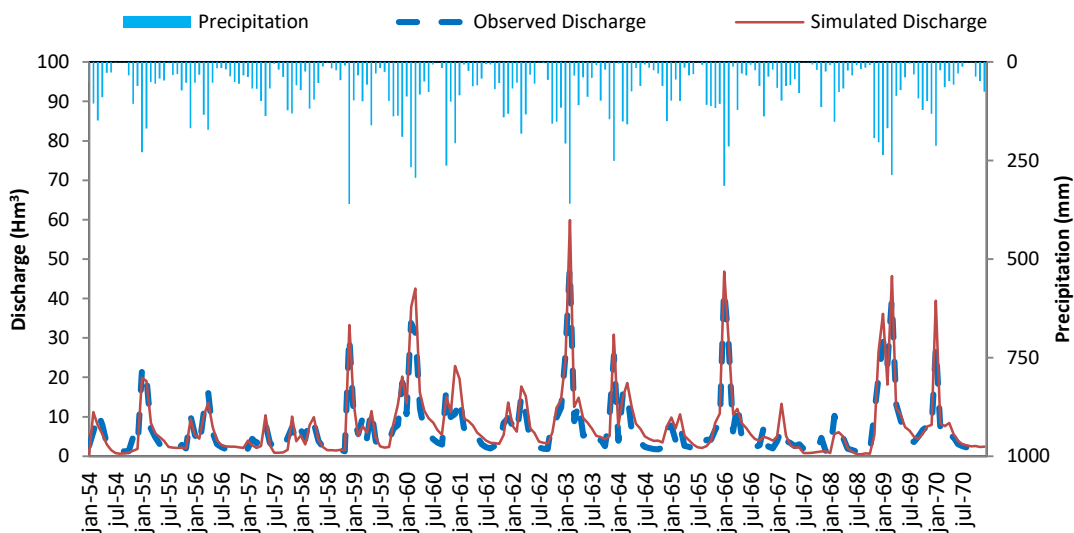
Figure 9. Calibration (1954–1963) and validation (1964–1970) results of SWAT model in Anchuricas Reservoir

streamflow discharge during the period 1996–2015 (Figure 10). The values of model evaluation statistics such as NSE, R^2, PBIAS and RSR were 0.72, 0.85, 21.93 and 0.53, respectively (Table 11). These values indicate that the calibrated model satisfactorily simulates the monthly runoff.
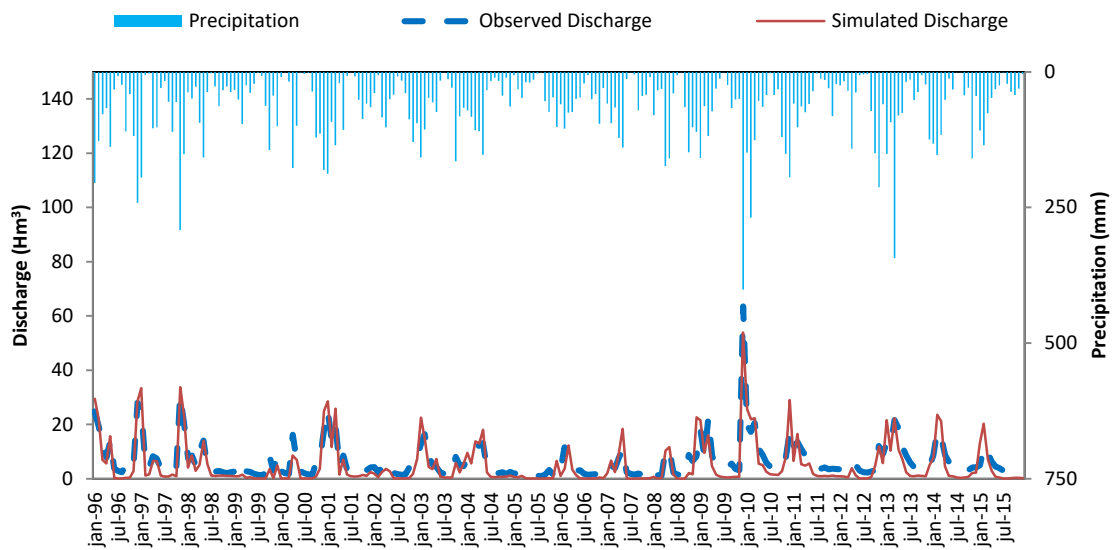
Figure 10. Observed and simulated monthly discharge data for the period 1996−2015 (scenario C) in Anchuricas Reservoir

IV.4.1.4 Impacts of climate and LCLU changes on Runoff and ET at HWSRB

Table 12 shows the annual mean runoff and ET simulated by SWAT under the three different scenarios analyzed.

Table 12. Simulated average annual runoff and ET under various scenarios.

Scenarios	Climate	LUCC	P (mm)	Runoff (mm)	ET (mm)	Runoff change	ET change
A	1951–1970	1956	895.4	363.7	493.1		
B	1996–2015	1956	814.1	302.0	479.9	−61.7	−13.2
C	1996–2015	2007	814.1	267.9	524.9	−95.8	+31.8

The results show how both climate variability and reforestation plans decreased runoff. Compared with Scenario A, the simulated runoff decreased by 95.8 mm in Scenario C, which was a combined effect of climate change and the reforestation. When compared Scenarios A and B with the impact of climate change, it showed that surface runoff decreased significantly by 61.7 mm, which accounted for 64.4% of the total runoff reduction.

ET was discovered that increased by 31.8 mm with the combined effect of climate and LCLU changes. Even the temperature increased slightly but with the significant decrease in precipitation, the climate change caused a decrease of 13.2 mm in ET. This suggested that the reforestation planscontributed to a 45 mm increase in ET values, greatly exceeding the impact of the climate variability on ET.

IV.4.2 Coupling SWAT model and CMB method for modelling of high–permeability bedrock basins receiving Interbasin Groundwater Flow

IV.4.2.1 Estimating IGF using CMB datasets

As introduced in Section III.1, the entire hydrogeological system that contributes to streamflow at the CRB headwater outlet encompasses the CRB headwater surface as well as some hydraulically related nearby areas from the GRW and SRW. Once a steady hydrogeological functioning without land-use changes and water usages was proven, the 10 km × 10 km nodal mean values and standard deviations of R from the CMB method (Alcalá and Custodio, 2014; 2015) can be considered to be identical to nodal mean values and standard deviations of baseflow.

For the control period (1996–2005), nodal mean R varied between 143 and 332 mm/year, implying recharge–to–precipitation ratios of 0.29–0.37; mean R standard deviation varied between 39 and 90 mm/year, implying that the given coefficients of variation of mean annual R (mean value/standard deviation) were in the 0.27–0.30 range (Table 13).

Fitting parameters were determined to construct the yearly R data series in the CRB and upstream GRW and SRW contributing areas for the control period (1996–2005), which are shown in Table 14. The resultant surface–weighted yearly P and R series are shown in Table 15.

Table 13. For the 10 km × 10 km cells covering the CRB and upstream GRW and SGW contributing areas, nodal mean values and standard deviations of precipitation and net aquifer recharge.

	CRB					GRW					SRW				
Cell [1]	S	P [2]	CVP	R	CVR	S	P	CVP	R	CVR	S	P	CVP	R	CVR
3200						3.2	894	0.31	315	0.27	0.8	894	0.31	315	0.27
3201	10.4	909	0.33	332	0.27	20.2	909	0.33	332	0.27					
3202	60.6	693	0.34	229	0.28	4.8	693	0.34	229	0.28					
3203	7.1	486	0.35	143	0.27										
3275						1.0	813	0.32	276	0.27	21.7	813	0.32	276	0.27
3276	22.0	668	0.33	206	0.29	14.5	668	0.33	206	0.29	25.0	668	0.33	206	0.29
3277	1.8	517	0.35	153	0.30	1.1	517	0.35	153	0.30					
3349						0.1	687	0.32	212	0.27	0.5	687	0.32	212	0.27
3350						2.0	612	0.33	186	0.28	0.5	612	0.33	186	0.28
Sum	101.9					46.9					48.4				
SWA [3]		692	0.34	227	0.28		787	0.33	269	0.28		736	0.32	239	0.28

[1] Cell ID as in Figure 1c, after Alcalá and Custodio (2014; 2015). [2] S is surface in km², P and R are mean precipitation and mean net aquifer recharge over the control period (1996–2005) in mm year⁻¹, and CVP and CVR are the dimensionless coefficients of variation of mean P and R over the control period (1996–2005) as fractions. [3] SWA is surface–weighted average.

Table 14. Fitting parameters for the CRB and upstream GRW and SGW areas

Parameter [1]	CRB	GRW	SRW
$\Delta\mu$	–0.67	–0.66	–0.67
$\Delta\sigma$	–0.73	–0.71	–0.72
μ_C	227	269	239
σ_C	63.1	74.9	66.8

[1] $\Delta\mu$ and $\Delta\sigma$ are dimensionless, and μ_C and σ_C are in mm year⁻¹.

Table 15. For the control period (1996–2005), surface–weighted yearly series of (i) P and R in the CRB and in upstream GRW and SRW areas, and (ii) IGF from GRW and SRW area contributing to CRB.

Year	P [1]	Pni [1]	R, CRB [1]	R, GRW	R, SRW	IGF,GRW+SRW [2]
1996	1037.9	1.76	338.5	401.4	357.1	378.9
1997	978.9	1.47	319.8	379.2	337.3	357.9
1998	472.3	−1.08	159.2	188.7	167.4	177.9
1999	575.4	−0.56	191.9	227.5	202.0	214.6
2000	669.5	−0.09	221.7	262.9	233.6	248.0
2001	742.6	0.28	244.9	290.4	258.1	274.0
2002	616.8	−0.35	205.0	243.1	215.9	229.3
2003	723.7	0.19	238.9	283.3	251.8	267.3
2004	641.5	−0.23	212.9	252.4	224.2	238.1
2005	406.9	−1.40	138.5	164.1	145.5	154.7
Mean [3]	686.6		227.1	269.3	239.3	240.1
SD	199.2		63.1	74.9	66.8	66.8
CV	0.29		0.28	0.28	0.28	0.28

[1] P and R are annual precipitation and net aquifer recharge in mm year^{-1}, and Pni is dimensionless normalized yearly P. [2] IGF is Interbasin Groundwater Flow in mm year^{-1}. [3] Mean and SD are mean and standard deviation over the control period (1996–2005) in mm year^{-1}, and CV is dimensionless coefficient of variation as a fraction.

Yearly R and P series for the control period (1996–2005) were compared in each area. The resulting parametric functions allowed for the extension of the calculated yearly R series to cover the yearly P full record in the 1951–2016 period (Figure 11). Figure 12 depicts the yearly baseflow series supplied by the CBR, as well as the yearly surface–weighted IGF series given by upstream GRW and SRW regions. IGF was slightly higher than baseflow supplied within the CRB and accounted for around 51% of total CRB baseflow.
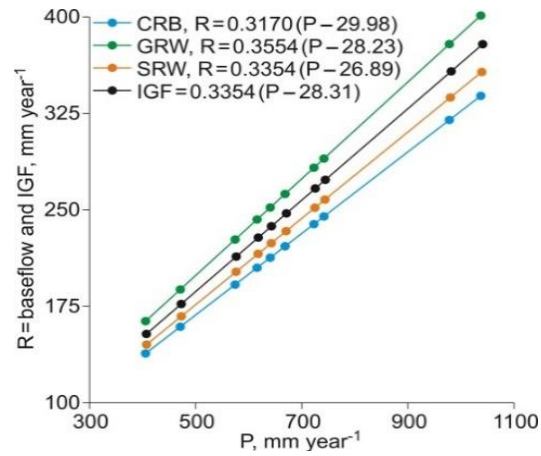
Figure 11. For the control period (1996–2005), parameterization of yearly P–R functions in the CRB and upstream GRW and SRW contributing areas; yearly R equals yearly baseflow. Yearly IGF series refers to the surface–weighed sum of upstream R = baseflow from GRW and SRW areas contributing to the CRB streamflow. In all cases, the Pearson coefficient of correlation is 1.
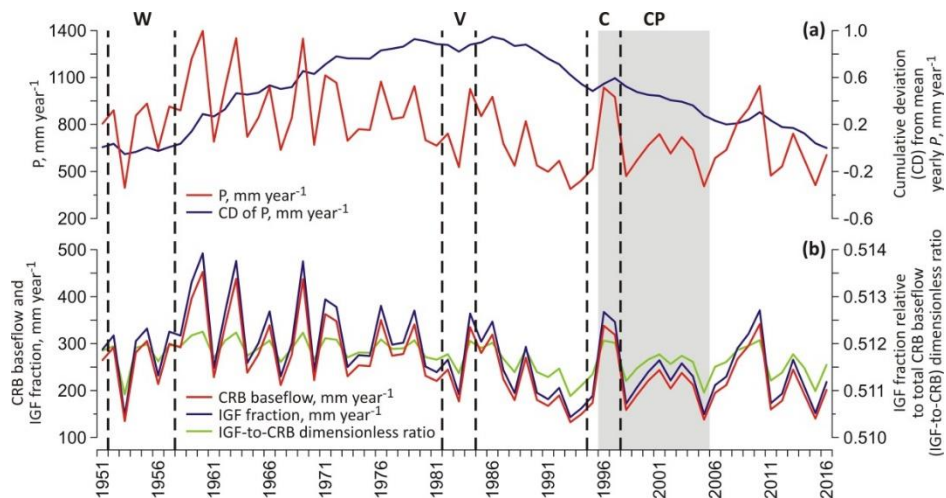
Figure 12. For the full period (1951–2016), (a) surface–weighted yearly P series in the area compiled from the AEMET grid version 1.0 and cumulative deviation (CD) from mean yearly P in mm year^{-1}; and (b) generated yearly baseflow series in the CRB and yearly surface–weighed IGF series from upstream GRW and SRW contributing areas in mm year^{-1}, and IGF fraction relative to total CRB baseflow (IGF-to-CRB) dimensionless ratio. The control period (1996–2005) is grey shallowed (CP). Vertical dotted lines indicate selected time intervals for the SWAT model warm–up (W), calibration (C), and validation (V) phases.

IV.4.2.2 Comparison of SWAT model results with and without IGF

The CRB was divided into 29 subbasins after DEM analysis and SWAT Model implementation. A total of 149 HRUs were created using a combination of land uses, soil types, and slope ranges (<2%, 2–8%, >8%). To improve model processing, the HRU definition thresholds were set to 5%. The Hargreaves non–global method was used to simulate potential evapotranspiration experiences (Hargreaves G.H. and Samani Z.A., 1982), so only the precipitation and temperature data were required to run SWAT model.

The SWAT model was implemented on a monthly scale with and without IGF from 1995 to 1997. When IGF was not included, the observed and initial simulated streamflows differed significantly (Figure 13). The discrepancy between observed and corrected simulated streamflow shrank dramatically when IGF was added as an additional baseflow fraction. The statistics NSE and PBIAS improved when IGF was counted, according to this preliminary evaluation of model performance (Figure 13). In absolute terms, the model's performance improved by nearly 100%.

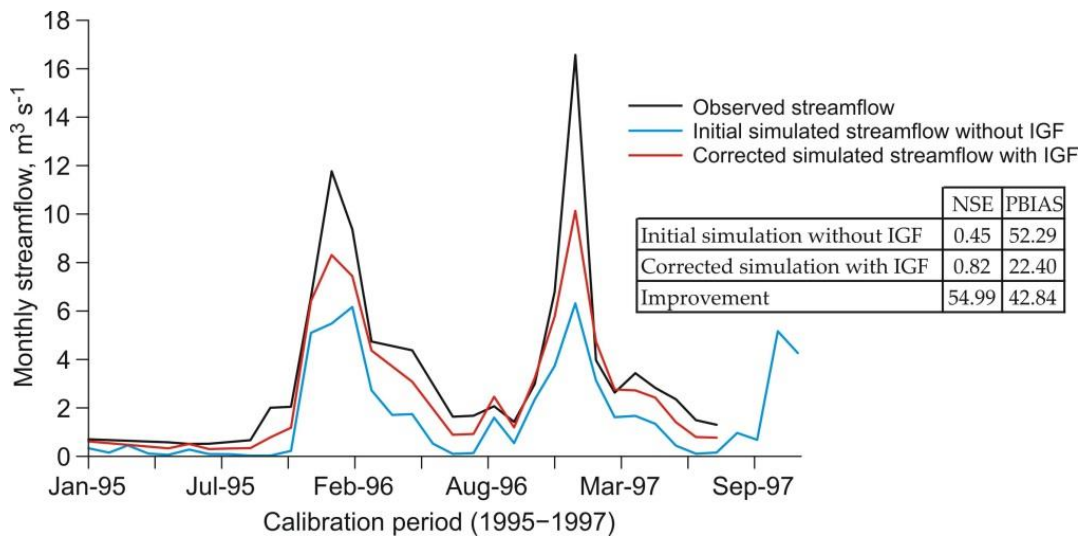|	NSE	PBIAS
Initial simulation without IGF	0.45	52.29
Corrected simulation with IGF	0.82	22.40
Improvement	54.99	42.84

Figure 13. For the selected calibration period (1995−1997) and on a monthly scale, observed streamflow compared to (i) initial simulated streamflow without IGF and (ii) corrected simulated streamflow with IGF. The statistics NSE and PBIAS show the model performance achieved in each simulation.

IV.4.2.3 Calibration and validation of SWAT model including IGF

The following datasets were used to establish the SWAT model: (1) the 25-m resolution DEM from the Spanish National Geographic Institute (IGN); (2) the land-use map (scale 1:25,000) from the Andalusian Environmental Information Network (REDIAM); (3) the 1-km resolution georeferenced soil data from the World Soil Coordination Map; (4) the 5-km resolution nodal daily precipitation series cover the period 1951–2017 in Spain from the AEMET grid version 1.0; (5) the 10-km resolution nodal daily temperature series for the period 1951–2016 from the fifth version of the high resolution SPAIN02 grid; and (6) the 24-h streamflow records downloaded from the CEDEX website.

The SUFI–2 algorithm of SWAT–CUP (Calibration and Uncertainty Programs) to calibrate and validate the SWAT model was used. Twenty-one commonly used flow calibration parameters and their ranges were first selected based on the past simulation experiences (Senent-Aparicio J. et al., 2017; Jimeno-Sáez P. et al., 2018). The final ranges used and the final fitted values of these parameters are given in Table 16.

Two iterations (representing 500 simulations each) were undertaken with the goal of attaining an acceptable calibration, the first including 13 parameters on a monthly scale and the second including 8 parameters on a daily scale. A five-year warm-up period was given to reduce the effect of the initial soil-water condition (Abbaspour K.C. et al., 2016). The calibration and validation phases were chosen from the 1995-1997 and 1982-1984 periods, respectively. Because the downloaded daily streamflow series was discontinuous, the calibration and validation time intervals were carefully chosen to minimize the impact of existing data gaps. The statistics NSE, lnNSE, R^2, PBIAS, RMSE, and RSR were used to determine model efficiency criteria.

The magnitude of calibrated GW_REVAP, ESCO, LAT_TTIME, GWQMN, and ALPHA_BF parameters were quite close to those obtained in previously-modelled regions with similar orography, geology, climate, and land use (Senent-Aparicio J. et al., 2017; Jimeno-Sáez P. et al., 2018). The ESCO was similarly comparable to those used in other Mediterranean karst regions, where annual actual evapotranspiration is typically 0.7–0.9 times annual precipitation (Alcalá F.J. et al., 2011; Andreu J.M. et al., 2011; Vanderlinden K. et al., 2004). ALPHA BF's low

value suggested a delayed aquifer reaction (Arnold J.G. et al., 2019; Moral F. et al., 2008).

Table 16. Description of parameters used for SWAT model calibration in the CRB headwater.

Parameter[1]	Description	Range used in calibration	Fitted value
r_CN2.mgt	SCS runoff curve number.	–0.1 to 0.1	0.08
v_ALPHA_BF.gw	Baseflow alpha factor (day^{-1}).	0 to 1	0.11
a_GW_DELAY.gw	Groundwater delay time (day).	0 to 60	2.82
a_GWQMN.gw	Threshold depth of water in the shallow aquifer for return flow to occur (mm).	–200 to 1000	898.00
v_GW_REVAP.gw	Groundwater revap coefficient.	0.02 to 0.1	0.09
a_RCHRG_DP.gw	Deep aquifer percolation fraction.	–0.05 to 0.05	0.04
a_REVAPMN.gw	Threshold depth of water in shallow aquifer for revap or percolation to deep aquifer to occur (mm).	–500 to 500	–61.00
v_CANMX.hru	Maximum canopy storage (mm).	0 to 8	0.47
v_EPCO.bsn	Plant uptake compensation factor.	0.5 to 1	0.56
v_ESCO.bsn	Soil evaporation compensation factor.	0.3 to 0.8	0.61
r_SOL_AWC.sol	Available water capacity of the soil layer (mm H_2O/mm soil).	–0.02 to 0.02	–0.02
v_LAT_TTIME.hru	Lateral flow travel time (day).	0 to 180	76.50
v_SLSOIL.hru	Slope length for lateral subsurface flow (m).	0 to 150	1.35
r_SLSUBBSN.hru	Average slope length (m).	–0.5 to 0.5	0.08
r_HRU_SLP.hru	Average slope steepness (m/m).	–0.5 to 0.5	0.40
v_OV_N.hru	Manning's 'n' value for overland flow.	0.01 to 1	0.61

r_CH_S1.sub	Average slope of tributary channels (m/m).	–0.5 to 0.5	0.26
v_CH_N1.sub	Manning's 'n' value for the tributary channels.	0.01 to 30	1.68
r_CH_S2.rte	Average slope of main channel along the channel length (m/m).	–0.5 to 0.5	–0.04
v_CH_N2.rte	Manning's 'n' value for the main channel.	0.01 to 0.3	0.04
v_SURLAG.bsn	Surface runoff lag coefficient.	0.05 to 24	20.71

[1] (r_) refers to relative change, i.e., the current parameter must be multiplied by (1 + the value obtained in calibration), (v_) means that the existing parameter value must be replaced by the value obtained in calibration, and (a_) refers to absolute change, i.e., the fitted value must be added to the existing value of the parameter.

Model calibration (1995–1997) and validation (1982–1984) were conducted using corrected streamflow records with IGF. During the calibration and validation periods, observed streamflow and corrected simulated streamflow were compared on monthly (Figure 14) and daily (Figure 15) scales. The fitted SWAT model matched the trend of the streamflow hydrograph nearly precisely. Both monthly and daily streamflow simulations revealed that the higher fluctuations in the simulated peaks and the lesser ones in low flows.
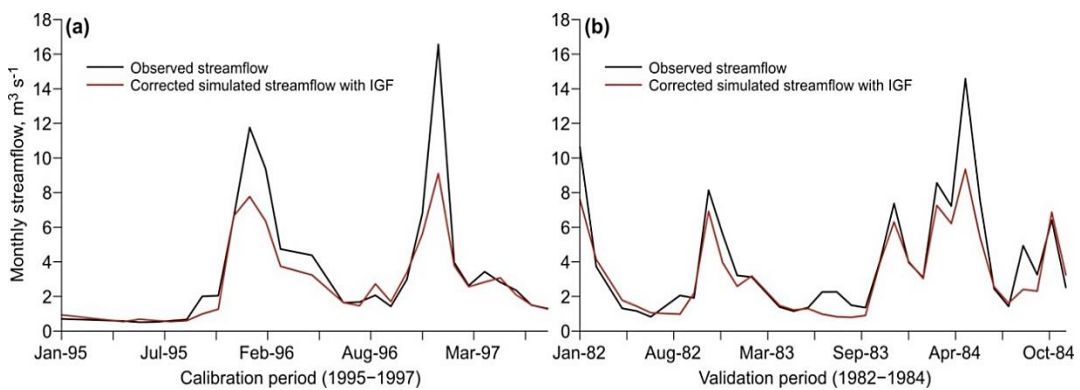
Figure 14. On a monthly scale, observed streamflow compared to corrected simulated streamflow with SWAT model for the calibration (a) and validation (b) phases.
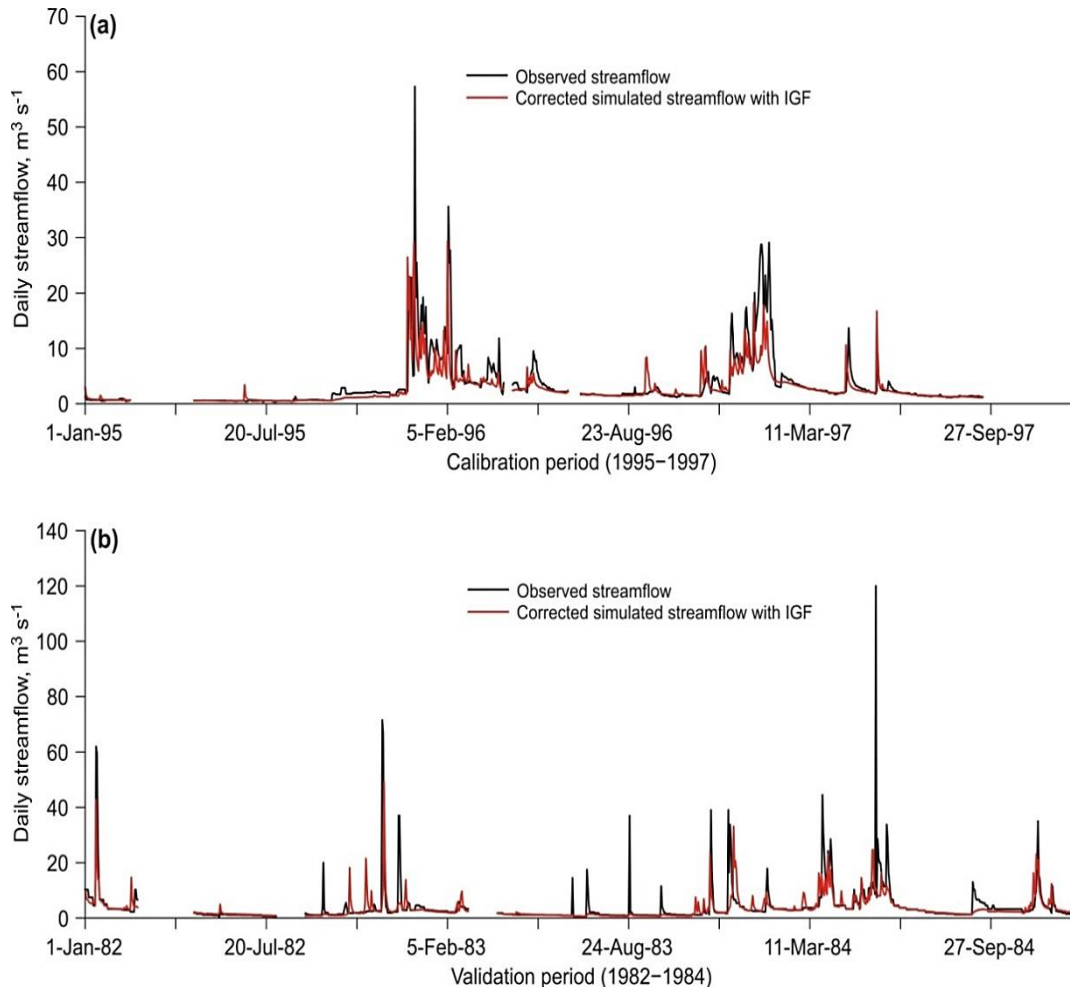
Figure 15. On a daily scale, observed streamflow compared to corrected simulated streamflow with SWAT model for the calibration (a) and validation (b) phases.

The SWAT model performance for high and normal flows reduces in the face of predominant low flows, as many other SWAT modellers have shown in other similar aquifer-fed karst regions (Jimeno-Sáez P. et al., 2018; Senent-Aparicio J. et al., 2019). It was also can be seen in Figure 15, low flows predominate in the CRB daily streamflow record. NSE and lnNSE were used respectively to measure the high flows and the low flows to reduce the problem of the squared differences, and the resulting sensitivity to extreme values of NSE. The model performance statistics for monthly and daily simulations in Table 17 revealed that calibration and

validation of monthly corrected streamflow showed good agreement between simulated and observed data.

Table 17. SWAT model performance statistics for corrected simulated monthly and daily streamflow during calibration and validation phases.

Statistic	Time step	Calibration	Validation
NSE	Monthly	0.77	0.8
R^2	Monthly	0.92	0.89
PBIAS	Monthly	19.82	17.25
RSR	Monthly	0.48	0.44
lnNSE	Daily	0.81	0.64

As a result, the SWAT model performed well and can be utilized for further research in the CRB and other comparable high-permeability bedrock basins, where IGF has a large influence on the baseflow component. This requires a confidence assessment of IGF or, at the very least, a trustworthy external assessment. The SWAT–CMB application indicated the following overall difficulties, as discussed for other groundwater and surface water coupling models: (1) groundwater and surface water bodies have different spatial (size and volume) and temporal (renovation rate) scales, although the coupling model can only replicate the same spatial and temporal scale in both types of bodies; (2) the coupling models exhibited flaws in the coupling mechanism processing, necessitating significant simplification of the coupling process, resulting in model distortion; and (3) this coupling model was developed for a specific region or problem, and although good results were obtained, there was no general adaptability, necessitating additional hydrogeological knowledge of local applications to contribute for changes in scale effects, actual flow conditions water uses, and sources of chloride in the case of the CMB method.

IV.4.3 Impact of dam construction on ecohydrological conditions

The following data were used in this paper: (1) A 25-m resolution DEM from the Spanish National Geographic Institute (IGN). (2) Land use map at a scale of 1:25,000 was provided by the Andalusian Network of Environmental Information (REDIAM). (3) Soil data were obtained from the World Soil Coordination Map with the resolution of 1 km. (4) Precipitation was obtained from the AEMET grid version 1.0, which provided daily rainfall in Spain from 2001 to 2018 with the resolution of 5 km. (5) Temperature data from 2001 to 2018 were provided from the fifth version of a high-resolution (approximately 10 km) dataset called SPAIN02. (6) The streamflow discharge data were collected on the CEDEX website.

The open source QGIS interface for SWAT (QSWAT 1.8) was used to set up the SWAT model. The SUFI–2 algorithm of SWAT–CUP (Calibration and Uncertainty Programs) to calibrate and validate the SWAT model was used.

IV.4.3.1 Inter-annual variability of natural and dam-controlled Castril River streamflow

The IAHRIS divided the 17 years of the research period into wet, normal and dry years according to the 25th and 75th percentiles of the annual volume in natural regime, which is named natural volume in Table 18. By comparing the natural annual regime with the altered annual regime, which is named altered volume in Table 18, it can be seen that the dam adjusted the annual flow according to the actual situation of each year (Figure 16). The patterns in both series are pretty similar as shown in Figure 16. However, in dry and normal years, the volume in the dam-controlled stream was virtually always higher than in the natural regime. Indeed, in the regulated regime, two of the years that would be considered dry in the natural regime (2001–2002 and 2005–2006) were normal, decreasing the number of dry years. In wet years the opposite is true, with a 7.72 percent fall in peak volume on average. The exception is the final year of the study (2017–2018), when annual volume increased by 20.39 percent, transforming the year from normal to wet under the altered regime. In the period 2001–2018, the inter-annual water balance shows a volume increase of 9.64 percent in the altered regime compared to the natural regime. While the overall inter-annual picture is fairly favourable in terms of environmental challenges, intra-annual changes in streamflow are critical to the conservation and livelihood of the riverine ecosystem (Richter B.D. et al.,

1996, Li F. et al., 2014). To ensure the river's health, a regulated flow regime should replicate natural flow regimes as closely as feasible, including in-stream and out-of-stream situations (IFC, 2004).

Table 18. Characterization of the inter-annual variability of natural and dam-controlled Castril River streamflow.

			Type of year					
	Wet[1]			Normal[1]			Dry[1]	
Year	Natural Volume	Altered Volume	Year	Natural Volume	Altered Volume	Year	Natural Volume	Altered Volume
2008–2009	106,807	104,566	2002–2003	73,001	85,020	2001–2002	39,551	59,456
2009–2010	144,569	131,733	2003–2004	74,797	84,182	2004–2005	27,120	25,407
2010–2011	109,821	103,285	2006–2007	61,122	67,063	2005–2006	38,136	58,139
2012–2013	162,440	139,806	2007–2008	49,920	59,625	2011–2012	41,318	40,789
			2013–2014	100,447	83,745			
			2014–2015	59,226	66,044			
			2015–2016	62,217	62,620			
			2016–2017	42,485	53,282			
			2017–2018	89,669	107,952			

[1] Wet year if annual volume (Mm^3) is $\geq$ 103,627; normal year if annual volume (Hm^3) is < 103,627 and > 41,902; dry year if annual volume (Hm^3) is $\leq$ 41,902.
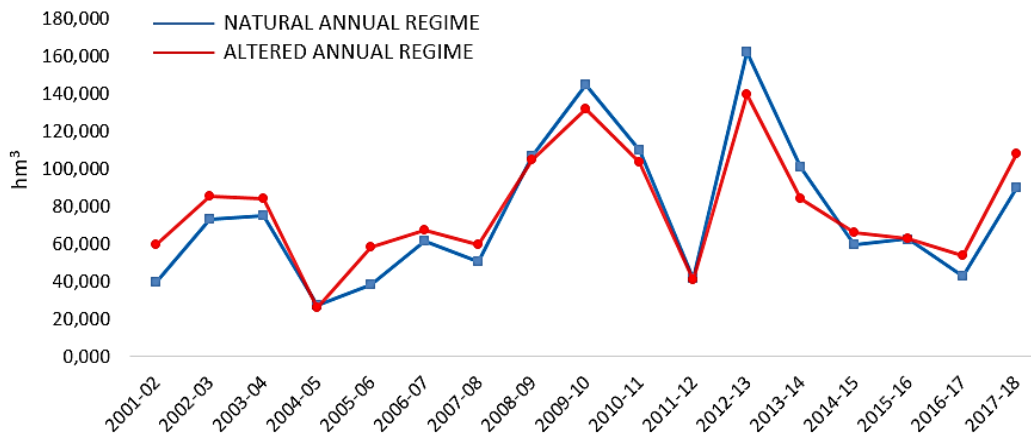
Figure 16. Comparison of natural and altered inter-annual regime of the Castril River streamflow.

IV.4.3.2 *Intra-annual variability of natural and dam-controlled Castril River streamflow*

The monthly volumes in natural and altered regime are showed in Figure 17 and Figure 18, respectively. As shown, the natural flow regime hydrograph is compared to the hydrograph altered by the dam. Intra-annual variability analysis shows the separation of two main seasonal periods: a low flow period from May to October and a spring higher water volume period from November to April, peaking in March. Although the tendencies in the three types of years (wet, normal, and dry) follow similar patterns in general, the variances in steepness and peaks are important. Autumn and winter could see more big changes in the flow regime. Indeed, in wet years, the difference in volume between the altered and natural regimes was 106.38 percent in October, while in normal years, the gap was 122 percent in December and 77 percent in November. Except in August when there was a lack of rainfall during the summer season, and in spring during wet and normal years when the greatest values were recorded, volumes were often larger in the altered regime. Despite this, in dry and normal years, the natural regime was below the altered regime for nine and eight months, respectively. The results of the preceding studies all point to the same conclusion: the El Portillo Reservoir has a strong regulatory effect on the watershed's volume regimes. The river's maximum flow regime decreased following the dam's completion during high-volume periods due to flood retention and peak reduction in wet years, while the river's

minimum flow increased in dry years to meet downstream water requirements. Despite the fact that the annual average volumes for all year types were higher in the altered regime than in the natural regime, seasonality variations, particularly during wet years, might significantly alter floodplain conditions (Zheng Y. et al., 2019) and the river eco-environment (Ngor P.B. et al., 2019; Lin Z. and Qi J., 2017; Pool T. et al., 2017; Zhang Z. et al., 2016; Arias M.E. et al., 2014; Junk W.J. et al. 1989).
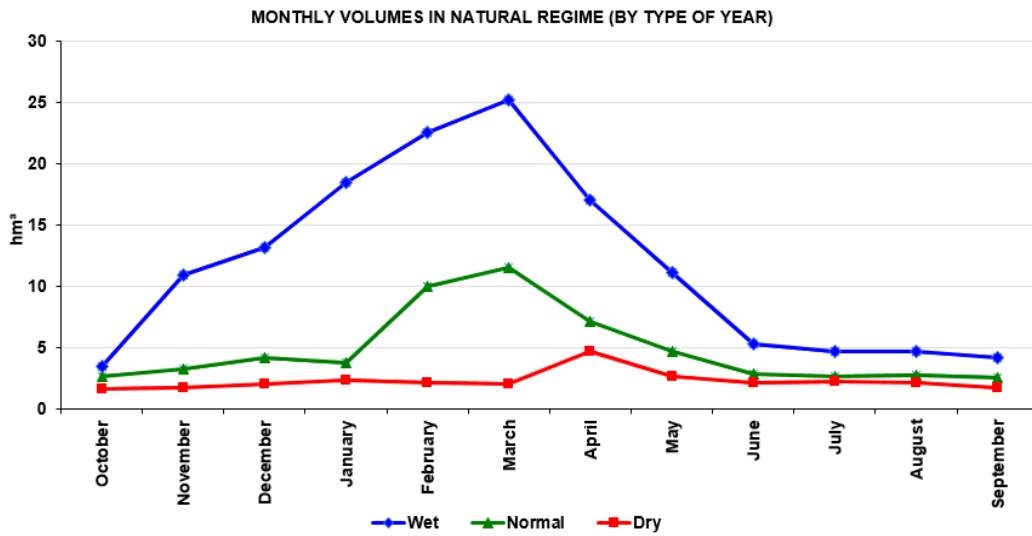

Figure 17. Monthly volumes in natural regime, clustering the data by type of year: wet, normal and dry.
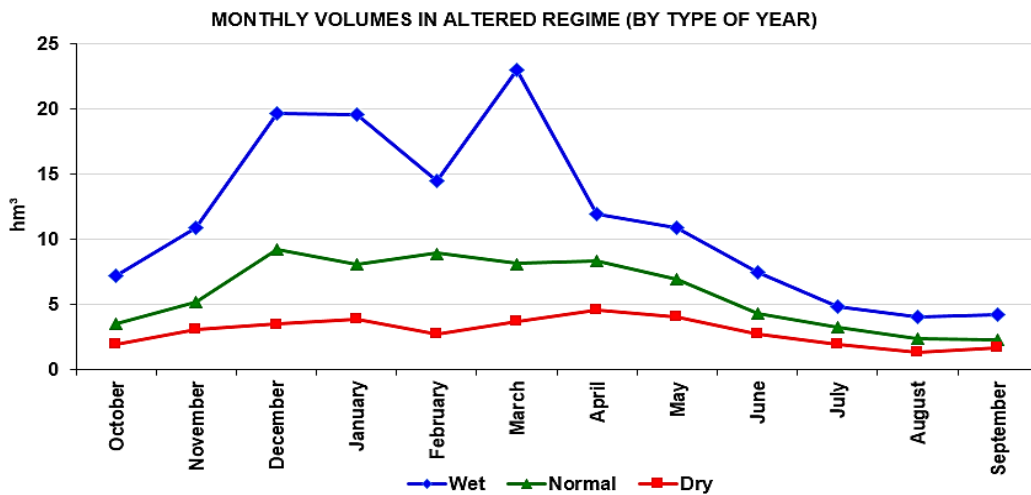

Figure 18. Monthly volumes in altered regime, clustering the data by type of year: wet, normal and dry.

IV.4.3.3 Indicators of hydrological alteration

In the period 2001–2018, IAHRIS parameters were used to compare the regulated-altered and natural-modelled volumes in the Castril River under the influence of dam construction. Table 19 shows the typical values for the normal, wet and dry years, as well as the weighted year.

The average annual volume differences between the natural and altered regimes were less than 10% in normal and wet years, but reached 20.49 percent in dry years. The average annual volume in the weighted year was 3.76 percent more than in the natural regime due to dam regulation. Under both regimes, maximum volumes remained between March and April, and the minimum volumes were moved forward from September to October in the natural regime and in August in the altered regime. In all of the year types, seasonality produced the most significant changes. In normal years, it ranged from 0.70 (good) to 0.91 (excellent), but the seasonality of minimum values in wet (0.46) and dry (0.33) years resulted a moderate alteration in minimum values in the weighted year (0.55). During the summer season, the average number of days with a flow below the 95th percentile in the examined series increased in the regulated regime, particularly in August (5.2 days) and September (3.3 days). During the rest of the year the number of days with extremely low volumes (below the 95th percentile) decreased, especially in the autumn, when the difference reached an average of 6.2 days in November. In nearly half of the indicators for the three year types, the magnitude and variability showed inverse values, indicating that the altered volumes were higher than in the natural regime. This ensures the required availability of habitat for aquatic and terrestrial organisms (Gonçalves Moreira De Jesús M.T., 2003), riverine soil moisture, spawning area access (Friday M. and Haxton T., 2021; Hayes D.S. et al., 2018), habitat heterogeneity and quality and non-exclusive competition between species (Arthington A.H., 2012).

The hydrological status of the river is summarized in Table 20. Overall, the usual value results indicated a good hydrological state. The IAG calculation result was between 0.47 and 0.65, which showed that the hydrological state was good, especially in the normal years.

Table 19. Indicators of hydrological alteration (IHA) of habitual values for the natural and altered regimes; asterisk (*) denotes inverse values.

Group	Aspect	Code	Value	Spider Chart
Usual Values – Wet year	Magnitude	IAH1	0.92	
		IAH2	0.72*	
	Variability	IAH3	0.67*	
		IAH4	0.67	
	Seasonality	IAH5	0.88	
		IAH6	0.46	
Usual Values – Normal year	Magnitude	IAH1	0.87*	
		IAH2	0.71*	
	Variability	IAH3	0.83	
		IAH4	0.82*	
	Seasonality	IAH5	0.91	
		IAH6	0.70	
Usual Values – Dry year	Magnitude	IAH1	0.81	
		IAH2	0.68*	
	Variability	IAH3	0.81	
		IAH4	0.71*	
	Seasonality	IAH5	0.79	
		IAH6	0.33	
Usual Values – Weighted year	Magnitude	IAH1	0.87	
		IAH2	0.70	
	Variability	IAH3	0.77	
		IAH4	0.76	
	Seasonality	IAH5	0.87	
		IAH6	0.55	

Table 20. Index of global alteration (IAG) of habitual values for the natural and altered regime.

Aspect	Value	Code	Level
Usual Values – Wet year	0.51	IAG$_{H\ WET\ YEAR}$	Good
Usual Values – Normal year	0.65	IAG$_{H\ NORMAL\ YEAR}$	Excellent
Usual Values – Dry year	0.47	IAG$_{H\ DRY\ YEAR}$	Good
Usual Values – Weighted year	0.54	IAG$_{H\ WEIGTHED\ YEAR}$	Good

Table 21 and Table 22 show the calculated results of extreme values which are floods and droughts. The IAG value of droughts was 0.69 which means an excellent status, and IAG value of floods was 0.35 in a moderate status close to the threshold of good (0.36). This indicated that the extreme values in floods were more deficient than extreme values in droughts.

As shown in Table 21, the flood spider chart revealed the most attenuation in the studied area. Regarding to the IHA values of floods, it can be seen that the results of frequency of connectivity flow (IAH9) and floods duration (IAH13) were both deficient, with values of 0.28 and 0.37, respectively. These altered regimes showed a significant reduction in flow connectivity (QCONEC). This volume is especially important in terms of riparian habitat dynamics and flood-dependent ecosystems. This connectivity ensures access to this band as well as enough moisture, both of which are critical for various degrees of biota and habitat rejuvenation (Martinez C. and Fernández J.A., 2010a and 2010b). Moreover, numerous researchers have looked into the consequences of altered flood regimes on river fauna and flora (Hickey J.T. and Salas J.D., 1995; Richter B.D. and Richter H.E., 2000; Whipple A.A. et al., 2016). Macroinvertebrate communities require transversal connectivity in order to preserve their variety and functionality (Collier K.J. and Scarsbrook M.K., 2000). Furthermore, erosion and sedimentation processes may be jeopardized, and hydraulic variability in riverbeds and floodplains may be reduced, according to geomorphological considerations (Guo L. et al., 2018; Wohl E. et al., 2015; Thoms M.C. and Sheldon F., 2002). In addition, the magnitude of maximum floods (IAH7) and variability of maximum floods (IAH11) were moderate, with values of 0.55 and 0.53, respectively. This indicated that flood flows

can be well controlled under the influence of dams in flood conditions, but the decline in hydrological connectivity to flood plains can lead to a biodiversity loss. The spider-chart visually showed the values of each indicators of floods.

For the droughts, the number of days of null flow (IAH20) was 1, and the magnitude of usual droughts (IAH16) and duration of droughts (IAH19) were in close proximity to 1, both with values of 0.98. And as with the normal values, the seasonality of droughts was the most affected parameter. The IAH21 for droughts (seasonality) had a value lower than 0.6, which is the threshold between moderate and good status. As can be seen from the spider-chart, the seasonality of droughts of the inner polygons shrunk the most inward with the calculated value 0.56. During the driest seasons, these variances can have an impact on water quality, phenological synchronism among numerous vegetal and animal species (Naiman R.J. et al., 2002) and the colonization of exotic species (Bunn S. and Arthington A., 2002). The worst results were recorded between August and November, when the year's driest season ended. The rest of the indicators stayed in the good–excellent range, indicating that there will be no major issues during droughts that could harm the riverine environment or hydraulic conditions. Indeed, dam regulation moderating droughts ensures habitat availability and aquatic habitat sustainability (Bae M.J. and Park Y.S., 2019, Aspin T.W.H. et al., 2019).

Table 21. Indicators of hydrological alteration (IAH) extreme values for the natural and altered regimes; asterisk (*) denotes inverse values.

Group	Aspect	Code	Value	Spider Chart
Floods	Magnitude and frequency	IAH7	0.55*	
		IAH8	0.81*	
		IAH9	0.28	
		IAH10	0.92	
	Variability	IAH11	0.53	
		IAH12	0.72	
	Duration	IAH13	0.37	
	Seasonality	IAH14	0.86	

	Magnitude and frequency	IAH15	0.82*
		IAH16	0.98*
	Variability	IAH17	0.76
Droughts		IAH18	0.74*
	Duration	IAH19	0.98
		IAH20	1.00
	Seasonality	IAH21	0.56

Table 22. Index of global alteration (IAG) of extreme values for the natural and altered regimes.

Aspect	Value	Code	Level
Floods	0,35	IAG$_F$	Moderate
Droughts	0,69	IAG$_D$	Excellent

IV.4.3.4 Flow Duration Curve and Ecosystem

Annual eco-surplus and eco-deficit were used to analyze in flow regime annual changes. The flow duration curve (FDC) was produced by using natural and altered regime flows with the effect of El Portillo Reservoir, which is shown in Figure 19. According to the curve, the altered regime in the range of 4% to 26%, showed a decrease in peak flows under the influence of dam, which can be regarded as eco-deficit. In addition, the altered regime was higher than the natural regime, both were eco-surplus.

Based on previous analyses of the IHA indicators and the FDC eco-surplus and eco-deficit, the El Potillo Reservoir significantly altered the hydrological situation of the lower reaches. The magnitude, frequency, timing, duration, and rate of change of hydrological conditions are five key components of flow regime that measure ecological processes in river ecosystems. Ecological deficits and ecological surpluses can be used to assess the impact of dam construction on the trade-off between ecological and human activities on water demand.
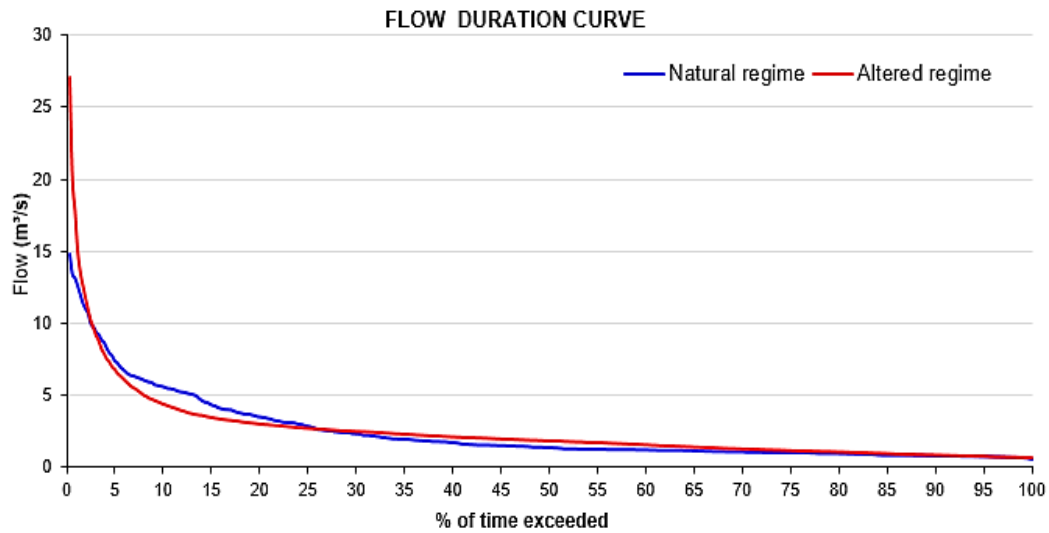
Figure 19. Flow duration curve (FDC) of the natural and altered regime.

These results demonstrate how the lower reaches of the dam generally maintained the hydrological seasonality but with a large variation due to the increase in low flows and the decrease in high flows between the natural and altered regimes. The changes in maximum and minimum flows, reduction of the hydrological connectivity, and high duration in floods affect the inundation of floodplains and river habitat ecosystems downstream. Moderate changes in droughts through the regulation of dams ensure the availability and sustainability of aquatic habitats (Bae M.J. and Park Y.S., 2019; Aspin T. W. H. et al., 2019). Previous studies have mentioned that increasing low flows has a positive impact on both the structure and function of river ecosystems (Rolls R. J., Leigh C., and Sheldon F., 2012; Poff N. L. and Zimmerman J. K. H.., 2001; Marchetti M. P. and Moyle P. B., 2001). But there were also other analyses of the effects of low-flow restoration on the long-term structure of aquatic populations and communities in river ecosystems have been met with mixed results (Daufresne M. et al., 2015; Bradford M. J. et al., 2011). The decrease of high flows reduced the transport of sediment and organic resources that caused a decline in the habitat suitability. Hydrological connectivity between the river and floodplain is essential for floodplain habitats and biodiversity. The loss of connectivity to floodplains means that the riparian habitats cannot be restored but only continue to age, and species

regeneration is seriously endangered (Nilsson C. and Svedmark M., 2002). It may also lead to a reduction in habitat availability for aquatic organisms and a reduction in the food supply of aquatic animals (Gao B. et al., 2012).

V – CONCLUSIONS AND FUTURE RESEARCH DIRECTIONS

V- CONCLUSIONS AND FUTURE RESEARCH DIRECTIONS

The use of SWAT applications in hydrological modeling has been widely promoted in the scientific community in order to protect the sustainable development of ecosystems under the combined influence of climate change and human activities, and its simulation results will influence water resource management decision-making. This PhD Thesis proposes methodological innovations around the SWAT model to try to solve complex hydrological and eco-systemic problems that involve (totally or partially) the groundwater component and the regulation of streamflow in semi-arid basins in southeastern Spain. The experimental implementation has focused on two basins at the headwaters of the Segura River and the Guadalquivir River, while scientific advances have been channeled through three articles published in high-impact indexed journals.

The **Publication 1** used the SWAT model to identify the influences of climate variability and human activities on water resources in the HWSRB, the first study area. The SWAT model was shown to be capable of reproducing the hydrological conditions of the HWSRB. The statistical results of calibration were NSE = 0.86, RSR = 0.38 and PBIAS = –14.11, while the validation results were NSE = 088, RSR = 0.35 and PBIAS = −17.23, indicating that the SWAT model performed well. The decrease of rainfed agriculture and shrubland areas, and the increase of forests, was the main trend in land–use/land-cover change, both of which are a result of the reforestation plan carried out during the 1970s. Both the climate change and reforestation lead to a reduction of the HWSRB's streamflow. Climate change contributed 64.4 percent more than the replanting plan (35.6 percent). However, for the ET in the HWSRB, the results demonstrated that the reforestation plan had a greater impact than climate variability.

To sum up, the reforestation plan can prevent soil erosion but cause the reduction of runoff. These findings could have far-reaching consequences for a region that is already under water stress. In order to sustain the water yield, future reforestation plans in this area should focus on strengthening native shrub vegetation rather than expanding the forested area. In order to build sustainable strategies, the reforestation plan's effects should be factored into water resource management plans.

The **Publication 2** combined the SWAT model and the CMB method to simulate streamflow in the CRB headwater. This second study area is a representative high-permeability bedrock basin where streamflow is considerably influenced by IGF from upstream areas. The SWAT model should not be used alone to model these aquifer–fed mountain basins, so it can be used in conjunction with other specific methods to appropriately quantify IGF. On the basis of the available, well-checked CMB datasets in continental Spain, the well-known hydrogeological functioning of the area, the negligible use of groundwater and the absence of non-atmospheric sources of chloride, the CMB method was applied for the IGF that adds to the baseflow produced within the CRB.

When using simulated streamflow with IGF, the SWAT model's performance improved considerably. The SWAT model exhibited good performance both in daily and monthly simulations when using the CMB-based IGF estimates for streamflow adjustment. So, the CMB was revealed to be a feasible method for IGF, allowing for similar net aquifer recharge to the baseflow contributing to streamflow in the headwater of large river watersheds.

IGF accounts for around 51% of total baseflow in the CRB. As a result of its significant impact, IGF should be addressed in order to improve water resource appraisal and management in basins like the CRB. But as methiond before, although good results have been achieved, this coupling model was developed for a specific region has no general adaptability. Assessment of IGF must rely on other methods or techniques specifically adapted to the hydrogeological features of the studied area.

The **Publication 3** used the IAHRIS software and the IHA method to investigate how the construction of the El Portillo Reservoir has impacted on the hydrological and ecological statuses of the Castril River downstream. The the IHA metrics and eco-flow metrics were obtained by comparing the natural flow without dam's influence to the altered flow under dam's influence. These representative factors might be considered in the design of dam operations for river ecosystem restoration and protection. More extensive information on changes in hydrological conditions can be found in IHA indicators. The influence of dam operation on river ecosystems under flow changes demonstrates the ecological surpluses and deficits.

To be specific, the river's flow regime was adjusted by the dam according to the actual status. The river's overall hydrological seasonality was preserved, with flow changes being more noticeable in autumn and winter than in other seasons. Extreme flows were managed at varying periods, with high flows being reduced during floods and low flows being increased during dry periods.

The altered regime resulted in a significant reduction in flow connectivity. Controlling flow peaks downstream of the dam has reduced river-riverine-flood-plain hydrological connectivity, potentially limiting sediment and organic resource transit and jeopardizing habitat rejuvenation and floodplain biodiversity.

The results of the flow duration curve (FDC) showed that the CRB's ecological and hydrological statuses had both eco-surplus and eco-deficit when the dam was operational. Due to the dam's high flow control, there was primarily an eco-deficit in the range of 4% to 26% of FDC. The eco-surplus in other intervals increased. The dam's regulation of high and low flow values can be considered as the cause of variations in the river's biological influence. The eco-flow metrics (eco-surplus, eco-deficit) have a strong relationship with the IHA indicators and may be cross-verified with the majority of ecological information.

VI – REFERENCES

VI- **REFERENCES**

Abbaspour, K.C. SWAT Calibration and Uncertainty Program—A User Manual; SWAT-CUP-2012; Swiss Federal Institute of Aquatic Science and Technology: Dubendorf, Switzerland, 2012.

Abbaspour, K. C., Johnson, C. A., & Van Genuchten, M. T. (2004). Estimating uncertain flow and transport parameters using a sequential uncertainty fitting procedure. Vadose Zone Journal, 3(4), 1340–1352.

Abbaspour, K.C., Rouholahnejad, E., Vaghefi, S., Srinivasan, R., Yang, H. & Kløve, B., 2015. A continental-scale hydrology and water quality model for Europe: Calibration and uncertainty of a high-resolution large-scale SWAT model. J. Hydrol. 2015, 524, 733–752.

Abbaspour, K.C.; Vaghefi, S.; Srinivasan, R. A guideline for successful calibration and uncertainty analysis for soil and water assessment: A review of papers from the 2016 International SWAT Conference. Water 2018, 10, 6.

Abbaspour, K. C., Yang, J., Maximov, I., Siber, R., Bogner, K., Mieleitner, J., ... & Srinivasan, R. (2007). Modelling hydrology and water quality in the pre-alpine/alpine Thur watershed using SWAT. Journal of Hydrology, 333(2–4), 413–430.

Abbott, M. B., Bathurst, J. C., Cunge, J. A., O'Connell, P. E., & Rasmussen, J. (1986). An introduction to the European Hydrological System—Systeme Hydrologique Europeen, "SHE", 1: History and philosophy of a physically-based, distributed modelling system. Journal of hydrology, 87(1–2), 45–59.

Alcalá, F.J.; Cantón, Y.; Contreras, S.; Were, A.; Serrano-Ortiz, P.; Puigdefábregas, J.; Solé-Benet, A.; Custodio, E.; Domingo, F. Diffuse and concentrated recharge evaluation using physical and tracer techniques: Results from a semiarid carbonate massif aquifer in southeastern Spain. Environ. Earth Sci. 2011, 63, 541–557.

Alcalá, F.J.; Custodio, E. 2008a. Atmospheric chloride deposition in continental Spain. Hydrol. Process. 2008, 22, 3636–3650.

Alcala, F.J.; Custodio, E. 2008b. Using the Cl/Br ratio as a tracer to identify the origin of salinity in aquifers in Spain and Portugal. J. Hydrol. 2008, 359, 189–207.

Alcalá, F.J.; Custodio, E. Spatial average aquifer recharge through atmospheric chloride mass balance and its uncertainty in continental Spain. Hydrol. Process. 2014, 28, 218–236.

Alcalá, F.J.; Custodio, E. Natural uncertainty of spatial average aquifer recharge through atmospheric chloride mass balance in continental Spain. J. Hydrol. 2015, 524, 642–661.

Alcalá, F.J.; Martínez-Valderrama, J.; Robles-Marín, P.; Guerrera, F.; Martín-Martín, M.; Raffaelli, G; Tejera de León, J.; Asebriy L. A hydrological-economic model for sustainable groundwater use in sparse-data drylands: application to the Amtoudi Oasis in southern Morocco, northern Sahara. Sci. Total Environ. 2015, 537, 309–322.

Alcalá, F.J.; Martín-Martín, M.; Guerrera, F.; Martínez-Valderrama, J.; Marín, P.R. A feasible methodology for groundwater resource modelling for sustainable use in sparse-data drylands: Application to the Amtoudi Oasis in the northern Sahara. Sci. Total Environ. 2018, 630, 1246–1257.

Andalusian Network of Environmental Information (REDIAM). Comparador WMS Ortofotos; Cartografía de Inundaciones en Febrero-Marzo 2010 en las Cuencas de los ríos Guadalquivir y Guadalete; Mapa de usos y Coberturas Vegetales Multitemporal. Available online: http://www.juntadeandalucia.es/medioambiente/site/rediam (accessed on 11 January 2018).

Andreu, J.M.; Alcalá, F.J.; Vallejos, Á.; Pulido-Bosch, A. Recharge to aquifers in SE Spain: Different approaches and new challenges. J. Arid Environ. 2011, 75, 1262–1270.

Aparicio, E., Vargas, M.J., Olmo, J.M., De Sostoa, A., 2000. Decline of native freshwater fishes in a Mediterranean watershed on the Iberian Peninsula: a quantitative assessment. Environ. Biol. Fish. 59 (1), 11–19.

Araque, Jiménez, E. Forest landscapes in the Prebetic Arc. The Segura and Cazorla Mountains. Rev. Estud. Reg. 2013, 96, 321–344.

Arias, M.E., Piman, T., Lauri, H., Cochrane, T.A., Kummu, M., 2014. Dams on Mekong tributaries as significant contributors of hydrological alterations to the Tonlé Sap Floodplain in Cambodia Hydrology and Earth System Sciences 18 (12), 5303.

Arnold, J. G., Allen, P. M., & Bernhardt, G. (1993). A comprehensive surface-groundwater flow model. Journal of hydrology, 142(1–4), 47–69.

Arnold, J.G.; Allen, P.M.; Muttiah, R.; Bernhardt, G. Automated Base Flow Separation and Recession Analysis Techniques. Ground Water 1995, 33, 1010–1018.

Arnold, J.G.; Kiniry, J.R.; Srinivasan, R.; Williams, J.R.; Haney, E.B.; Neitsch, S.L. Soil and Water Assessment Tool—Input/Output Documentation—Version 2012. Available online: http://swat.tamu.edu/documentation/ (accessed on 20 December 2019).

Arnold, J. G.; Srinivasan, R.; Muttiah, R. S.; Williams, J.R. Large area hydrologic modeling and assessment Part I: Model development. J. Am. Water Resour. Assoc. 1998, 34, 73–89.

Arthington, A.H., 2012. Environmental flows: saving rivers in the third millennium. University of California Press: Berkeley, 424. USA.

Aspin, T. W. H.; Khamis, K.; Matthews, T. J.; Milner, A. M.; O'Callaghan, M. J.; Trimmer, M.; Ledger, M. E. (2019). Extreme drought pushes stream invertebrate communities over functional thresholds. Global Change Biology 25: 230–244.

Bae, M.J.; Park, Y.S. (2019) Evaluation of precipitation impacts on benthic macroinvertebrate communities at three different stream types. Ecological Indicators 102: 446–456.

Baffaut, C.; Benson, V.W. Modeling flow and pollutant transport in a karst watershed with SWAT. Trans. ASABE 2009, 52, 469–479.

Batalla, R.J., Gomez, C.M., Kondolf, G.M., 2004. Reservoir-induced hydrological changes in the Ebro River basin (NE Spain). J. Hydrol. 290 (1–2), 117–136.

Bates, P.D., De Roo, A.P.J., 2000. A simple raster-based model for flood inundation simulation. Journal of Hydrology 236, 54–77.

Belmar, O.; Velasco, J.; Martinez-Capel, F. Hydrological classification of natural flow regimes to support environmental flow assessments in intensively

regulated Mediterranean rivers, Segura River Basin (Spain). Environ. Manag. 2011, 47, 992.

Beven, K. J. & Kirkby, M. J. (1979). A physically based, variable contributing area model of basin hydrology/Un modèle à base physique de zone d'appel variable de l'hydrologie du bassin versant. Hydrological Sciences Journal, 24(1), 43–69.

Beven, K. 2007. Towards integrated environmental models of everywhere: uncertainty, data and modelling as a learning process. Hydrol. Earth Syst. Sci. 2007, 11, 460–467.

Blanco-Gómez, P.; Jimeno-Sáez, P.; Senent-Aparicio, J.; Pérez-Sánchez, J. Impact of Climate Change on Water Balance Components and Droughts in the Guajoyo River Basin (El Salvador). Water 2019, 11, 2360.

Boix-Fayos, C.; de Vente, J.; Martinez-Mena, M.; Barbera, G.G.; Castillo, V. The impact of land use change and check-dams on catchment sediment yield. Hydrol. Process. 2008, 22, 4922–4935.

Bouaziz, L.; Weerts, A.; Schellekens, J.; Sprokkereef, E.; Stam, J.; Savenije, H.; Hrachowitz, M. Redressing the balance: Quantifying net intercatchment groundwater flows. Hydrol. Earth Syst. Sci. 2018, 22, 6415–6434.

Bosch, J.M.; Hewlett, J.D. A review of catchment experiments to determine the effects of vegetation changes on water yield and evapotranspiration. J. Hydrol. 1982, 55, 3–23.

Bradford, M. J., Higgins, P. S., Korman, J., & Sneep, J. (2011). Test of an environmental flow release in a British Columbia river: Does more water mean more fish? Freshwater Biology, 56, 2119–2134

Brown, A.E.; Zhang, L.; McMahon, T.A.; Western, A.W.; Verstessy, R.A. A review of paired catchment studies for determining changes in water yield resulting from alteration in vegetation. J. Hydrol. 2005, 310, 28–61.

Burnash, R. J., Ferral, R. L., & McGuire, R. A. (1973). A generalized streamflow simulation system, conceptual modeling for digital computers. Report by the Joliet Federal State River Forecasts Center, Sacramento, CA.

Bunn, S., Arthington, A., 2002. Basic Principles and Ecological Consequences of Altered Flow Regimes for Aquatic Biodiversity. Environmental Management 30, 492–507.

Cabezas, F., 2015. Análisis estructural de modelos hidrológicos y de sistemas de recursos hídricos en zonas semiáridas. PhD Thesis. University of Murcia. pp. 290. Available at: http://hdl.handle.net/10201/48218 (accessed on 26 Augest 2018).

Capel-Molina, J.J. Los climas de España. Ed.: Oikos-Tau. Barcelona, Spain, 1981; 403 pp.

Charlier, J.B., Ladouche, B., Maréchal, J.C., 2015. Identifying the impact of climate and anthropic pressures on karst aquifers using wavelet analysis. Journal of Hydrology 523, 610–623.

Chen YD, Yang T, Xu CY. 2010. Hydrologic alteration along the Middle and Upper East River (Dongjiang) basin, South China: a visually enhanced mining on the results of RVA method. Stochastic Environmental Research and Risk Assessment 24(1): 9–18.

Cibin, R., Sudheer, K. P., & Chaubey, I. (2010). Sensitivity and identifiability of stream flow generation parameters of the SWAT model. Hydrological processes, 24(9), 1133–1148.

Claasen, H.C.; Reddy, M.M.; Halm, D.R. Use of the chloride ion in determining hydrologic-basin water budgets: A 3-year case study in the San Juan Mountains, Colorado, USA. J. Hydrol. 1986, 85, 49–71.

Collier, K.J., Sacrsbrook, M.K., 2000. Use of riparian and hyporheic habitats. New Zealand Stream Invertebrates: ecology and implications for management. New Zealand Limnological Society. NIWA.

Crawford, N. H. & Linsley, R. K. (1966). Digital simulation in hydrology: Stanford Watershed Model IV. Tech. Rep. No. 39, Stanford Univ., Palo Alto, Calif.

Daufresne, M., Veslot, J., Capra, H., Carrel, G., Poirel, A., Olivier, J. M., & Lamouroux, N. (2015). Fish community dynamics (1985–2010) in multiple reaches of a large river subjected to flow restoration and other environmental changes. Freshwater Biology, 60, 1176–1191.

De Almeida Bressiani, D.; Srinivasan, R.; Jones, C.A.; Mendiondo, E.M. Effects of spatial and temporal weather data resolutions on streamflow modeling of a semi-arid basin, northeast Brazil. International Journal of Agricultural and Biological Engineering. 2015, 8, 125–139.

Dettinger, M.D. Reconnaissance estimates of natural recharge to desert basins in Nevada, U.S.A., by using chloride-balance calculations. J. Hydrol. 1989, 106, 55–78.

Döll, P., Fiedler, K., Zhang, J., 2009. Global-scale analysis of river flow alterations due to water withdrawals and reservoirs. Hydrol. Earth Syst. Sci. 13 (12), 2413.

Dong Z，Zhang J，Zhao J. Comments upon progress of environmental flows assessments [J]. Journal of Hydraulic Engineering, 2017, 48(6): 670–677

Dwivedi VK, Gupta SK, Pandey SN (2010) A study of environmental impact due to construction and operation of dam. In: National Conference on Eco friendly Manufacturing for Sustainable Development, 31, 1–6.

Eakin, T.E., 1966. A regional interbasin groundwater system in the White River Area, southeastern Nevada. Water Resources Research 2, 251–271.

Fantin-Cruz I, Pedrollo O, Girard P, Zeilhofer P, Hamilton, SK. 2015. Effects of a diversion hydropower facility on the hydrological regime of the Correntes River, a tributary to the Pantanal floodplain, Brazil. Journal of Hydrology 531:810–820

Fernández, J. A., Martínez C., Magdaleno, F., 2012 Application of indicators of hydrologic alterations in the designation of heavily modified water bodies in Spain, Environmental Science & Policy 16, 31–43,

Ficklin, D.L.; Luo, Y.; Zhang, M. Watershed Modelling of Hydrology and Water Quality in the Sacramento River Watershed, California. Hydrol. Process. 2012, 27, 236–250

Fossey, M.; Rousseau, A.N.; Savary, S. Assessment of the impact of spatio-temporal attributes of wetlands on stream flows using a hydrological modelling framework: A theoretical case study of a watershed under temperate climatic conditions. Hydrol. Process. 2016, 30, 1768–1781.

Fu, B.; Merritt, W.S.; Croke, B.F.W.; Weber, T.R.; Jakeman, A.J. A review of catchment-scale water quality and erosion models and a synthesis of future prospects. Environ. Model. Softw. 2019, 114, 75–97.

Francesconi, W.; Srinivasan, R.; Pérez-Miñana, E.; Willcock, S.P.; Quintero, M. Using the Soil and Water Assessment Tool (SWAT) to model ecosystem services: A systematic review. J. Hydrol. 2016, 535, 625–636.

Friday, M., Haxton, T., 2021. Evaluating the effects of controlled flows on historical spawning site access, reproduction and recruitment of lake sturgeon Acipenser fulvescens. Journal of Fish Biology 99 (6), 1940–1957.

Gao, B., Yang, D., Zhao, T., & Yang, H. (2012). Changes in the eco-flow metrics of the Upper Yangtze River from 1961 to 2008. Journal of Hydrology, 448–449, 30–38.

Gao, L.; Zhang, Y. Spatio-temporal variation of hydrological drought under climate change during the period 1960–2013 in the Hexi Corridor, China. J. Arid. Land 2016, 8, 157–171.

Gao, Y., Vogel, R. M., Kroll, C. N., Poff, N. L., & Olden, J. D. (2009). Development of representative Indicators of Hydrologic Alteration. Journal of Hydrology, 374, 136–147

García, C.; Amengual, A.; Homar, V.; Zamora, A. Losing water in temporary streams on a Mediterranean island: Effects of climate and land-cover changes. Glob. Planet Chang. 2017, 148, 139–152.

Gassman, P. W., Reyes, M. R., Green, C. H., & Arnold, J. G. (2007). The soil and water assessment tool: historical development, applications, and future research directions. Transactions of the ASABE, 50(4), 1211–1250.

Genereux, D.P.; Jordan, M.T.; Carbonell, D. A pired-watershed budget study to quantify interbasin groundwater flow in a lowland rain forest. Costa Rica. Water Resour. Res. 2005, 41, W04011.

Genereux, D.P., Wood, S., Pringle, C.M., 2002. Chemical tracing of interbasin groundwater transfer in the lowland rainforest of Costa Rica. Journal of Hydrology 258, 163–178.

Giorgi, F.; Lionello, P. Climate change projections for the Mediterranean region. Glob. Planet. Chang. 2008, 63, 90–104.

González del Tánago, M., Bejarano, M.D., García de Jalón, D., Schmidt, J.C., 2015. Biogeomorphic responses to flow regulation and fine sediment supply in Mediterranean streams (the Guadalete River, southern Spain). J. Hydrol. 528, 751–762.

Gonçalves Moreira De Jesús, M.T., 2003. Impacto de centrais mini-hídricas na qualidade biológica da água: a "Cascata" do Alva (Portugal). III Congreso Ibérico sobre gestión y planificación del agua." La Directiva Marco del Agua: realidades y futuros". Sevilla, Spain.

Grantham, T.E., Figueroa, R., Prat, N., 2013. Water management in Mediterranean river basins: a comparison of management frameworks, physical impacts, and ecological responses. Hydrobiologia 719 (1), 451–482.

Green, W.H. & Ampt, G.A. (1911). Studies on soil physics, 1. The flow of air and water through soils. Journal of Agricultural Sciences 4:11-24.

Grindlay, A.L., Zamorano, M., Rodríguez, M.I., Molero, E., Urrea, M.A., 2011. Implementation of the European water framework directive: integration of hydrological and regional planning at the Segura River basin, southeast Spain. Land Use Pol. 28 (1), 242–256.

Grusson, Y., Anctil, F., Sauvage, S., & Sánchez Pérez, J. M. (2017). Testing the SWAT Model with Gridded Weather Data of Different Spatial Resolutions. Water, 9(1), 54.

Guo, L., Su, N., Zhu, C., He, Q., 2018. How have the river discharges and sediment loads changed in the Changjiang River basin downstream of the Three Gorges Dam Journal of Hydrology 560, 259-274.

Hamlet AF, Mote PW, Clark MP (2007) Twentieth-century trends in runoff, evapotranspiration and soil moisture in the western United States. J Climate 20:1468–1486

Han, M.; Zhao, C.Y.; Šimůnek, J.; Feng, G. Evaluating the impact of groundwater on cotton growth and root zone water balance using Hydrus-1D coupled with a crop growth model. Agric. Water Manag. 2015, 160, 64–75.

Hargreaves, G. L., Hargreaves, G. H., & Riley, J. P. (1985). Agricultural benefits for Senegal River basin. Journal of irrigation and Drainage Engineering, 111(2), 113–124.

Hayes, D. S., Brändle, J. M., Seliger, C., Zeiringer, B. Ferreira, T., Schmutz, S., 2018. Advancing towards functional environmental flows for temperate floodplain rivers, Science of the Total Environment 633, 1089–1104.

Herrera, S.; Fernández, J.; Gutiérrez, J.M. Update of the Spain02 gridded observational dataset for EURO-CORDEX evaluation: Assessing the effect of the interpolation methodology. Int. J. Climatol. 2016, 36, 900–908.

Hickey, J. T., Salas, J. D., 1995. Environmental effects of extreme floods in Proceedings of the Italy Research Workshop on the Hydrometeorology, Impacts, and Management of Extreme Floods, Perugia, Italy.

Hojberg, A.L.; Refsgaard, J.C. Model uncertainty-parameter uncertainty versus conceptual models. Water Sci. Technol. 2005, 52, 177–186.

Hooke, J.M., 2006. Human impacts on fluvial systems in the Mediterranean region. Geomorphology 79 (3–4), 311–335.

Homa, E., Vogel, R.M., Smith, M.P., Apse, C.D., Huber-Lee, A. (2005). "An Optimization Approach for Balancing Human and Ecological Flow Needs", EWRI 2005 World Water and Environmental Resources Congress. Anchorage, Alaska.

Hu LiTang, Wang ZhongJing, Zhao JianShi, Ma YiHua. 2007. Advances in the Interactions and Integrated Model between Surface Water and Groundwater. Journal of Hydraulic Engineering 38(1), 54–59.

Hu W, Wang G, Deng W, Li SN. 2008. The influence of dams on eco-hydrological conditions in the Huaihe River basin, China. Ecological Engineering 33: 233–241.

Hudson, M.R., Mott, D.N., 1997. Faulting and coincident interbasin ground-water flow in a karst aquifer, Buffalo National River region, northwestern Arkansas. Geological Society of America Abstracts with Programs 29 (6), 181–182.

Hurrell, J.W. Decadal trends in the North Atlantic Oscillation, regional temperatures and precipitation. Nature 1995, 269, 676–679.

Hydrologic Engineering Center (HEC). 1981. HEC-1, Flood Hydrograph Package—User's Manual. US Army Corps of Engineers: Davis, CA.

IGME. Hydrogeological Map of Spain, scale 1: 200,000. Sheet nº 78, Baza. Geological Survey of Spain, Memory and Maps, 1988.

IGME. Hydrogeological Map of Spain, scale 1: 200,000. Sheet nº 71, Villacarrillo. Geological Survey of Spain, Memory and Maps, 1995.

ITGE-CGH-DGCA. Proyecto para la actualización de la infraestructura hidrogeológica de las Unidades 05.01 Sierra de Cazorla, 05.02 Quesada-Castril, 07.07 Sierras de Segura-Cazorla y el Carbonatado de la Loma de Úbeda, Madrid, 2001.

Jiang L, Ban X, Wang X, et al. Assessment of hydrologic alterations Cased by Three Gorges Dam in the middle and lower reaches of Yangtze River, China [J]. Water, 2014, 6(5): 1419–1434

Jimeno-Sáez, P.; Senent-Aparicio, J.; Pérez-Sánchez, J.; Pulido-Velazquez, D. A Comparison of SWAT and ANN models for daily runoff simulation in different climatic zones of peninsular Spain. Water 2018, 10(2), 192.

Jodar-Abellán, A., Pla-Bru, C. & Valdés-Abellán, J., 2019. Los modelos hidrológicos como sistemas de soporte en la toma de decisiones. Evolución histórica. Congreso Nacional del Agua 2019: innovación y sostenibilidad. Temática: aguas superficiales y subterráneas. ISBN: 978-84-1302-034-1. pp. 1269–1285

Junk, W.J., Bayley, P.B., Sparks, R.E., 1989. The flood pulse concept in river-floodplain systems. Canadian Special Publication of Fisheries and Aquatic Sciences 106, 110–127.

Karlsson, I. B., Sonnenborg, T. O., Refsgaard, J. C., Trolle, D., Børgesen, C. D., Olesen, J. E., … Jensen, K. H. (2016). Combined effects of climate models, hydrological model structures and land use scenarios on hydrological impacts of climate change. Journal of Hydrology, 535, 301–317.

Karr, J. R. (1991). "Biological integrity: A long-neglected aspect of water resource management." Ecol. Appl., 1(1), 66–84.

Kim, N.W.; Chung, I.M.; Won, Y.S.; Arnold, J.G. Development and application of the integrated SWAT-MODFLOW model. J. Hydrol. 2008, 356, 1–16.

Kiros, G., Shetty, A. & Nandagiri, L., 2015. Performance evaluation of SWAT model for land use and land cover changes under different climatic conditions: A review. J. Waste Water Treat. Anal. 2015, 6, 1–6.

Kliment Z, Matoušková M (2009) Runoff changes in the Šumava Mountains (Black Forest) and the Foothill Regions: extent of influence by human impact and climate change. Water Resour Manag 23:1813–1834

Knisel, W. G. (1980). CREAMS: a field scale model for Chemicals, Runoff, and Erosion from Agricultural Management Systems [USA]. United States. Dept. of Agriculture. Conservation research report (USA).

Kondolf, G.M., Batalla, R.J., 2005. Hydrological effects of dams and water diversions on rivers of Mediterranean-climate regions: examples from California. Dev. Earth Surf. Process 7, 197–211.

Krysanova, V. & Srinivasan, R., 2014. Assessment of climate and land use change impacts with SWAT. Reg. Environ. Chang. 2014, 15, 431–434.

Krysanova, V., & White, M. (2015). Advances in water resources assessment with SWAT—an overview. Hydrological Sciences Journal, 60(5), 771–783.

Ladouche, B., Marechal, J.C., Dorfliger, N., 2014. Semi-distributed lumped model of a karst system under active management. Journal of Hydrology 509, 215–230.

Lal, R., Pimentel, D., 2008. Soil erosion: a carbon sink or source? Science 319 (5866), 1040–1042.

Lee, J.; Kim, J.; Jang, W.S.; Lim, K.J.; Engel, B.A. Assessment of Baseflow Estimates Considering Recession Characteristics in SWAT. Water 2018, 10, 371.

Lee, M.-H.; Bae, D.-H. Climate Change Impact Assessment on Green and Blue Water over Asian Monsoon Region. Water Resour. Manag. 2015, 29, 2407–2427.

Li, F., Zhang, G., Xu, Y.J., 2014. Spatiotemporal variability of climate and streamflow in the Songhua River Basin, northeast China. Journal of Hydrology 514, 53–64.

Li, Y.Y.; Chang, J.X.; Wang, Y.M.; Jin, W.T.; Guo, A.J. Spatiotemporal impacts of climate, land cover change and direct human activities on runoff variations in the Wei River Basin, China. Water 2016, 8, 220.

Li, Z.; Deng, X.; Wu, F.; Hasan, S.S. Scenario analysis for water resources in response to land use change in the middle and upper reaches of the Heihe River Basin. Sustainability 2015, 7, 3086–3108.

Lim, K.J.; Engel, B.A.; Tang, Z.; Choi, J.; Kim, K.S.; Muthukrishnan, S.; Tripathy, D. Automated web GIS based hydrograph analysis tool, WHAT. J. Am. Water Resour. Assoc. 2005, 1407–1416.

Lin, Z., Qi, J., 2017. Hydro-dam – A nature-based solution or an ecological problem: The fate of the Tonlé Sap Lake. Environmental Research 158, 24–32.

Llorens, P.; Latron, J.; Oliveras, I. Modelización del efecto del Cambio Global en la hidrología superficial. Ejemplo de aplicación a una cuenca Mediterránea de montaña. In Proceedings of the 3rd Asamblea Hispano-Portuguesa de Geodesia y Geofísica, Valencia, Spain; García, F., Berné, J.L., Eds; Universidad Politécnica de Valencia: Valencia, Spain, 2003; Volume 3, pp. 1679–1681.

Lobera, G., Besné, P., Vericat, D., López-Tarazón, J.A., Tena, A., Aristi, I., Díez, J.R., Ibisate, A., Larrañaga, A., Elosegi, A., Batalla, R.J., 2015. Geomorphic status of regulated rivers in the Iberian Peninsula. Sci. Total Environ. 508, 101–114.

Lorenzo-Lacruz, J., Vicente-Serrano, S.M., López-Moreno, J.I., Morán-Tejeda, E., Zabalza, J., 2012. Recent trends in Iberian streamflows (1945–2005). J. Hydrol. 414, 463–475.

Lorup, J.K., Refsgaard, J.C., Mazvimavi, D., 1998. Assessing the effect of land use change on catchment runoff by combined use of statistical tests and hydrological modelling: case studies from Zimbabwe. J. Hydrol. 205 (3–4), 147–163.

Luo, Y.; Arnold, J.; Allen, P.; Chen, X. Baseflow simulation using SWAT model in an inland river basin in Tianshan Mountains, Northwest China. Hydrol. Earth Syst. Sci. 2012, 16, 1259–1267.

Ma, L., Ascough II, J. C., Ahuja, L. R., Shaffer, M. J., Hanson, J. D., & Rojas, K. W. (2000). Root zone water quality model sensitivity analysis using Monte Carlo simulation. Transactions of the ASAE, 43(4), 883.

Magilligan, F. J., & Nislow, K. (2005). Changes in hydrologic regime by dams. Geomorphology, 71, 61–78.

MAGRAMA (Ministerio de Agricultura y Pesca, Alimentación y Medio Ambiente). Sistema de Información del Anuario de Aforo. Available online: http://sig.magrama.es/aforos (accessed on 1 February 2018).

Malagó, A.; Efstathiou, D.; Bouraoui, F.; Nikolaidis, N.P.; Franchini, M.; Bidoglio, G.; Kritsotakis, M. Regional scale hydrologic modeling of a karst-

dominant geomorphology: the case study of the island of Crete. J. Hydrol. 2016, 540, 64–81.

Marchetti, M. P., & Moyle, P. B. (2001). Effects of flow regime on fish assemblages in a regulated California stream. Ecological Applications, 11, 530–539.

Marhaento, H.; Booij, M.J.; Rientjes, T.H.M.; Hoekstra, A.Y. Attribution of changes in the water balance of a tropical catchment to land use change using the SWAT model. Hydrol. Process. 2017, 31, 2029–2040.

Martínez, C., 2006. El régimen natural de caudales: una diversidad imprescindible, una diversidad predecible. Revista Invest Agrar: Sist Recur For Fuera de Serie, 15(1), 153–165.

Martínez, C., Fernández, J. A., 2010a. IAHRIS 2.2 Indicators of Hydrologic Alteration in Rivers: Free software. http://ambiental.cedex.es/docs/IHARIS_v2.2.zip

Martínez, C., Fernández, J. A., 2010b. IAHRIS 2.2 Indicators of Hydrologic Alteration in Rivers: Methodological Reference Manual. http://ambiental.cedex.es/docs/IHARIS_v2.2.zip

Matteau, M., Assani, A. A., and Mesfioui, M. (2009). "Application of multivariate statistical analysis methods to the dam hydrologic impact studies." J. Hydrol. (Amsterdam), 371(1–4), 120–128.

Maxwell, R. M.; Miller, N. L., 2005. Development of a coupled land surface and groundwater model. Journal of Hydrometeorology 6: 233–247.

McMahon, P.B.; Plummer, L.N.; Bohlke, J.K.; Shapiro, S.D.; Hinkle, S.R. A comparison of recharge rates in aquifers of the United States based on groundwater-based data. Hydrogeol. J. 2011, 19, 779–800.

McManamay RA, Bevelhimer MS (2013) A Holistic framework for environmental fows determination in hydropowercontexts. Oak Ridge National Laboratory, Oak Ridge. http://www.osti.gov/ bridge

Meaurio, M.; Zabaleta, A.; Angel, J.; Srinivasan, R.; Antigüedad, I. Evaluation of SWAT models performance to simulate streamflow spatial origin. The case of a small forested watershed. J. Hydrol. 2015, 525, 326–334.

Mitra S, Singh A (2018) Assessment of environmental fow requirements of damodar river basins by using fow duration indices method – a case study. Int J Hydrol 2(3):281–283

MMA (Ministerio Medio Ambiente), 2006. Inventario de Presas Españolas. Publicaciones Ministerio de Medio Ambiente, Madrid, Spain.

Molina-Navarro, E.; Andersen, H.E.; Nielsen, A.; Thodsen, H.; Trolle, D. Quantifying the combined effects of land use and climate changes on stream flow and nutrient loads: A modelling approach in the Odense Fjord catchment (Denmark). Sci. Total Environ. 2018, 621, 253–264.

Monteith, J.L. 1965. Evaporation and the environment. p. 205-234. In The state and movement of water in living organisms. 19th Symposia of the Society for Experimental Biology. Cambridge Univ. Press, London, U.K.

Morán-Tejeda, E.; Ceballos-Barbancho, A.; Llorente-Pinto, J.; López-Moreno, J.I. Land-cover changes and recent hydrological evolution in the Duero Basin (Spain). Reg. Environ. Chang. 2012, 12, 17–33.

Moral, F.; Cruz-Sanjulian, J.J.; Olias, M. Geochemical evolution of groundwater in the carbonate aquifers of Sierra de Segura (Betic Cordillera, Southern Spain). J. Hydrol. 2008, 360, 281–296.

Moriasi, D.N.; Wilson, B.N.; Douglas-Mankin, K.R.; Arnold, J.G.; Gowda, P.H. Hydrologic and water quality models: Use, calibration, and validation. Trans. ASABE 2012, 55, 1241–1247.

Moussa, R., Bocquillon, C., 2009. On the use of the diffusive wave for modelling extreme flood events with overbank flow in the floodplain. Journal of Hydrology 374, 116–135.

Mul M L, Mutiibwa R K, Foppen J W A, Uhlenbrook S, Savenije H H G. 2007. Identification of groundwater flow systems using geological mapping and chemical spring analysis in South Pare Mountains, Tanzania. Phys. Chem. Earth. 32 (15–18), 1015–1022.

Nachtergaele, F.O.; Van Velthuizen, H.; Verelst, L.; Wiberg, D. Harmonized World Soil Database, version 1.2; IIASA: Laxenburg, Austria, 2012.

Naiman, R.J., Bunn, S.E., Nilsson, C., Petts, G.E., Pinay, G., Thompson, L.C., 2002. Legitimizing Fluvial Ecosystems as Users of Water: An Overview. Environmental Management 30 (4), 455–467.

Nathan, R.J.; McMahon, T.A. Evaluation of automated techniques for base-flow and recession analyses. Water Resour. Res. 1990, 26, 1465–1473.

Neitsch, S. L., Arnold, J. G., Kiniry, J. R., & Williams, J. R. (2011). Soil and water assessment tool theoretical documentation version 2009. Texas Water Resources Institute.

Ngor, P.B., Oberdorff, T., Phen, C., Baehr, C., Grenouillet, G., Lek, S., 2018. Fish assemblage responses to flow seasonality and predictability in a tropical flood pulse system. Ecosphere 9(11), e02366.

Nguyen, V.T.; Dietrich, J.; Uniyal, B. Modeling interbasin groundwater flow in karst areas: Model development, application, and calibration strategy. Environ. Modell. Softw. 2020, 124, 104606.

Nilsson, C.; Svedmark, M. (2002) Basic principles and ecological consequences of changing water regimes: riparian plant communities. Environmental Management 30(4): 468–480.

Nikolaidis, N.P.; Bouraoui, F.; Bidoglio, G. Hydrologic and geochemical modeling of a karstic Mediterranean watershed. J. Hydrol. 2013, 477, 129–138. #

Obuobie E. Estimation of groundwater recharge in the context of future climate change in the White Volta River basin, West Africa. Germany. PhD Thesis, Rheinischen Friedrich-Wilhelms-Universität, Bonn, Germany, 2008, 165 pp.

Olden, J. D., & Poff, N. L. (2003). Redundancy and the choice of hydrologic indices for characterizing streamflow regimes. River Research and Applications, 19(2), 101–121.

Palanisamy, B.; Workman, S.R. Hydrologic modeling of flow through sinkholes located in streambeds of Cane Run stream, Kentucky. J. Hydrol. Eng. 2014, 20, 04014066.

Panday, P. K., Coe, M. T., Macedo, M. N., Lefebvre, P., & de Almeida Castanho, A. D. (2015). Deforestation offsets water balance changes due to climate variability in the Xingu River in eastern Amazonia. Journal of Hydrology, 523, 822–829.

Parker, J.M., Foster, S.S.D., Gomez-Cruz, A., 1988. Key hydrogeological features of a recent andesitic complex in Central America. Geolis II (1), 13–23.

Paz, C.; Alcalá, F.J.; Carvalho, J.M.; Ribeiro, L. Current uses of ground penetrating radar in groundwater-dependent ecosystems research. Sci. Total Environ. 2017, 595, 868-885.

Pedro-Monzonis M, Ferrer J, Solera A, Estrela T, Paredes-Arquiola J. 2014. Key issues for determining the exploitable water resources in a Mediterranean river basin. Science of the Total Environment 503-504: 319–328.

Peral García, C.; Navascués Fernández-Victorio, B.; Ramos Calzado, P. Serie de precipitación diaria en rejilla con fines climáticos. Nota técnica 24 de AEMET; Spanish Meteorological Agency (AEMET): Madrid, Spain, 2017.

Pérez-Sánchez, J., Senent-Aparicio, J., Martínez Santa-María, C., López-Ballesteros, A. 2020. Assessment of Ecological and Hydro-Geomorphological Alterations under Climate Change Using SWAT and IAHRIS in the Eo River in Northern Spain. Water 12(6),1745.

Plesca, I.; Timbe, E.; Exbrayat, J.-F.; Windhorst, D.; Kraft, P.; Crespo, P.; Vaché, K.B.; Frede, H.-G.; Breuer, L. Model intercomparison to explore catchment functioning: Results from a remote montane tropical rainforest. Ecol. Model. 2012, 239, 3–13.

Poff, N.L., Olden, J.D., Merritt, D.M., Pepin, D.M., 2007. Homogenization of regional river dynamics by dams and global biodiversity implications. Proc. Natl. Acad. Sci. Unit. States Am. 104 (14), 5732–5737.

Poff, N. L., et al. (1997). "The natural flow regime: A paradigm for river conservation and restoration." BioScience, 47(11), 769–784.

Poff, N. L., & Zimmerman, J. K. H. (2010). Ecological responses to altered flow regimes: A literature review to inform the science and management of environmental flows. Freshwater Biology, 55, 194–205.

Pool, T., Holtgrieve, G., Elliott, V., McCann, K., McMeans, B., Rooney, N., Smits, A., Phanara, T., Cooperman, M., Clark, S., Phen, C., Chhuoy. S., 2017. Seasonal increases in fish trophic niche plasticity within a flood-pulse river ecosystem (Tonle Sap Lake, Cambodia). Ecosphere 8(7).

Priestley, C. H. B., & Taylor, R. J. (1972). On the assessment of surface heat flux and evaporation using large-scale parameters. Monthly weather review, 100(2), 81–92.

Pulido-Velazquez, D.; Collados-Lara, A.J.; Alcalá, F.J. Assessing impacts of future potential climate change scenarios on aquifer recharge in continental Spain. J. Hydrol. 2018, 567, 803–819.

Quiñonero-Rubio, J.M.; Nadeu, E.; Boix-Fayos, C.; de Vente, J. Evaluation of the effectiveness of forest restoration and check-dams to reduce catchment sediment yield. Land Degrad. Develop. 2016, 27, 1018–1031.

Rahayuningtyas, C.; Wu, R.S.; Anwar, R.; Chiang, L.C. Improving avswat stream flow simulation by incorporating groundwater recharge prediction in the upstream Lesti watershed, East Java, Indonesia. Terr. Atmos. Ocean. Sci. 2014, 25, 881–892.

Rahman, K., Maringanti, C., Beniston, M., Widmer, F., Abbaspour, K., & Lehmann, A. (2013). Streamflow modeling in a highly managed mountainous glacier watershed using SWAT: The Upper Rhone River watershed case in Switzerland. Water resources management, 27(2), 323–339.

Revenga, C., Brunner, J., Henninger, N., Kassem, K. and Payne, R. (2000) Pilot Analysis of Global Ecosystems: Freshwater Ecosystems. World Resources Institute (WRI), Washington DC.

Richter, B. D., Baumgartner, J. V., Powell, J. 1996. A method for assessing hydrologic alteration within ecosystems［J］. Conservation Biology, 10(4):1163–1174.

Richter, B.D., Richter, H.E., 2000. Prescribing Flood Regimes to Sustain Riparian Ecosystems along Meandering Rivers. Conservation Biology 14, 1467–1478.

Rockwood D. M, Davis E.D., & Anderson J. A. (1972). User Manual for COSSARR Model. US Army Engineering Division, North Pacific: Portland, OR.

Rolls, R. J., Leigh, C., & Sheldon, F. (2012). Mechanistic effects of low-flow hydrology on riverine ecosystems: Ecological principles and consequences of alteration. Freshwater Science, 31, 1163–1186

Routschek, A., Schmidt, J., Kreienkamp, F., 2014. Impact of climate change on soil erosion — a high-resolution projection on catchment scale until 2100 in Saxony/Germany. Catena 121, 99–109.

Rutledge, A.T.; Mesko, T.O. Estimated Hydrologic Characteristics of Shallow Aquifer Systems in the Valley and Ridge, the Blue Ridge, and the Piedmont Physiographic Provinces Based on Analysis of Streamflow Recession and Base Flow. U.S. Geological Survey: Reston, VA, USA, 1996; 58 pp.

Sahin, V.; Hall, M.J. The Effects of Afforestation and Deforestation on Water Yields. J. Hydrol. 1996, 178, 293–309.

Sakaris PC. 2013. A review of the effects of hydrological alteration on fisheries and biodiversity and the management and conservation of natural resources in regulated river systems. INTECH Open Access Publisher: Rijeka, Croatia; 273–297.

Sami, K.; Hughes, D.A. A comparison of recharge estimates to a fractured sedimentary aquifer in South Africa from a chloride mass balance and an integrated surface-subsurface model. J. Hydrol. 1996, 179, 111–136.

Scanlon, B.R.; Healy, R.W.; Cook, P.G. Choosing appropriate techniques for quantifying groundwater recharge. Hydrogeol. J. 2002, 10, 18–39.

Scanlon, B.R.; Keese, K.E.; Flint, A.L.; Flint, L.E.; Gaye, C.B.; Edmunds, W.M.; Simmers, I. Global synthesis of groundwater recharge in semiarid and arid regions. Hydrol. Process. 2006, 20, 3335–3370.

Senent-Aparicio, J., Alcalá, F.J., Liu, S. & Jimeno-Sáez, P., 2020. Coupling SWAT Model and CMB Method for Modeling of High-Permeability Bedrock Basins Receiving Interbasin Groundwater Flow. Water 2020, 12, 657.

Senent-Aparicio, J., Liu, S., Pérez-Sánchez, J., López-Ballesteros, A. & Jimeno-Sáez, P., 2018a. Assessing impacts of climate variability and reforestation activities on water resources in the headwaters of the Segura River Basin (SE Spain). Sustainability 2018, 10, 3277.

Senent-Aparicio, J., López-Ballesteros, A., Pérez-Sánchez, J., Segura-Méndez, F. & Pulido-Velazquez, D., 2018b. Using Multiple Monthly Water Balance Models to Evaluate Gridded Precipitation Products over Peninsular Spain. Remote Sens. 2018, 10, 922.

Senent-Aparicio, J.; Jimeno-Sáez, P.; Bueno-Crespo, A.; Pérez-Sánchez, J.; Pulido-Velazquez, D. Coupling machine-learning techniques with SWAT model for instantaneous peak flow prediction. Biosyst. Eng. 2019, 177, 67–77.

Senent-Aparicio, J.; Pérez-Sánchez, J.; Carrillo-García, J.; Soto, J. Using SWAT and Fuzzy TOPSIS to assess the impact of climate change in the headwaters of the Segura River Basin (SE Spain). Water 2017, 9, 149.

Serra, P.; Pons, X.; Sauri, D. Land-cover and land-use change in a Mediterranean landscape: A spatial analysis of driving forces integrating biophysical and human factors. Appl. Geogr. 2008, 28, 189–209.

Shiau JT, Wu FC. 2004. Assessment of hydrologic alterations caused by Chi-Chi diversion weir in Chou-Shui Creek, Taiwan: opportunities for restoring natural flow conditions. Regulated Rivers: Research & Management 20: 401–412.

Singh, V. & Woolhiser, D.A., 2002. Mathematical modeling of watershed hydrology. J. Hydrol. Eng. 2002. 7:270–292.

Sloan, P.G., Morre, I.D., Coltharp, G.B., & Eigel, J.D. (1983). Modeling surface and subsurface stormflow on steeply-sloping forested watersheds. Water Resources Inst. Report 142. University. Kentucky, Lexington.

Sophocleous M. 2002. Interactions between groundwater and surface water: the state of the science. Hydrogeology Journal 10: 52–67.

Spanish National Geographic Institute (IGN). Plan Nacional de Ortofotografía Aérea. Available online: http://pnoa.ign.es/ (accessed on 3 January 2018).

Sugawara, M., Ozaki, E., Wantanabe, I., & Katsuyama, Y. (1976). Tank Model and its Application to Bird Creek, Wollombi Brook, Bihin River, Sanaga River, and Nam Mune. National Center for Disaster Prevention, Tokyo, Research Note, 11, 1–64.

Sun, G.; Zhou, G.; Zhang, Z.; Wei, X.; McNulty, S.G.; Vose, J.M. Potential water yield reduction due to forestation across China. J. Hydrol. 2006, 328, 548–558.

Srivastava, P., McNair, J. N., & Johnson, T. E. (2006). Comparison of process-based and artificial neural network approaches for streamflow modeling in an agricultural watershed. JAWRA Journal of the American Water Resources Association, 42(3), 545–563.

Tague, C., Grant, G., Farrell, M., Choate, J., & Jefferson, A. (2008). Deep groundwater mediates streamflow response to climate warming in the Oregon cascades. Climatic Change, 86, 189–210

The Brisbane Declaration (2007) Environmental flows are essential for freshwater ecosystem health and human well-being. In: The 10th International River symposium and International Environmental Flows Conference. Brisbane, Australia

Thoms, M.C., Sheldon, F., 2002. An ecosystem approach for determining environmental water allocations in Australian dryland river systems: the role of geomorphology. Geomorphology 47, 153–168.

Thyne, G.D., Gillespie, J.M., Ostdick, J.R., 1999. Evidence for interbasin flow through bedrock in the southeastern Sierra Nevada. Geological Society of America Bulletin 111 (11), 1600–1616.

Todini, E. (1996). The ARNO rainfall—runoff model. Journal of hydrology, 175(1-4), 339–382.

Tomer, M. D., & Schilling, K. E. (2009). A simple approach to distinguish land-use and climate-change effects on watershed hydrology. Journal of Hydrology, 376, 24–33

Tonkin JD, Jähnig SC, Haase P (2014) The rise of riverine fow-ecology and environmental fow research. Springer 1:323–330

To´th, J.A., 1963. A theoretical analysis of groundwater flow in small drainage basins. Journal of Geophysical Research 68 (16), 4795–4812.

Trigo, R.; Pozo-Vázquez, D.; Osborn, T.; Castro-Díez, Y.; Gámiz-Fortis, S.; Esteban-Parra, M. North Atlantic oscillation influence on precipitation, river flow and water resources in the Iberian Peninsula. Int. J. Climatol. 2004, 24, 925–944.

Trolle, D.; Hamilton, D.P.; Hipsey, M.R.; Bolding, K.; Bruggeman, J.; Mooij, W.M.; Janse, J.H.; Nielsen, A.; Jeppesen, E.; Elliott, A.; Makler–Pick, V.; Petzoldt, T.; Rinke, K.; Flindt, M.R.; Arhonditsis, G.B.; Gal, G.; Bjerring, R.; Tominaga, K.; 't Hoen, J.; Downing, A.S.; Marques, D.M.; Fragoso, C.R.J.; Søndergaard, M.; Hanson, P.C. A community–based framework for aquatic ecosystem models. Hydrobiologia 2012, 683, 25–34.

USD-SCS (1972). National Engineering Handbook. Section 4. Hydrology. Department of Agriculture. Soil Conservation Service. Washington.

Vanderlinden, K.; Giraldez, J.V.; Van Meirvenne, M. Assessing Reference Evapotranspiration by the Hargreaves Method in Southern Spain. J. Irrig. Drain. Eng. 2004, 130, 184–191.

Vogel, R. M., J. Sieber, S. A. Archfield, M. P. Smith, C. D. Apse, and A. Huber-Lee. (2007). "Relations among storage, yield, and instream flow". Water Resources Research. 43, W05403.

Vörösmarty C, Lettenmaier D, Leveque C, Meybeck M, Paht Wostl C, Alcamo J, Cosgrove W, Grassl H, Hoff H, Kabat P, Lansigan F, Law ford R, Naiman R (as Members of the Framing Committee of the GWSP). 2004. Humans Transforming the Global Water System. Eos, Transactions, American Geophysical Union 85: 48

Vorosmarty CJ, Green P, Salisbury J, Lammers RB (2000) Global water resources: vulnerability from climate change and population growth. Science 289:284–288

Vogel, R.M.; Sieber, J.; Archfield, S.A.; Smith, M.P.; Apse, C.D.; Huber-Lee, A. Relations among storage, yield and instream flow. Water Resour. Res. 2007, 43.

Vogel, R.M., Fennessey, N.M. (1995). "Flow duration curves II: a review of applications in water resources planning". Water Resources Bulletin 31 (6), pp. 1029–1039.

Wagner, P.D.; Waske, B. Importance of spatially distributed hydrologic variables for land use change modeling. Environ. Model. Softw. 2016, 83, 245–254.

Wang, G., Yang, H., Wang, L., Xu, Z., & Xue, B. (2014). Using the SWAT model to assess impacts of land use changes on runoff generation in headwaters. Hydrological Processes, 28(3), 1032–1042.

Wang Y, Wang D, Wu J. 2015. Assessing the impact of Danjiangkou reservoir on ecohydrological conditions in Hanjiang river, China. Ecological Engineering 81:41–52.

WCD (2000) Dams and development: a new framework for decisionmaking. Earthscan Publications Ltd, London.

Water Framework Directive (2000/60/EC). European Communities Official Journal L327 22.12.2000, pp.1–72

Wei, X., Liu, W., & Zhou, P. (2013). Quantifying the relative contributions of forest change and climatic variability to hydrology in large watersheds: A critical review of research methods. Water, 5, 728–746.

Whipple, A.A., Viers, J.H., Dahlke, H.E., 2017. Flood regime typology for floodplain ecosystem management as applied to the unregulated Cosumnes River of California, United States. Ecohydrology 10, e1817.

Williams J. R. & Hann R. W. (1973). HYMO: Problem-Oriented Language for Hydrologic Modeling—User's Manual. USDA: ARS-S-9.

Wohl, E., Bledsoe, B. P., Jacobson, R. B., LeRoy Poff, N., Rathburn, S. L., Walters, D. M., Wilcox, A. C., 2015. The Natural Sediment Regime in Rivers: Broadening the Foundation for Ecosystem Management. *BioScience*, 65 (4), 358–371.

Woldesenbet, T.A.; Elagib, N.A.; Ribbe, L.; Heinrich, J. Hydrological responses to land use/cover changes in the source region of the Upper Blue Nile Basin, Ethiopia. Sci. Total Environ. 2017, 575, 724–741.

Wood, W.W.; Sanford, W.E. Chemical and isotopic methods for quantifying ground-water recharge in a regional, semiarid environment. Ground Water 1995, 33, 458–468.

Xia Jun. 2002. Hydrological Science Towards Global Change: Progress and Challenge. Resources Science 24(3).

Yan, R.; Zhang, X.; Yan, S.; Zhang, J.; Chen, H. Spatial patterns of hydrological responses to land use/cover change in a catchment on the Loess Plateau, China. Ecol. Indic. 2017, 92, 151–160.

Yang, J. H., & Chang, C. C. (2008). Efficient residue number system iterative modular multiplication algorithm for fast modular exponentiation. IET Computers & Digital Techniques, 2(1), 1–5.

Yang, L.; Feng, Q.; Yin, Z.; Wen, X.; Si, J.; Li, C.; Deo, R.C. Identifying separate impacts of climate and land use/cover change on hydrological processes in Upper Stream of Heihe River, northwest China. Hydrol. Process. 2017, 31, 1100–1112.

Yang YH, Tian F (2009) Abrupt change of runoff and its major driving factors in Haihe River Catchment, China. J Hydrol 374:373–383

Yang Z, Yan Y, Liu Q. 2012. Assessment of the flow regime alterations in the Lower Yellow River, China. Ecological Informatics 10: 56–64.

Zeiringer B, Seliger C, Greimel F, Schmutz S (2018) River hydrology, fow alteration, and environmental fow. Riverine ecosystem management. Springer, Cham, pp 67–89

Zhang, A.-J.; Wang, B.-D.; Cao, M.-L. Influence research of climate change and human activities on runoff contribution. Water Resour. Hydropower Northeast. China 2012, 1. Available online: https://en.cnki.com.cn/Article_en/CJFDTotal-DBSL201201001.htm

Zhang, L.; Karthikeyan, R.; Bai, Z.K.; Srinivasan, R. Analysis of streamflow responses to climate variability and land use change in the Loess Plateau region of China. Catena 2017, 154, 1–11.

Zhang, L., Jin, X., He, C., Zhang, B., Zhang, X., Li, J., Tian, J. & DeMarchi, C. (2016). Comparison of SWAT and DLBRM for hydrological modeling of a mountainous watershed in Arid Northwest China. Journal of Hydrologic Engineering, 21(5), 04016007.

Zhang, Q., Gu, X., Singh, V. P., & Chen, X. (2015). Evaluation of ecological instream flow using multiple ecological indicators with consideration of hydrological alterations. Journal of Hydrology, 529, 711–722.

Zhang, Y.; Guan, D.; Jin, C.; Wang, A.; Wu, J.; Yuan, F. Impacts of climate change and land use change on runoff of forest catchment in northeast China. Hydrol. Process. 2014, 28, 186–196.

Zhang, Z., Huang, Y., & Huang, J., 2016. Hydrologic alteration associated with dam construction in a medium-sized coastal watershed of southeast China. Water 8(8), 317.

Zhang, Z., Liu, J., Huang, J., 2020. Hydrologic impacts of cascade dams in a small headwater watershed under climate variability. Journal of Hydrology 590, 125426.

Zheng, Y., Zhang, G., Wu, Y., Xu, Y.J., Dai, C., 2019. Dam Effects on Downstream Riparian Wetlands: The Nenjiang River, Northeast China. *Water 11*, 2038.

Zuo Q, Liang S. Effects of dams on river flow regime based on IHA/RVA [J]. Proceedings of the International Association of Hydrological Sciences, 2015 (368): 275–280.

APPENDIX: QUALITY OF PUBLICATIONS

APPENDIX: QUALITY OF PUBLICATIONS

Publication 1: Sustaibility by MDPI

Sustaibility Magazine Statistics:
- ISSN: 2071-1050
- Founded in 2009
- 50,403 published articles
- 71,638 total citations

Impact Factor:
- Impact Factor: 3.251 (2020)
- 5-Year Impact Factor: 3.473 (2020)
- Ranking of the category JCR 2020: 53/123 (Q2) in *Environmental Studies (SSCI);* 120/265 (Q2) in *Environmental Sciences (SCIE);* 26/41 (Q3) in *Green & Sustainable Science & Technology (SCIE)*
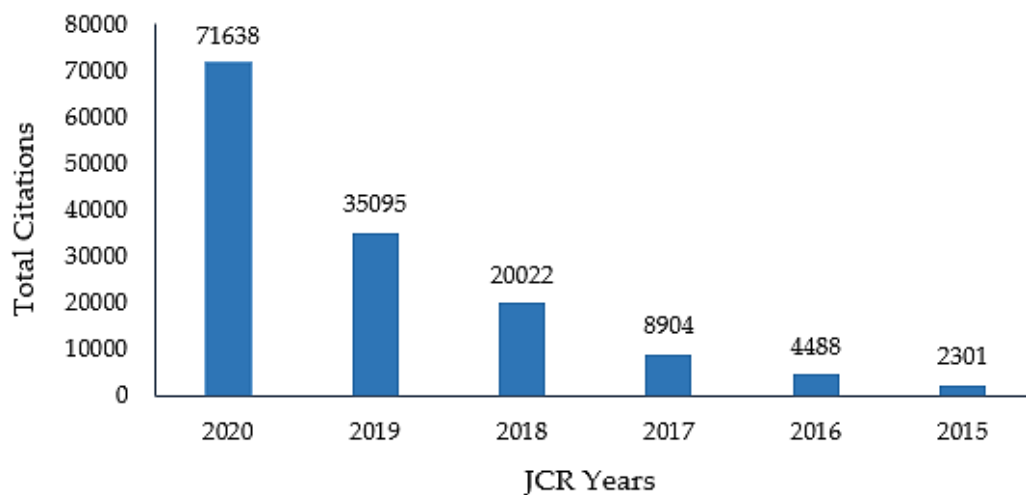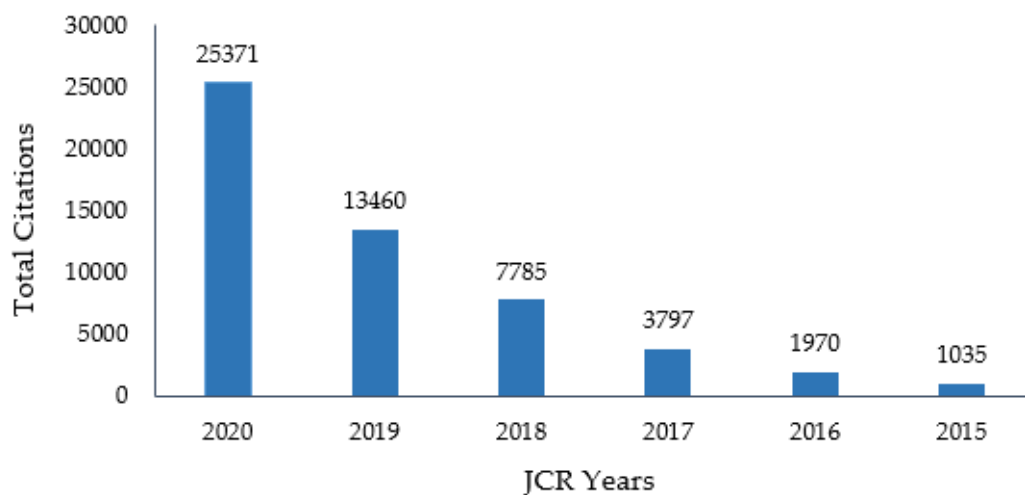
Publication 2: Water by MDPI

Water Magazine Statistics:
- ISSN: 2073-4441
- Founded in 2009
- 16,258 published articles
- 25,371 total citations

Impact Factor:
- Impact Factor: 3.103 (2020)
- 5-Year Impact Factor: 3.229 (2020)
- Ranking of the category JCR 2020: 31/94 (Q2) in *Water Resources*

Publication 3: Ecohydrology & Hydrobiology by Elsevier

Ecohydrology & Hydrobiology Magazine Statistics:
- ISSN: 1642-3593
- Founded in 2001

Impact:
- Impact Factor: 2.957 (2021)
- Ranking of the category JCR 2021: 84/173 (Q2) in *Ecology*
- CiteScore: 5.1 (2021)
- Ranking of the CiteScore 2021: 40/234